# A NEURAL BASIS FOR THE BEHAVIORAL EFFECTS OF ANXIETY

by

Junchol Park

Bachelor of Arts, Korea University, 2006

Master of Science, Korea University, 2009

Submitted to the Graduate Faculty of the

Kenneth P. Dietrich school of Arts and Science in partial fulfillment

of the requirements for the degree of

Doctor of Philosophy

University of Pittsburgh

2017

UNIVERSITY OF PITTSBURGH

DIETRICH SCHOOL OF ARTS AND SCIENCES

This dissertation was presented

by

Junchol Park

It was defended on

December 12, 2016

and approved by

Susan Sesack, PhD, Professor, Neuroscience, Psychiatry

Marlene Cohen, PhD, Assistant Professor, Neuroscience

Robert Kass, PhD, Professor, Statistics, Machine Learning, Carnegie Mellon University

Anne-Marie Oswald, PhD, Assistant Professor, Neuroscience

Naoshige Uchida, PhD, Professor, Molecular and Cellular Biology, Harvard University

Dissertation Advisor: Bita Moghaddam, PhD, Neuroscience, Psychiatry

**A NEURAL BASIS FOR THE BEHAVIORAL EFFECTS OF ANXIETY**

Junchol Park, PhD

University of Pittsburgh, 2017

Anxiety represents a state of high arousal and negative valence that leads to enhanced vigilance in the absence of concrete and immediate threat. Anxiety has profound impacts on ongoing behaviors. It can be an adaptive reaction to stressful or unpredictable life events, but excessive and persistent anxiety produces adverse cognitive effects that disrupt ongoing behavior and contribute to the clinical manifestation of anxiety disorders. Numerous studies have associated anxiety with deficits in cognitive control of behavior, and with perseverative behavioral tendencies. In addition, the adverse impact of anxiety is characterized in part by deficits in reward-related behavioral domains such as anhedonia and aberrant reward-associated perception.

This dissertation study focuses on the neural basis of the behavioral impacts of anxiety. The neural circuit, comprising the prefrontal cortex (PFC) and the ventral tegmental area (VTA), is thought to be critically involved in anxiety-induced behavioral disruptions. Numerous neurophysiological and neurochemical studies suggest that the mesoprefrontal circuit preferentially responds to aversive stimuli, stressors, and resultant anxiety. However, it is largely unknown how VTA and mPFC individual neurons and neuronal ensembles represent cognitive, motivational, and emotional behavioral changes in anxiety. To address this, we studied animals engaged in well-characterized motivated and cognitive behavioral tasks in the absence or presence of varying degrees of an anxiogenic perturbation. By electrophysiologically recording the activity of VTA and mPFC single neurons and local field potential (LFP) signals from the

task-performing animals, we demonstrate that anxiety-related behavioral alterations can be attributed to specific changes in the activity of VTA and mPFC neurons and neuronal populations. Collectively, our neurophysiological findings suggest that anxiety “hijacks” the VTA-mPFC neural circuit by profoundly modulating the spontaneous and task-related neural activity at the individual neuron-, neural population-, and neural circuit levels. Anxiety-induced neural changes in the VTA-mPFC circuit were systematically associated with anxiety-like changes in motivated and cognitive behaviors, even on a single-trial basis, providing insights that could contribute to therapeutic interventions for the behavioral symptoms of anxiety disorders.

**TABLE OF CONTENTS**

## LIST OF TABLES

## LIST OF FIGURES

# PREFACE

In the recent six years, I have been extremely fortunate to interact with many great scientists and friends in the laboratory of Dr. Bita Moghaddam and in the center for neuroscience. I owe much to former members of the lab intellectually – Yunbok Kim, Jesse Wood, Corina Bondi, David Sturman, Adria Martig, Nick Simon, and Alberto Del Arco. Yunbok and Jesse provided me with thorough training for collection and analysis of neurophysiological data. Jesse and Nick significantly contributed to invention of the risky reward-seeking task, which was one of the most important experimental challenges. Current members of the Moghaddam lab – Sweyta Lohani, Meredyth Wegener, Tara Chowdhury, and Sara Morrison – have provided critical and constructive discussion on experimental data, and they have also provided helpful comments and edits on my manuscripts and presentations.

It has been great pleasure to interact with great scientists who kindly served in my dissertation committee – Susan Sesack, Marlene Cohen, Rob Kass, Anne-Marie Oswald, Nao Uchida, and Bita Moghaddam. Our discussion at every meeting significantly influenced how I think about my data and how I communicate my findings to fellow scientists. I am also sincerely grateful to each of the committee members for being such a great model with their excellent science and career.

Most importantly, I would like to express my sincere gratitude to my awesome mentor Bita Moghaddam. None of this dissertation work was possible without her generous intellectual

and financial supports. Bita has provided mentorship with an excellent balance between guidance and sufficient degree of freedom for me to explore different possibilities with trials-and-errors, which gave rise to enormous amount of learning and training. I believe that Bita's persistent passion and dedication to the neural basis of mental health will continue to shine with outlasting success in her science, which will continue to be much appreciated by the neuroscientific community.

I would love to thank very much to my sister Jiyoon and my parents Sookja and Jinho for their continued unconditional love and supports for me. Finally, I would like to express my sincere love and thanks to my wonderful wife and physician scientist Dr. Hannah Hoeun Lee, who have made this entire dissertation process and my life in general much more likable and enjoyable.

# 1.0 INTRODUCTION

Anxiety represents a state of high arousal and negative valence, leading to elevated vigilance in the absence of concrete and immediate threat (Calhoon and Tye, 2015). Anxiety has profound impacts on ongoing behaviors. It can be an adaptive reaction to stressful and unpredictable life events, as physiological and emotional stress and resultant anxiety may enable animals to avoid dangers and to achieve goals. However, excessive and persistent anxiety may cause detrimental impacts on cognitive control of behavior: i.e., the ability to flexibly guide behavior to gain/avoid appetitive/aversive outcomes, respectively, in an ever-changing environment utilizing reinforcement history and learned "rule of the game" (Park et al., 2016). The negative impacts of anxiety are characterized in part by profound deficits in reward-related behavioral domains such as anhedonia and aberrant reward-associated perception (Russo and Nestler, 2013). Furthermore, numerous studies have associated pathological anxiety with deficits in cognitive control of behavior, as patients with anxiety disorders exhibit perseverative cognitive and/or emotional behavioral patterns: i.e., inability to shift to a novel task strategy or a new affective state (Bishop, 2007; Eysenck et al., 2007).

The mesoprefrontal neural circuit comprising the prefrontal cortex (PFC) and the ventral tegmental area (VTA) is thought to be critically involved in anxiety-induced behavioral disruptions for the following reasons. First, mesoprefrontal neural activity, specifically dopamine (DA) neurotransmission in the PFC, plays a role in "normal" cognitive functions in a non-

anxious state: e.g., cognitive flexibility, working memory and decision making (Arnsten, 2015; Floresco, 2013). Either excessive or deficient DA transmission may result in suboptimal cognitive performance. Second, the mesoprefrontal DA system preferentially responds to stressful and anxiogenic perturbations, even to mild ones that do not affect mesolimbic or mesostriatal DA transmission (Abercrombie et al., 1989; Bradberry et al., 1991a; Moghaddam et al., 1990; Thierry et al., 1976). Consistent with this, VTA DA neurons projecting to the mPFC receive preferential input from the lateral habenula (LHb) neurons that are selectively tuned to aversion and omission of reward (Lammel et al., 2012) (Figure 1-1). Furthermore, photostimulation of VTA dopaminergic input to the mPFC elicits anxiety-like behavior (Gunaydin et al., 2014; Lammel et al., 2012).

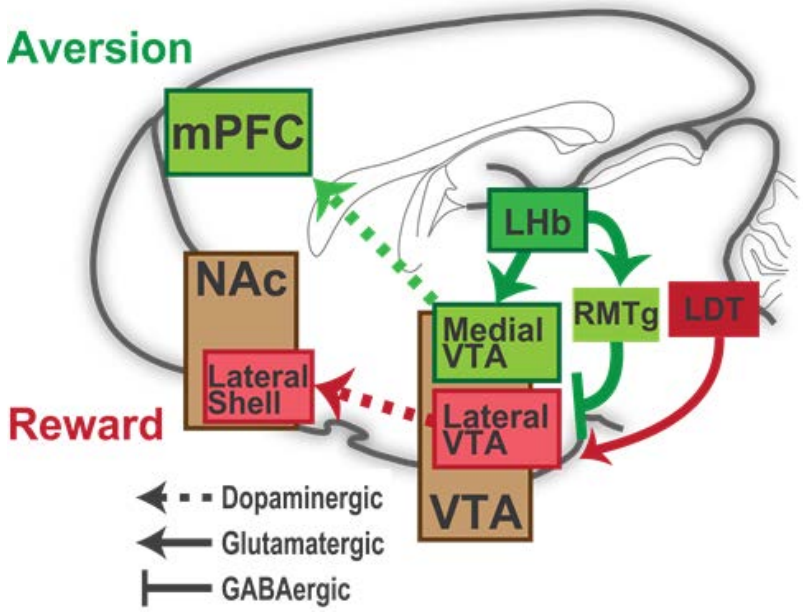


**Figure 1-1 A simplified functional circuit mapping of the mesocorticolimbic structures implicated in aversion- and reward-related behaviors.**

The mesocorticolimbic structures that are associated with aversive behavior appear in green, while the structures associate with reward-related behavior are in red. Connections among these structures are indicated with different types of lines (legend) depending on the primary neurotransmitters in the relevant synapses. mPFC = medial prefrontal cortex; NAc = nucleus accumbens; LHb = lateral habenula; VTA = ventral tegmental area; RMTg = rostromedial tegmental nucleus; LDT = laterodorsal tegmental nucleus.

These lines of evidence converge onto the hypothesis that anxiety may place the VTA-mPFC neural circuit in an aberrant state of disrupted ongoing and task-relevant neural activity, which may result in deficits in flexible cognitive control of behavior. The current dissertation study has been designed to test this hypothesis and, more generally, to unravel the nature of PFC and VTA neural substrates underlying cognitive and motivated behavioral changes in anxiety. To more thoroughly address the neural basis of behavioral changes in anxiety, we used experimental designs combining an animal model of anxiety and a behavioral task in which performance has been well characterized. While animals performed this task, we recorded the activity of single neurons and local field potential (LFP) signals. In the first set of experiments, we investigated how the VTA-mPFC neural circuit represents varying degrees of punishment risk and risk-based anxiety-like changes in simple instrumental behavior by simultaneously recording the neural activity in medial PFC (mPFC) and VTA. In the second set of experiments, we focused on the neural basis of disruptions in PFC-dependent cognitive functions in anxiety by recording mPFC and orbitofrontal PFC (OFC) activity from rats performing a task requiring cognitive flexibility.

Before we delve into our findings, we begin by discussing the role of the PFC in the cognitive control of goal-directed behavior. We also review the literature describing the importance of the mesoprefrontal circuit, especially dopaminergic neuromodulation, for proper

PFC-mediated cognitive functions. Then we review human and animal studies illustrating cognitive behavioral deficits that are associated with anxiety. Finally, we discuss the literature demonstrating the susceptibility of the mesoprefrontal neural circuit to aversive, stressful and anxiogenic stimuli, which may engender disruptions of the cognitive functions subserved by the VTA-mPFC neural circuit in anxiety.

## 1.1 THE ROLE OF PFC IN FLEXIBLE COGNITIVE CONTROL OF BEHAVIOR

Before discussing prefrontal cortical function in cognitive flexibility, it is informative to consider behaviors that do not primarily depend on PFC functions. The PFC is not critically involved in performing simple, automatic behaviors, which can be guided by first-order associations between a stimulus and an outcome (S-O) or an action and an outcome (A-O) (Balleine and Dickinson, 1998; Euston et al., 2012; Miller and Cohen, 2001). These behaviors can be innate or learned by experience, and can be evoked simply by the right stimulus or context, facilitating prompt reactions in familiar situations. On the other hand, behaviors that depend on a simple association are prone to form habits, which may be characterized as inflexible, stereotyped behaviors in that they are difficult to update, unlearned, and generalized to novel situations. Numerous studies have shown that lesion or pharmacological inactivation of the PFC does not impair learning and expression of simple S-O or A-O behaviors per se, suggesting that they may primarily depend on "bottom-up" processing subserved by subcortical circuits (Balleine and Dickinson, 1998; Birrell and Brown, 2000; Miller and Cohen, 2001; Naneix et al., 2009).

In contrast, the PFC plays a critical role when "top-down" processing is required for behavioral guidance. In real-life situations, S-O and/or A-O relationships are abstract, noisy, and

ever-changing. Thus, adaptive behavior requires up-to-date representations of the higher-order statistics underlying the complex S-O and, A-O relationships. In addition, the internal motivational and emotional states that affect animals' "goal state" in a given situation also vary over time. Given these external and internal sources of variance, the "rules of the game" – i.e., internal representations of goals and the means to achieve them – need to be configured in a highly flexible manner to achieve the best available outcome. This integrative function has been termed "cognitive flexibility" or "behavioral flexibility". Converging lines of theoretical and experimental evidence have suggested cognitive flexibility as a cardinal function of the PFC (Cohen and Servan-Schreiber, 1992; Kehagia et al., 2010; Miller and Cohen, 2001; Wise et al., 1996). Lesions of PFC have been associated with response perseveration – i.e. behavioral inflexibility, which renders an animal unable to discontinue a learned response that is no longer effective (Fuster, 1989).

A comprehensive literature has demonstrated that functional integrity of PFC is essential for cognitive flexibility in rodents (Ragozzino et al., 2003; Rich and Shapiro, 2009; Stefani et al., 2003; Stefani and Moghaddam, 2010), non-human primates (Dias et al., 1996; Nakahara et al., 2002; Wallis et al., 2001; White and Wise, 1999) and humans (Konishi et al., 1998; Nagano-Saito et al., 2008; Nakahara et al., 2002). Behavioral paradigms that measure cognitive flexibility test the ability to guide goal-directed actions based on two or more discriminative rules, and to shift from one rule to another on the basis of the feedback (i.e. response outcome). Among many versions of these tasks, the Wisconsin Card Sorting Task (WCST; Figure 1-2a) has been used most commonly for rule-based flexible control of behavior in humans (Nyhus and Barcelo, 2009). In the WCST, participants are required to match test cards with a sample card according to one of multiple possible rules (Figure 1-2a; e.g. color rule, shape rule), with changes in the

matching rule occurring without subjects' knowledge, thus requiring flexible adjustment of the sorting strategy based on feedback. Studies have shown that, when performing the WCST, individuals with ventromedial PFC lesion fail to shift to a response strategy that is more advantageous in the long run (Bechara et al., 2000; Bechara et al., 1996). This is consistent with earlier work demonstrating that human subjects with frontal lobe injury show marked deficits in shifting from one mode of solution to another on a sorting task (Milner, 1963).

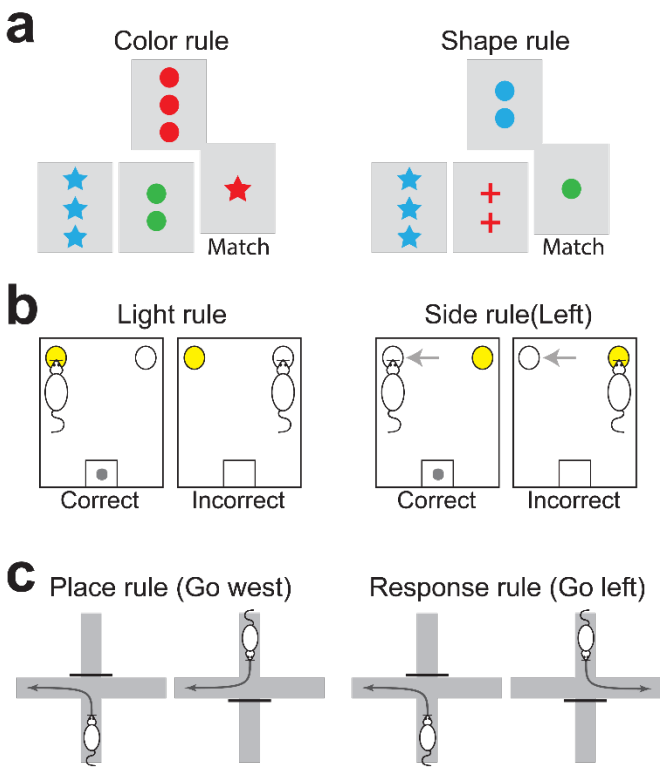


**Figure 1-2 Tasks measuring cognitive flexibility in humans and rodents.**

(a) Example trials in the WCST. The top card is the test card. The bottom three cards are the reference cards. During the matching period, the subject selects the reference card that matches the test card based on the currently valid sorting rule: e.g., matching based on the color or shape. Feedback is provided after each selection. An extra-

dimensional set-shift then occurs to another rule on a distinct perceptual dimension; this shift is not signaled to the subject, who should respond to the shift according to task feedback. (b) A rodent version of a set-shifting task in an operant chamber. In this task, rats learn to guide their instrumental behavior based on two rules in distinct perceptual dimensions, and shift between them based on task feedback (reward delivery or omission). In the "light rule," a nose poke (or a lever press) to the illuminated port is correct, whereas in the "side rule," a nose poke to the valid location (e.g. left port) is a correct response regardless of the illumination. The gray arrows indicate the current valid side (invisible to rats). (c) A rodent set-shifting task in a plus maze. In the "place rule", rats are required to enter one goal arm (east or west) from both starting arms (north and south). In the "response rule", one body turn response (right or left) should be made from either starting arm. Gray arrows indicate correct trajectories in either rule.

Animal studies have successfully used different version of the WCST (Figure 1-2b-c) to investigate neural substrates of flexible rule-based decision making in rodents and primates. In these tasks, behavior is guided by the currently valid rule among two or more rules that refer to distinct perceptual dimensions. Rule shifting can occur between different perceptual dimensions (extra-dimensional shifting) or within a dimension (intra-dimensional shifting or reversal). Lesions or pharmacological manipulations of the rat medial PFC (mPFC) result in markedly impaired performance in these and other set-shifting tasks that assess behavioral flexibility (Birrell and Brown, 2000; Bissonette et al., 2008; Darrah et al., 2008; Floresco et al., 2008; Ragozzino et al., 2003; Stefani et al., 2003; Stefani and Moghaddam, 2010) (Figure 1-3). This is similar to performance deficits observed after dorsolateral PFC lesion in non-human primates (Dias et al., 1996, 1997) and in humans with PFC damage (Anderson et al., 1999).

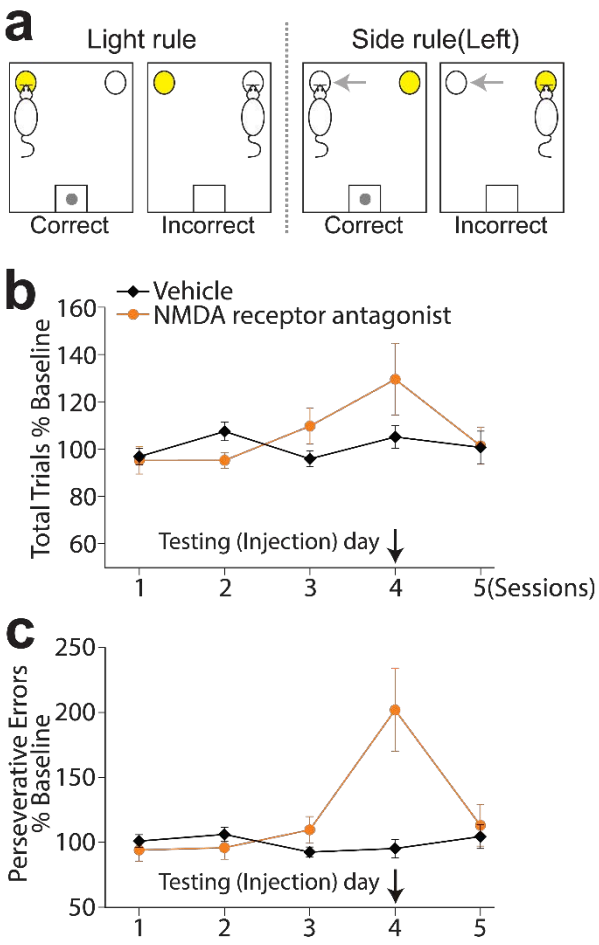


**Figure 1-3 Set-shifting task performance is impaired by intracranial microinjection of the NMDA receptor antagonist MK801 in mPFC.**

(a) The extra-dimensional set-shifting task used for this experiment. In each session, rats performed the operant task based on two alternating rules in distinct perceptual dimensions. Three extra-dimensional rule-shifts had to be made to complete a session (i.e., a total of four sets with two light- and two side-rule sets interleaved in a pseudo-randomized order). (b) Rats underwent a total of five sessions with injections made only on the 4th session, indicated with an arrow. MK801 significantly increased the number of total trials to complete the task, indicating impaired task performance. (c) The most pronounced drug effect was an increased number of perseverative errors, scored when rats produced an error by making a choice based on the previously effective rule. This result indicates that the blockade of glutamatergic neurotransmission mediated by NMDA receptors in PFC leads to cognitive inflexibility. Figure 1-3b-c adapted from Darrah et al. (2008).

Cognitive flexibility involves multiple dynamic processes that monitor ongoing actions and action-outcome relationships, and then adjusts future actions based on outcome. This process can be subdivided into various constructs such as representations of the rule, performance errors, conflict among different response tendencies, and the risk/uncertainty contingent on the action. Human and primate studies using functional magnetic resonance imaging (fMRI) have shown that different but overlapping subregions of the PFC are activated in correlation with these constructs using multiple tasks (Carter et al., 1998; Clark et al., 2008; Kerns et al., 2004; O'Doherty, 2004). For example, fMRI studies have shown transient activation of PFC during rule shifting (Konishi et al., 1998; Nakahara et al., 2002), retrieval, and maintenance of abstract rules for decision making (Bunge et al., 2003).

While human neuroimaging data have informed us about the general involvement of PFC subregions in cognitive-flexibility tasks, invasive electrophysiological recordings in laboratory animals have demonstrated the dynamic nature of neuronal encoding during these tasks. For example, studies in primates have revealed that PFC single neuron firing rates during different task states (e.g., baseline, cue, delay and response periods) vary as a function of the current task rule (Asaad et al., 2000; Fuster et al., 2000; Hoshi et al., 1998; White and Wise, 1999).

Electrophysiological studies in rodents have demonstrated that PFC subregions – including prelimbic PFC (PL), infralimbic PFC (IL), and orbitofrontal cortex (OFC) – are differentially involved in extra-dimensional set-shifting tasks. In an elegant study, Rich and Shapiro recorded from single neurons in rats navigating a plus maze with two alternating response strategies: one based on egocentric path and one based on spatial location (Figure 1-2c; e.g. “go left” or “go west”) (Rich and Shapiro, 2009). Subpopulations of PL and IL neurons

encoded the strategy shift, even when neuronal activity during the two strategies was compared between trials with seemingly identical navigation. The PL encoding of a strategy shift temporally preceded both the behavioral shift and IL encoding, suggesting that dorsal rather than ventral medial PFC neurons drive the behavioral shift. Neurons in the OFC have been suggested to play a dissociable role that is more specialized for signaling outcome expectancy (Schoenbaum et al., 2009). This view is supported by behavioral studies indicating a role of OFC in representation of outcome value and expectancy (Bissonette et al., 2008; Burke et al., 2009; Dias et al., 1996, 1997; McAlonan and Brown, 2003; Rudebeck et al., 2006). Neurophysiological studies suggest that OFC neurons signal outcome expectancy as well as reversal in cue-outcome association (Bissonette et al., 2015; Morrison and Salzman, 2009; Roesch and Olson, 2004; Simon et al., 2015).

Recent neurophysiological studies have delved into PFC population-level codes that may underlie rule-based flexible control of behavior. Investigating the coordinated activity of neural populations is particularly important when examining the neural basis of rule-based behavior because such tasks require encoding of multiple task features to which individual PFC neurons are dynamically tuned. Dynamic neuronal tuning properties have been uncovered by studies that investigated the population-level activity of PFC and other high-order cortical structures during flexible decision making (Karlsson et al., 2012; Ma et al., 2014; Mante et al., 2013; Raposo et al., 2014; Rigotti et al., 2013). These studies show that the majority of PFC neurons have mixed selectivity: i.e., their responses are linearly or nonlinearly correlated with diverse combinations of task-relevant features (such as the sensory stimuli, task rules or motor responses) rather than being purely selective for individual features (e.g., Figure 1-4). In fact, mixed selectivity is suggested to be a key computational property of PFC neurons that leverages the dimensionality

of population-activity space related to cognitive task performance (Rigotti et al., 2013). For example, Fusi and colleagues have recently demonstrated the advantages of PFC neuronal mixed selectivity by showing that the degree of dimensionality of the neuronal population activity space is correlated with actual choice behavior (Rigotti et al., 2013; Rigotti et al., 2010), suggesting that the high dimensionality of PFC population encoding is causally associated with decision-making capability.

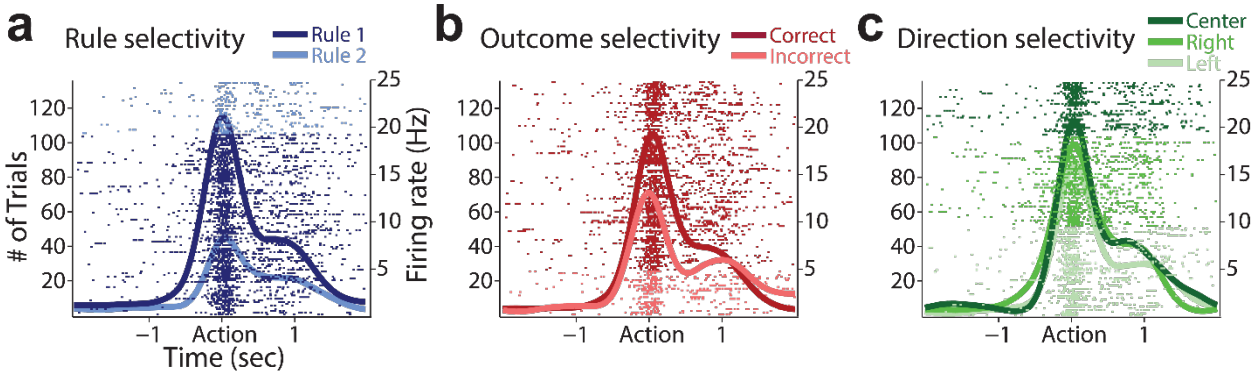


**Figure 1-4 Example of an mPFC neuron with mixed selectivity for multiple task variables, recorded from a rat performing the extra-dimensional set-shifting task.**

This neuron encoded three different task variables: the task rule (a), the response outcome (b), and the response direction (c), in overlapping or non-overlapping time bins around the time of the action, according to a multiple linear regression analysis (Section 3).

Recent studies provide convincing evidence that some unique properties of PFC neuronal encoding are revealed only when the ensemble-level activity is examined in a high-dimensional space. Seamans and colleagues addressed this experimentally by comparing the individual- and

population-level neuronal discriminability of simultaneously recorded neurons in the anterior cingulate region of the PFC (ACC), and in the dorsal striatum (DS) (Ma et al., 2014). The individual neuronal discriminability of different action sequences did not differ between the two regions, whereas the ACC outperformed the DS as an ensemble in all ensemble-based discriminability measures. This suggests that coordinated activity of PFC neurons leads to more information-rich ensembles as compared to the striatum.

Other studies have used trial-by-trial population trajectories to investigate the dynamic properties of PFC-neuronal representations of flexible decision making. Stokes et al. (2013), for example, analyzed PFC neural populations in monkeys performing a cue-target matching task with three possible cue-target pairs; monkeys were required to choose the matching target after viewing a cue in the presence of distractors. By tracing population states in the high-dimensional space constructed by all neurons in the network, the authors found that the PFC population was dynamically tuned to represent momentary task demands – i.e., cue discrimination during the cue period and behavioral choice during the choice period – in a task-context dependent manner. This suggests that complex rule-based choices can be mapped onto high-dimensional PFC neural states that are tuned to reflect the current task requirement (Stokes et al., 2013). On a larger timescale, the PFC rule-learning process has been depicted as a rapid shift in the neuronal ensemble state, suggesting that the task-rule shift is represented by a sustained alteration in PFC population activity that occurs abruptly – an "a-ha" moment (Durstewitz et al., 2010; Powell and Redish, 2016).

Synchronization via coherent gamma oscillations (γ; 30~120 Hz) may subserve the formation and communication of functional ensembles in the PFC and other cortical brain regions (Buschman et al., 2012; Cardin et al., 2009; Fries, 2005, 2015; Sirota et al., 2008; Sohal

et al., 2009; Uhlhaas and Singer, 2010). During task-related processes, neuronal ensembles tend to engage in rhythmic synchronization that can temporally coordinate neuronal activity by creating a sequence of excitatory and inhibitory cycles (Figure 1-5). Phase-locking of relevant ensembles into coherent excitation-inhibition sequences can facilitate communication between them while blocking 'noise' from incoherent ensembles. This may provide a mechanism for selecting and binding the neural ensembles that encode the currently relevant features of the task while deselecting the irrelevant ensembles.

Consistent with this model, distinctly synchronous PFC ensembles have been shown to be associated with different task rules suggesting that a rule-dependent emergence of synchronous ensembles may be a neural substrate of the cognitive flexibility (Buschman et al., 2012). An additional causal relationship has been suggested between task-relevant gamma oscillations and cognitive flexibility by Sohal and colleagues (Cho et al., 2015). The authors found that disruption of baseline and task-evoked gamma oscillations in a mouse model of deficient development of fast-spiking interneurons (FSINs) led to cognitive inflexibility. By optogenetically enhancing the activity of FSINs in these mice, the task-related gamma oscillations, as well as the rule-shifting behavior, could be rescued, suggesting a role of FSIN-mediated PFC gamma oscillations in cognitive flexibility. Collectively, these studies suggest that cognitive inflexibility may be associated with disruptions in baseline and/or task-evoked oscillations in the PFC.

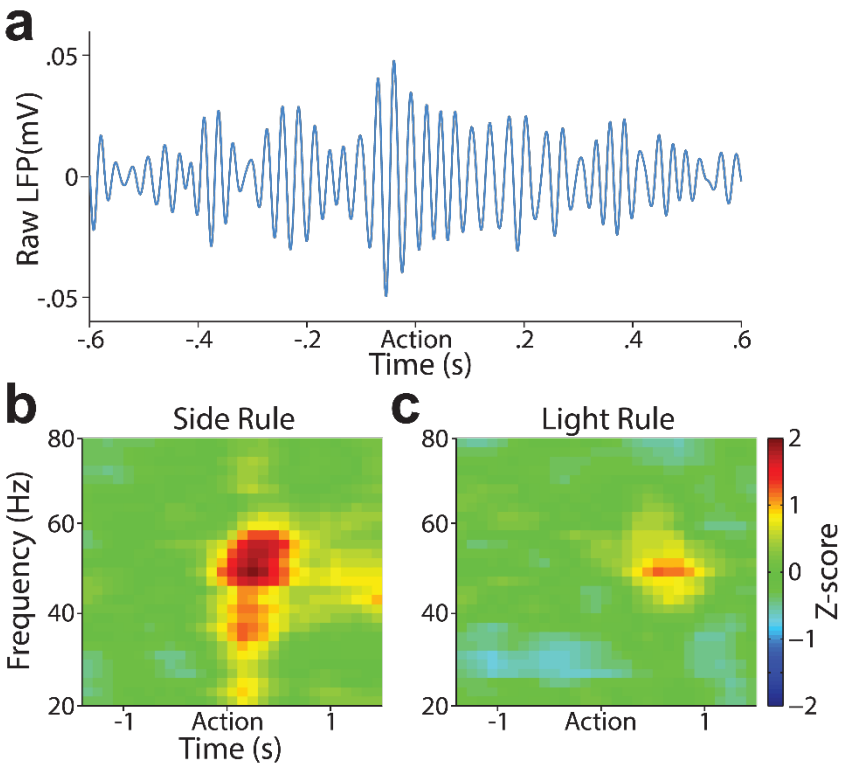


**Figure 1-5 A rule-based behavior is accompanied by an increase in prefrontal gamma oscillations specifically at the time of the action.**

(a) An example mPFC local field potential trace recorded from rats performing the extra-dimensional set-shifting task described in Figure 1-2b. This example trace shows enhanced gamma oscillatory power in the 30 to 60 Hz band, specifically at the peri-action window. (b-c) The z-score normalized power spectral densities show that the peri-action gamma oscillations were discriminative of the task rule, as a much more pronounced increase in gamma power was observed in side-rule than light-rule trials.

## 1.2 THE ROLE OF THE VTA-PFC NEURAL CIRCUIT IN COGNITIVE CONTROL OF BEHAVIOR

In the previous section, we reviewed the literature supporting the idea that the PFC plays a central role in flexible cognitive control of goal-directed behavior. Mesencephalic dopamine (DA) projections from the ventral tegmental area (VTA) exert an important neuromodulatory control over a wide variety of cognitive functioning in the mammalian PFC. Even in invertebrate nervous systems – e.g., *Drosophila* – different types of dopamine neurons subserve distinct roles in writing and updating appetitive or aversive memories, demonstrating the evolutionarily profound role of the DA system in cognition (Aso and Rubin, 2016). Here, we discuss the role of dopaminergic neuromodulation in PFC neural processing of cognitive functions.

As discussed in the previous section, the PFC exerts top-down control of behavior to achieve goals via actions appropriate to a given environment. To estimate the most appropriate action at the moment, it is critical to represent the possible outcomes associated with each action. These action-outcome associations are learned through experiences that reinforce associations among stimuli (or contexts), actions and outcomes that successfully lead to a goal state (i.e., reward), while weakening the unsuccessful ones. Reinforcement learning theories suggest that such learning requires a 'teaching signal' that selectively reinforces successful associations, while degrading ineffective ones (Mackintosh, 1975; Pearce and Hall, 1980; Rescorla and Wagner, 1972; Sutton and Barto, 1998). Mesencephalic dopamine neurons are thought to subserve this role by signaling 'reward prediction errors (RPE)'. The reward prediction error is simply the discrepancy between expected rewards and received rewards; for instance, a positive RPE is generated (and DA neurons increase their firing) when an animal receives an unexpected reward. Importantly, DA neurons no longer respond to the reward per se if it is predicted by

experience; instead they will respond to the earliest predictor of the reward – i.e., preceding action or stimulus. Conversely, if an expected reward is omitted or a smaller reward is provided, a negative RPE is generated and DA neuronal firing is depressed. These positive and negative RPE signals are thought to provide a teaching signal by strengthening or weakening the synapses that are associated with reward or no reward, respectively. This simple rule turns out to be highly powerful in promoting adaptive action selection and decision making even within a complex task structure.

In addition to value-based RPE signaling, DA neurons also encode other environmental features that are not intrinsically rewarding, but are relevant for cognitive control of behavior. Many DA neurons respond to a salient sensory stimulus (or context) in a value-free manner. For example, exposure to a novel stimulus (or "novelty salience") can activate DA neurons. This fast response to novelty is thought to promote attention toward the stimulus, thereby providing an opportunity to detect a potential reward association (Bromberg-Martin et al., 2010; Redgrave and Gurney, 2006; Schultz, 2016). Further, a subpopulation of DA neurons responds to stimuli with high motivational/emotional salience of either valence – including aversive events or punishment – or even to stimuli that are simply physically salient. Importantly, such a response pattern is distinct from RPE coding: in contrast to RPE-coding neurons, these salience-coding neurons treat reward and punishment similarly responding with firing rate changes in the same direction. Novel and aversive events are as important as rewarding events in cognitive control of behavior: they enable detection of cues of high potential importance and avoidance of unpleasant events. Likewise, the salience-signaling DA neurons are thought to play a crucial role in triggering attention and cognitive processing of novel and punishing events, thereby contributing to achieving goal states in a complex environment.

Thus far we have discussed the idea that DA neurons convey two indispensable signals – value-based RPE coding and salience coding – that are critical for cognitive control of goal-directed behavior. Numerous studies have tested the notion that DA transmission in downstream frontal and striatal structures are critical for cognitive processing required for adaptive behavioral control. For example, some studies use variants of the delayed response task, in which the ability to actively maintain an association among stimuli, actions and outcomes – i.e., working memory – is critical to guide action or decision. The effects of systemic or local manipulation of DA transmission in this task have been tested in monkeys and rats. In a seminal study, Brozoski et al (1979) found that the local depletion of DA in dorsolateral PFC (dlPFC) impaired a delayed alteration task performance in monkeys. Similar results were found in rodent studies. Likewise, clinical studies showed that working memory deficits are present in Parkinsonian patients with degeneration of DA neurons (Gotham et al., 1988; Levin et al., 1989).

Meanwhile, neurophysiological studies have revealed that PFC neurons show persistent activation during the delay period in a working memory task, which is thought to be a neural substrate of mnemonic representation (Funahashi et al., 1989, 1990; Fuster and Alexander, 1971; Kubota and Niki, 1971). Studies suggest that DA neurotransmission in PFC provides a "fine-tuning" of neuronal delay-period activity, in that pharmacological manipulation of D1 receptors generates a characteristic "inverted-U" shaped dose response. In other words, either "too little" or "too much" DA exerts detrimental effects on PFC neuronal mnemonic processing as well as behavioral working memory performance (Vijayraghavan et al., 2007; Williams and Goldman-Rakic, 1995). These findings suggest that DA transmission adjusts PFC neuronal cognitive processing such that an optimal range of DA-mediated neuromodulation is required for effective cognitive coding.

Tasks assessing cognitive flexibility require integrated functioning of prefrontal and striatal regions. Human and animal studies have revealed that dopamine and other neuromodulators play critical roles in frontostriatal cognitive functioning underlying behavioral flexibility. One simple form of flexibility is extinction learning, in which a learned association between a stimulus/action and an outcome (S-O or A-O relationship) is extinguished due to changes in the outcome contingency. Psychopharmacological studies have shown that extinction of an appetitive or aversive S-O and A-O association requires dopaminergic neuromodulation in the PFC (Mueller et al., 2010; van der Meulen et al., 2007).

Another commonly studied form of cognitive flexibility is reversal learning. Reversal learning requires the ability to switch responding to a previously non-reinforced stimulus while simultaneously withdrawing from responding to an outdated cue. Unlike extra-dimensional set-shifting, reversal learning paradigms require rule-switching within the same stimulus dimension: i.e., use the same basic principle, but respond to a different stimulus. Reversal shifts comprise dual problems: inhibiting response to an outdated cue, while promoting response to a newly effective cue. This bidirectional modulation of the two competing associations can be framed within reinforcement learning theory in that positive and negative prediction errors may provide the teaching signal for reversal. Lesions or pharmacological manipulations of the orbital PFC (OFC) and medial striatum resulted in deficits in reversal shifts that were associated with disruptions in positive and negative reinforcement processes (Clarke et al., 2008; Kehagia et al., 2010; van der Meulen et al., 2007). Impaired reversal in association with the reinforcement process suggest disruptions in DA neuronal activity and DA neuromodulation in frontostriatal functioning. Correspondingly, a reversal shift enhances DA concentration in the rat mPFC, especially in the early but not the late phase of the reversal in which the prediction error

signaling is thought to be more pronounced (van der Meulen et al., 2007). Further, human neuroimaging studies have demonstrated a linkage between abnormal DA neuromodulation and impairments in the reversal related OFC neural activation as well as reversal behavior (Cohen et al., 2007; Jocham et al., 2009).

In the natural environment, animals confront even more convoluted tasks requiring shifts between strategies and rules based on distinct perceptual dimensions, such that attention needs to be focused on distinct aspects of the complex environment. This phenomenon referred to as extradimensional or attentional set-shifting may involve switching between different types of strategies that depend on sensory cues vs an internal representation of space. Extradimensional set-shifting involves a multitude of cognitive constructs involving the DA neuronal teaching signal. First, shifting between strategies must be guided by the outcome (feedback) of each action – i.e., delivery or omission of reward – which may be provided by VTA DA neuronal positive and negative prediction error signaling. Second, attention to a novel aspect of environmental context may require DA neuronal encoding of motivational and/or novelty salience.

Collectively, the literature suggests that DA neuromodulation in PFC might play a critical role in extradimensional set-shifting. In support of this, using in vivo microdialysis Stefani and Moghaddam (2006) showed that PFC DA concentration increases during learning of the initial rule and rule shifting. Importantly, the authors did not observe this DA increase in yoked control animals that experienced a similar amount of reward randomly provided regardless of animals' choice, demonstrating that PFC DA levels are specifically sensitive to rule learning and shifting. Likewise, psychopharmacological studies have revealed that dopaminergic neuromodulation

facilitates attentional set-shifting; for example, blockade of mPFC D1 receptors induced severe perseverative errors (Ragozzino, 2002).

Some important distinctions have been suggested between the role of PFC DA neuromodulation in working memory vs extradimensional set-shifting. First, unlike the lack of effects observed on working memory, D2 receptor blockade resulted in poor set-shifting performance (Floresco et al., 2006). Secondly, stimulating D1 receptor activity did not impact set-shifting performance, in contrast to the inverted U-shaped relationship observed in working memory. Furthermore, D4 receptor activity blockade or stimulation resulted in impaired or enhanced set-shifting performance, respectively. Collectively, these data illustrate that DA-mediated neuromodulation is critical for the fine-tuning of PFC neural activity that enables PFC-dependent cognitive functioning such as working memory and cognitive flexibility. Likewise, disruptions in PFC and mesoprefrontal neural processing may underlie anxiety-related changes in cognitive control of behavior. In the next section, we discuss evidence for the sensitivity of the mesoprefrontal neural circuit to stressful and anxiogenic situations.

## 1.3 IMPACT OF ANXIETY ON FLEXIBLE COGNITIVE CONTROL OF BEHAVIOR

Numerous human and animal studies have demonstrated anxiety-related deficits in flexible cognitive control of goal-directed behavior such as cognitive and emotional perseveration and biases in decision-making. Here, we review some of these important studies, and discuss the current state of the field, as well as remaining questions that motivated my dissertation study.

### 1.3.1 Human studies

Human behavioral and neuroimaging studies have investigated the impact of anxiety on decision-making in healthy individuals and in patients with clinical anxiety (Hartley and Phelps, 2012). For example, Bishop et al. have shown that PFC recruitment during attentional control over conflict elicited by distractors is reduced in individuals with high trait anxiety in correlation with impaired cognitive task performance (Bishop et al., 2004; Bishop, 2009). In addition, a series of human neuroimaging studies have used fear conditioning and extinction paradigms to model perseverative conditioned fear responses – i.e., "emotional perseveration" – revealing PFC involvement (Phelps et al., 2004; Pitman et al., 2012; Shin et al., 2001). In these studies, a neutral conditioned stimulus (CS) is paired with an aversive outcome (i.e., mild shock) during the conditioning session. This is then followed by an extinction session during which the CS is repeatedly presented without the aversive outcome. fMRI results show that successful extinction is correlated with increased activation of the ventromedial PFC (vmPFC) but reduced activation of the amygdala (for a review, see Pitman et al., 2012). This bidirectional modulation of the vmPFC-amygdala circuitry is impaired in PTSD patients with perseverative conditioned fear responses even after extinction (Phelps et al., 2004; Pitman et al., 2012; Rauch et al., 2006). Related neuroimaging studies have reported dysregulated prefrontal control of subcortical neural activity in a population genetically vulnerable to developing anxiety disorders (Bertolino et al., 2005; Hariri et al., 2005; Hariri et al., 2003; Hariri et al., 2002; Meyer-Lindenberg et al., 2006; Pezawas et al., 2005).

Collectively, human studies suggest that anxiety biases information processing during flexible behavior. This can be manifested in at least two ways. First, anxiety biases attention to threat-related stimuli. This is measured as a faster response time detecting threat-related stimuli

and as increased distractibility by these stimuli at the expense of attention to task-relevant stimuli (Bar-Haim et al., 2007; Cisler and Koster, 2010; Mogg and Bradley, 1998). Likewise, anxiety also results in heightened distractibility by non-threatening stimuli, as suggested by poor concentration and reduced multi-tasking capability in anxious individuals (Eysenck et al., 2007; Mineka et al., 1998). Second, anxious individuals favor negative interpretations of neutral or ambiguous stimuli. When presented with emotionally ambiguous stimuli, such as facial expressions or face-voice pairings, anxious individuals disproportionately interpret these stimuli as possessing negative valence (Koizumi et al., 2011; Richards et al., 2002). Anxiety also is associated with increased expectation of negative outcomes in decision making involving risk or ambiguity in the action-outcome relationship. On a variety of choice tasks, anxious individuals show heightened risk aversion and favor safe alternatives (Anderson et al., 2012; Hartley and Phelps, 2012; Maner et al., 2012; Raghunathan and Pham, 1999).

These anxiety-related behavioral biases most likely involve PFC-mediated cognitive processing. Notably, there is an association between disrupted PFC neural activity and anxiety-related behavioral phenotypes, such as impulsivity and risk-aversion in healthy individuals, although the association needs to be further examined in patients with clinical anxiety (Giorgetta et al., 2012; Knoch et al., 2006; Li et al., 2009; Perugi et al., 2011). In addition, studies of blood oxygenation level dependent (BOLD) signals during risk-based decision-making tasks, which may be associated with increased anxiety, show reduced activity in PFC subregions in contrast to increased activity in subcortical regions such as the amygdala and the ventral striatum (Christopoulos et al., 2009; Clark et al., 2008; Fecteau et al., 2007; Knoch et al., 2006). Along the same lines, economic decision-making studies show that BOLD activity in the dorsolateral PFC is enhanced when the subject chooses the larger but more delayed reward during

intertemporal choices, whereas an impulsive choice was associated with decreased BOLD signal (Kim and Lee, 2011; McClure et al., 2004). Collectively, these data suggest that dysregulated prefrontal control of subcortical neural activity may be associated with anxiety-related behavioral biases such as risk-aversion and/or impulsive decision-making.

### 1.3.2 Animal studies: Current state of the field

Numerous studies have focused on PFC individual neuronal representations of fear and anxiety (Baeg et al., 2001; Burgos-Robles et al., 2009; Davis, 2006; Milad and Quirk, 2002; Morgan and LeDoux, 1995; Quirk and Beer, 2006). Findings from these studies have been corroborated by recent research that has further dissected the functional neuroanatomy of fear using various techniques of circuit manipulation, such as optogenetics (for a review, see Calhoon and Tye, 2015). These studies have confirmed that highly interlinked neural structures comprising the amygdala, the bed nucleus of the stria terminalis, the ventral hippocampus and the mPFC represent information about threats, defensive behavior, and constructs relevant to anxiety (Adhikari et al., 2010; Duvarci and Pare, 2014; Felix-Ortiz et al., 2013; Herry et al., 2008; Kim et al., 2013; Lesting et al., 2011; Likhtik et al., 2014; Namburi et al., 2015). In PFC, subpopulations of neurons respond preferentially to a conditioned stimulus associated with an aversive event, tracking alterations in the CS-US association – e.g. extinction (Baeg et al., 2001; Burgos-Robles et al., 2009; Courtin et al., 2014; Milad and Quirk, 2002). Moreover, the PFC interacts with other regions such as the amygdala and the ventral and dorsal hippocampus via pair-wise neuronal correlations and neural synchrony – particularly theta oscillations – to regulate conditioned fear responses and explorative behavior in anxiogenic environments such as

the open field test and the elevated plus maze test (Adhikari et al., 2010; Karalis et al., 2016a; Kumar et al., 2014; Lesting et al., 2011; Likhtik et al., 2014; Livneh and Paz, 2012).

While these studies have provided key information about how the PFC represents fear or anxiety *per se*, little is known about how anxiety affects PFC processing of cognitively relevant behavior. This includes a near-total lack of neurophysiological studies that have investigated the impact of anxiety on PFC neural correlates of cognitive flexibility. To this end, an important prerequisite for these studies is an appropriate experimental model of anxiety that mimics the physiological and behavioral phenotypes of anxiety while allowing animals to perform cognitive tasks. Fear conditioning paradigms are limited in two ways for this purpose: first, animals' fearful responses (freezing and/or avoidance) disrupt cognitive task performance. Second, a fearful state elicited by an imminent and concrete threat might be dissimilar to an anxious state, which is a temporally diffuse state often not associated with a specific event, and which may even be internally generated (Sylvers et al., 2011). Behavioral tests of anxiety based on explorative behavior – e.g. the open-field test and the elevated plus maze test – also are limited due to the lack of cognitive behavioral constructs in these assays.

In order to investigate the impact of anxiety on cognitive processing, experimental models that produce a sustained state of anxiety while allowing for cognitive task performance need to be designed and implemented. Only by using such models can we unravel anxiety-induced changes in cognitive flexibility at individual neuronal and neural population levels in the PFC on multiple timescales. Therefore, my dissertation study utilized experimental designs that combine an animal model of anxiety and performance of a well-characterized goal-directed behavior with simultaneous electrophysiological monitoring of VTA and mPFC neural activity.

## 1.4 SENSITIVITY OF THE MESOPREFRONTAL NEURAL CIRCUIT TO AVERSION AND ANXIETY

In the current section, we review evidence suggesting that the mesoprefrontal (VTA-mPFC) neural circuit preferentially responds to aversive, stressful and anxiogenic behavioral states. In this regard, the role of the dopaminergic projection to the mPFC has been extensively studied. We begin by reviewing classic and recent works suggesting that the VTA DA projection to mPFC comprises a specific subpopulation of DA neurons tuned for aversive stimuli. Then we briefly discuss evidence demonstrating the roles of VTA non-DA neurons and reciprocal mPFC-to-VTA projections in representing aversive states.

Classic works have suggested that DA neurons generate characteristic phasic excitation to reward and reward-predicting stimuli (Schultz, 1997; Ungless et al., 2004). Extensive recording studies have suggested that the DA neuronal reward response profile was associated with signaling the temporal reward prediction error (RPE): i.e., the difference in value between a received reward and a predicted reward at each moment in time (for a review, see Schultz, 2016).

In addition to robust evidence in support of the RPE hypothesis, numerous studies have shown that subpopulations of DA neurons are activated by non-rewarding and even aversive events. Indeed, it is well established that aversive, stressful and anxiogenic events can activate midbrain DA neurons and enhance DA release in target regions (Abercrombie et al., 1989; Bradberry et al., 1991b; Brischoux et al., 2009; Butts et al., 2011; Guarraci and Kapp, 1999; Murphy et al., 1996b; Ungless et al., 2010; Young, 2004). Recent recording studies targeted pharmacologically or optogenetically labeled DA neurons, and found that equivalent proportions of them exhibited excitatory or inhibitory responses to aversive stimuli (Cohen et al., 2012; Zweifel et al., 2008). Importantly, microdialysis studies found that the mesoprefrontal neural

circuit was preferentially activated by stressful and anxiogenic manipulations as evidenced by greater increase in DA release in PFC compared to other target structures such as the striatum (Abercrombie et al., 1989; Bradberry et al., 1991a; Moghaddam et al., 1990; Thierry et al., 1976). These results suggested functional and anatomical segregation of the mesoprefrontal circuit from the mesolimbic (VTA-NAc) circuit, such that the two pathways may comprise different DA neuron populations with distinct responses to rewarding vs aversive events.

Likewise, recent recording studies have found that subpopulations of identified VTA DA neurons exhibit 'unconventional' electrophysiological properties, opposing the traditionally used profile for classification of DA neurons (Ikemoto, 2007; Lammel et al., 2008; Margolis et al., 2008). In addition, these unorthodox DA neurons tended to be localized in the medial VTA nuclei, whereas DA neurons with a conventional profile were situated in the lateral VTA and SNc (Lammel et al., 2011). Combining viral tracing and electrophysiology, recent studies have found that distinct VTA DA neuron populations with different physiological and geographical profiles displayed separable input-output connectivity (Lammel et al., 2012). The DA neurons with conventional properties tended to project to the lateral shell of the NAc, and received excitatory input from the laterodorsal tegmentum (LDT). The unconventional DA neurons projected to the mPFC, the medial shell of the NAc, and the amygdala, and received projections from the lateral habenula (LHb).

Importantly, the excitatory input from LDT generates phasic bursting in the 'conventional' DA neurons that in turn project to the lateral shell of the NAc, which plays an important role in reward-mediated reinforcement process (Forster and Blaha, 2000; Lodge and Grace, 2006) (Figure 1-1). On the other hand, LHb neurons are activated by aversive events and omission of reward (Hikosaka, 2010; Hong et al., 2011). The LHb innervates the DA neurons

that project to the mPFC as well as the GABA neurons in the rostromedial tegmental nucleus (RMTg), which exerts inhibitory control over the DA neurons projecting to the NAc lateral shell (Lammel et al., 2012; Stamatakis and Stuber, 2012) (Figure 1-1). Collectively, these data illustrate parallel circuits involving distinct DA neuron groups with heterogeneous profiles and input-output connectivity, which may be functionally diversified to selectively represent rewarding vs aversive states.

Lammel et al. (2011) provided evidence supporting this parallel circuit notion, first by showing that the excitatory input synapses of the mesoprefrontal and mesolimbic DA neurons were selectively potentiated by aversive vs rewarding stimuli, respectively. Further, the same group optogenetically stimulated the LDT innervated mesolimbic DA neurons or the LHb innervated mesoprefrontal DA neurons, and found that stimulating the two pathways resulted in conditioned place preference vs aversion, respectively (Lammel et al., 2012). Consistent with this, photostimulation of NAc projecting VTA DA neurons resulted in prosocial behavior, whereas stimulation of the VTA DA terminals in mPFC led to antisocial and anxiety-related behaviors (Gunaydin et al., 2014). These results suggest that parallel mesoprefrontal and mesolimbic pathways arise from separable DA neuronal subpopulations with distinct afferent inputs, such that the two pathways are associated with profoundly different behavior.

Approximately 20-40% of VTA cells are GABAergic, comprising most of the non-DA neuronal population in the VTA (Carr and Sesack, 2000a; Nair-Roberts et al., 2008; Swanson, 1982). VTA GABA neurons consist of local inhibitory interneurons innervating neighboring DA neurons and long-range projection neurons that innervate target structures such as the NAc and mPFC (Fields et al., 2007; Omelchenko and Sesack, 2009). The GABAergic projection comprises approximately 58% of all mesoprefrontal neurons in the VTA (Carr and Sesack,

2000a). Recent studies have shown that photostimulation of VTA GABA neurons elicited aversive behavior such as conditioned place aversion, disrupted food consumption, and extinction of appetitive associative memory, which were mediated by inhibition of VTA DA neurons (Pan et al., 2013; Tan et al., 2012; van Zessen et al., 2012). Although the functional significance of the VTA GABA projection to the mPFC remains to be addressed, it is plausible that the VTA GABA neurons may comprise a critical component in the mesoprefrontal representation of aversive behavioral states.

The mPFC sends excitatory projections to the VTA specifically onto the DA neurons projecting back to mPFC, completing the mesoprefrontal 'loop', while the mPFC projection targets VTA GABA neurons projecting to the NAc (Carr and Sesack, 2000a). The mPFC neuronal innervation of mesoprefrontal DA neurons is consistent with electrophysiological data showing that mPFC stimulation produces a short latency response in DA neurons antidromically activated from the PFC (Gariano and Groves, 1988; Thierry et al., 1979). Likewise, neurochemical data show that stimulation of mPFC by local infusion of glutamate agonists increases DA levels within the PFC (Jedema and Moghaddam, 1996). Collectively, these data suggest that the mPFC neuronal subpopulation activated by aversive stimuli may contribute to preferential activation of the mesoprefrontal DA cells in stressful and anxiogenic situations. In a recent study, Ye et al. (2016) used activity-dependent whole brain mapping to show that mPFC neuronal populations projecting to distinct target structures differently responded to rewarding vs aversive experiences. The mPFC axonal projections to LHb and VTA responded to an aversive stimulus to a much greater degree compared to the mPFC-to-NAc projection, which preferentially responded to an appetitive but not to an aversive stimulus (Ye et al., 2016). Taken

together these data suggest that the reciprocal mesoprefrontal circuit plays a vital role in representing aversive behavioral states in stressful and anxiogenic situations.

## 1.5 PURPOSE OF DISSERTATION

This dissertation study addresses the mesoprefrontal (VTA-mPFC) neural basis of the adaptive and maladaptive behavioral impacts of anxiety. As discussed in previous sections, the mesoprefrontal neural circuit plays a critical role in flexible cognitive control of goal-directed behavior (Floresco, 2013). Importantly, the mesoprefrontal circuit exhibits preferential responses to aversive, stressful and anxiogenic stimuli, compared to other circuits within the mesocorticolimbic system (Abercrombie et al., 1989; Bradberry et al., 1991b; Moghaddam et al., 1990). Therefore, investigating how spontaneous and task-related mesoprefrontal neural activity is modulated in association with behavioral changes in anxiety may be the key for understanding the neural basis of behavioral impacts of anxiety.

To this end, we first set out to unravel how the mesoprefrontal neural circuit encodes anticipation of an aversive event – i.e., punishment risk – that induces anxiety-like behavioral changes. Although the general activation of the mesoprefrontal circuit in an aversive state has long been established, it remains to be addressed how individual neurons and ensembles of neurons encode punishment risk and risk-based anxiety-like behavioral changes. Importantly, the lack of simultaneous recording data from mPFC and VTA has hindered 1) valid characterization and comparison between VTA and mPFC neural coding schemes, 2) discovery of interregional neural codes for punishment. To address this, we designed a risky reward-seeking task, in which rats engaged in a simple instrumental action with varying degrees of punishment risk contingent

on the action. We confirmed that punishment risk induced anxiety-like changes in the instrumental behavior, which was reversed by pretreatment with an anxiolytic, diazepam. Using *in vivo* electrophysiology, we recorded single-unit spike activity and local field potentials simultaneously in VTA and mPFC from task-performing animals. Using exhaustive data analyses, we found that the mesoprefrontal circuit utilizes multiple layers of coding schemes to represent punishment and risk-based anxiety-like behavioral modulation at the individual neuronal, neural population, and neural circuit levels.

In a separate set of experiments, we focused on the detrimental aspects of anxiety, since anxiety has been associated with disruptions in PFC-mediated executive functions, such as flexible cognitive control of behavior. We trained animals on a rodent task requiring cognitive flexibility: an extradimensional set-shifting task. The task required rats to select their instrumental action based on two rules involving distinct perceptual dimensions, and to switch between the rules based on the task feedback. Previous studies have suggested that the set-shifting task requires higher-order, hierarchical neural processing in the network of cortical and subcortical structures, with the PFC playing an integrative role. By recording neural activity in animals performing this task, we could examine PFC neuronal encoding of task variables relevant to cognitive set-shifting in a non-anxious state. Then, within the same task context, we applied a clinically substantiated anxiogenic treatment to induce a sustained state of anxiety. It is important to note that the anxiogenic drug (FG7142) we used has been shown to activate the mesoprefrontal neural circuit in association with anxiety-like behavioral changes, including cognitive deficits in rodents, primates, and even in humans (Dorow, 1987; Evans and Lowry, 2007; Murphy et al., 1996b; Ninan et al., 1982). Therefore, we concluded that the pharmacological model of anxiety was appropriate to our purpose of investigating the

mesoprefrontal neural basis of anxiety. Animals performed the set-shifting task under systemic injection of different doses of the anxiogenic drug (FG7142). The impact of anxiety was subtle; however, consistent with human data, behavior was selectively impaired when previously correct conditions were presented as conflicting choices. This impairment was associated with reduced recruitment of mPFC neurons that selectively represented task rules at the time of action. We also examined how the spontaneous activity of PFC neurons was modulated in the sustained state of anxiety, and found that anxiety induced persistent suppression of PFC neuronal spike activity – i.e., hypofrontality.

Collectively, findings from my dissertation study demonstrate that anxiety "hijacks" the mesoprefrontal neural circuit by profoundly modulating spontaneous and task-related neural activity at the individual neuron-, neural population-, and neural circuit levels. Anxiety-induced neural changes in the mesoprefrontal circuit were systematically associated with anxiety-like changes in motivated and cognitive behaviors, providing insights relevant to the therapeutic interventions for the behavioral symptoms of anxiety disorders.

# 2.0 VTA AND PFC NEURAL REPRESENTATION OF THE IMPACT OF PUNISHMENT RISK ON REWARD-SEEKING BEHAVIOR

## 2.1 INTRODUCTION

Avoiding danger and approaching reward are fundamental functions of all nervous system. In a causally and socially complex world, this dual problem often needs to be concurrently resolved, as a reward-seeking behavior may involve risk of an aversive event, i.e., punishment risk, e.g. an animal foraging with risk of encountering a predator. Proper neural representations of punishment risk and accordingly guiding behavior are critical for survival and adaptive behavior. Deficient or exaggerated representation of risk is associated with maladaptive behavioral patterns observed in neuropsychiatric conditions such as addiction or anxiety-related disorders (Bechara et al., 2000; Gillan et al., 2016; Hartley and Phelps, 2012; Lee, 2013; Mineka et al., 1998).

In the present study, we sought to unravel how risk of punishment contingent on reward-seeking behavior is encoded in the neural circuit comprising the midbrain ventral tegmental area (VTA) and the medial prefrontal cortex (mPFC). We focused on the two regions first because they have been implicated in flexible cognitive control of goal-directed behavior (Floresco et al., 2006; Kehagia et al., 2010; Mueller et al., 2010; Popescu et al., 2016; Ragozzino, 2002; Stefani and Moghaddam, 2006). In addition, the VTA and mPFC have long been implicated in signaling aversive behavioral states. The mPFC neurons encode innate and conditioned aversive states to

modulate aversive behavior in concert with diverse cortical and subcortical structures (Adhikari et al., 2010; Karalis et al., 2016b; Kumar et al., 2014; Likhtik et al., 2014; Ye et al., 2016). VTA dopamine (DA) neurons have long been suggested to primarily encode reward-related events such as the reward prediction error (RPE), i.e. discrepancy between expected and actual outcomes (Cohen et al., 2012; Roesch et al., 2007; Schultz, 1998; Wise, 2004). However, mounting evidence suggests that various motivational features of appetitive, aversive and alerting events might be coded by heterogeneous subgroups of VTA DA and non-DA neurons (Bromberg-Martin et al., 2010; Horvitz, 2000; Kim et al., 2010; Matsumoto et al., 2016; Matsumoto and Hikosaka, 2009; Tan et al., 2012; van Zessen et al., 2012). At the neural circuit level, the mPFC and VTA (both DA and non-DA neurons) send reciprocal projections to each other (Berger et al., 1976; Carr and Sesack, 2000a, b). The DA neurons projecting to mPFC has been shown to preferentially respond to stressful and anxiogenic perturbations even to mild ones that scarcely affect the mesolimbic or mesostriatal DA transmission (Abercrombie et al., 1989; Bradberry et al., 1991a; Moghaddam et al., 1990; Thierry et al., 1976). In line with this, the VTA DA neurons projecting to the mPFC receive preferential input from the lateral habenula (LHb) neurons that are selectively tuned to aversion and omission of reward (Lammel et al., 2012). Further, photostimulation of the VTA dopaminergic input to the mPFC elicited anxiety-like behavior (Gunaydin et al., 2014; Lammel et al., 2012), suggesting a more causal role of this neural circuit in aversive behavior. Together these suggest that the VTA and mPFC may play a key role in representation of punishment risk contingent on a reward-seeking action and risk-based modulation of the action. However, the lack of simultaneous recording data from the two regions in reward-seeking animals with risk of punishment has hindered 1) valid characterization

and comparison of the VTA and mPFC coding schemes, and 2) discovery of interregional neural codes, for punishment risk and risk-based modulation of appetitive behavior.

Here we recorded single unit and local field potential (LFP) signals from rats performing a risky reward-seeking task, wherein an instrumental action constantly procured a reward but probabilistically led to punishment with varying degrees of risk. Our data show that the majority of VTA and mPFC neurons encode punishment risk and risk-based behavioral modulation. Accordingly, punishment risk could be accurately decoded from the activity of both VTA and mPFC neuronal populations. Furthermore, the neuronal population activity even tracked the risk-based trial-to-trial behavioral variation, demonstrating a solid link between aversive behavior and neuronal population activity in the presence of punishment risk. At the neural circuit level, we found that coherent theta oscillations synchronized the VTA and mPFC in a bottom-up direction, effectively phase-modulating the neuronal spike activity in the two regions during the risk-free actions. This oscillation-mediated neural synchrony declined as a function of risk, suggesting that the asynchrony between the two regions may signal risk of punishment contingent on the reward-seeking action. Taken together, these results demonstrate multiple layers of VTA-mPFC coding schemes for punishment risk at the single neuronal-, neuronal population- and circuit-levels.

## 2.2 METHODS

### 2.2.1 Subjects and surgical procedure

Male Long Evans rats weighing 300~400 g (Harlan) were singly housed on a 12 h light/dark cycle (lights on at 7 p.m.). All data were collected during the dark cycle. Microelectrode arrays were surgically implanted in ipsilateral mPFC and VTA (N = 10) or bilateral mPFC (N = 4) of isoflurane-anesthetized rats (Figure 2-3a). All mPFC electrode arrays were placed in the prelimbic subregion of the mPFC. The following coordinates relative to the bregma were used: mPFC = AP +3.0 mm, ML 0.7 mm, DV 4.0 mm; VTA = AP -5.3 mm, ML 0.8 mm, DV 8.2 mm (Paxinos and Watson, 1998). Behavioral training began after 1 week of postsurgical recovery. At the completion of all recordings, rats were anesthetized with 400 mg/kg chloral hydrate and perfused with saline and 10 % buffered formalin. Coronal brain slices of mPFC and VTA were collected and cresyl-violet stained. Placements of electrode arrays were verified under a light microscope. All procedures were in accordance with the National Institute of Health's Guide to the Care and Use of Laboratory Animals, and were approved by the University of Pittsburgh Institutional Animal Care and Use Committee.

### 2.2.2 Risky reward-seeking task

After the postsurgical recovery, rats were kept at 85 % of their free-feeding weight on a restricted diet of 13 g food pellets a day with free access to water. In an operant chamber, rats were fully trained to make an instrumental nose poke to the cue port to receive a sugar pellet at the food trough located in the opposite side of the chamber on the fixed ratio schedule of one,

namely FR1 (Figure 2-1a-b). After completion of three FR1 sessions consisting of 150 trials in 60 mins, rats were trained with the risky reward-seeking task consisting of three blocks, each containing 50 trials. Each block was assigned a punishment risk – 0, 0.06, or 0.1, i.e. the conditional probability of receiving an electric foot shock (0.3 mA, 300 ms) given an action. The action–reward contingency was kept at 1 across all training and recording sessions, i.e. every nose poke led to a reward delivery even in the shock trials, so there was no reward risk in our task. To minimize generalization of risk across blocks, they were organized in an ascending shock probability order – Block1: 0, Block2: 0.06, Block3: 0.1, and interleaved with 2-min timeout. In block 2 and 3 of each session, 3 and 5 trials were pseudo-randomly selected and followed by an electric foot shock. No explicit cue was provided on shock trials to keep the shock occurrence unpredictable (the cue onset only signaled initiation of a trial). Animals were informed of the block shift and risk increase by the 2-min darkened timeout in between blocks. In addition, the first shock trial of block 2 and the first two shock trials of block 3 were randomly selected from the initial 5 trials of each block. Also, animals completed two complete sessions of the risky reward-seeking task before the recording session, thus the shock occurrence and the task design including the ascending punishment risk were not novel to them at the time of the recording session. All training and recording sessions were terminated if not completed in 180 mins, and data from the completed sessions only were analyzed. Animals displayed stable behavioral performance overall without any sign of contextual fear conditioning as they performed fearless in the safe block across all sessions. In addition, there was no evidence for habituation to the shock as they showed equivalent risk-based behavioral changes across sessions. For the diazepam pretreatment experiment, a separate group of rats (N = 9) were trained using abovementioned procedure, and they underwent three test sessions with

intraperitoneal pretreatment of saline – diazepam (2 mg/kg, Hospira, Inc.) – saline. Injected animals were returned to their homecage for 10 minutes before they were placed in the operant chamber. Three days of washout period was allowed between sessions.

### 2.2.3 Electrophysiology

Single-unit activity and local field potentials (LFPs) were recorded simultaneously via a pair of eight channel Teflon-insulated stainless steel 50 μm microwire arrays (NB Laboratories). Unity-gain junction field effect transistor headstages were attached to a headstage cable and a motorized commutator nonrestrictive to the animals' movement. Signals were amplified via a multichannel amplifier (Plexon). Spikes were bandpass filtered between 220 Hz and 6 kHz, amplified ×500, and digitized at 40 kHz. Single-unit activity was then digitally high-pass filtered at 300 Hz and LFP were low-pass filtered at 125 Hz. Continuous single-unit and LFP signals were stored for offline analysis. Single units were sorted using the Offline Sorter software (Plexon). Only the single-units with a stable waveform throughout the recording session were further analyzed. If a unit presented a peak of activity at the time of the reference unit's firing in the cross-correlogram, only either of the two was further analyzed.

### 2.2.4 Neural data analysis

Single unit and LFP data analyses were conducted with Matlab (MathWorks) and SPSS statistical software (IBM). For single unit data analyses, 1-ms binned spike count matrix of the peri-cue, action, and reward periods (starting 2 s before each event and ending 2 s after each

event) were produced for each unit. The baseline period was a 2-s time window beginning 2.5 s before the trial onset.

#### 2.2.4.1 Trial-averaged firing-rate analysis

Spike count matrices were further binned using a 200 ms rectangular moving window with steps of 50 ms within the -2 to 2 s epoch aligned to the task event occurring at time = 0 for the firing rate analysis. Binned spike counts were transformed to firing rates and averaged across trials. The trial-averaged firing rate of each unit was Z-score normalized using the mean and standard deviation of its baseline firing rate.

#### 2.2.4.2 VTA cell classification

The VTA single units were classified into putative dopamine (DA) or non-dopamine (non-DA) neurons based on two criteria. First, units whose mean baseline firing rate slower than 12 Hz, waveform width greater than 1.2 ms were considered as potential DA units (Grace and Bunney, 1984; Kim et al., 2015; Schultz and Romo, 1987). This traditional classification, however, has been suggested to be potentially inaccurate (Margolis et al., 2006). Thus, the second criterion utilized the neuronal reward response properties for the putative DA and non-DA cell identification. Receiver-operating characteristic (ROC) curves were calculated by comparing the distribution of firing rates across trials in 100 ms bins (starting 0.5 s before reward delivery and ending 1 s after reward delivery) to the distribution of baseline firing rates (starting 2.5 s before the trial onset and ending 0.5 s before the trial onset). Principal component analysis was conducted using the singular value decomposition of the area under the ROC (auROC). Units were mapped in the 3-d space consisting of the top three principal components. Within the 3-d PC space, unsupervised clustering was conducted by fitting Gaussian mixture models using

the expectation-maximization algorithm. This method found two clusters: one with phasic excitation to reward (Type 1), one with sustained excitation or suppression to reward (Type 2) (Figure 2-4c-e). Units in the former class were classified as putative DA units, as previous studies have shown that optogenetically tagged DA neurons displayed similar phasic excitatory reward responses (Cohen et al., 2012; Eshel et al., 2015). Taken together, we defined a VTA unit satisfying both criteria as a putative DA unit and a unit that met either or none of the criteria as a putative non-DA unit (Figure 2-4). mPFC units were not classified based on their firing and spike-waveform properties. Only 2 out of the total 293 mPFC single units had the mean baseline firing rates higher than 20 Hz, thus few fast-spiking interneurons should be included in our data analysis.

#### 2.2.4.3 Spike rate selectivity

To quantify single neuronal encoding of blockwise punishment risk, we computed a bias-corrected percent explained variance (ωPEV) statistic with binned spike counts calculated in a 200 ms rectangular window moving with steps of 50 ms within the 2-s peri-event epochs (-1 to 1 s with an event occurring at time = 0).

$$\omega\text{PEV} = \frac{SS_{Blocks} - df_{Blocks}MS_{Error}}{SS_{Total} + MS_{Error}}$$

where $SS_{Blocks}$ and $SS_{Total}$ are the between-blocks (punishment risk) and total sums of squares, $df_{Blocks}$ is the blocks degrees of freedom, and $MS_{Error}$ is the mean squared error. This formulation resulted in an unbiased metric with an expected value of zero when there is no difference across blocks (Buschman et al., 2012; Keren, 1979). A unit was determined to encode punishment risk if its peri-event ωPEV surpassed 'the global ωPEV band', which was defined as the upper bound of the 99 % confidence interval of the trial-shuffled (1,000 times) surrogate ωPEV distribution,

i.e., fewer than 1 % of the trial-shuffled ωPEVs crossed the global band across all time bins in the peri-event epoch ($\alpha = 0.01$). To find the global ωPEV band, we computed the mean and standard deviation of the trial-shuffled ωPEV distribution. By stepping up from the mean by one-hundredth of the standard deviation, we found the pointwise band at each time bin and the global band across time bins both at $\alpha = 0.01$ (Figure 2-5). This approach effectively resolves the issue of multiple comparisons that can arise as statistical comparisons made separately across multiple time bins increase the rate of false rejection of the null hypothesis (Fujisawa et al., 2008). We repeated this analysis using the mutual information metric, and found that the two metrics yielded similar results.

#### 2.2.4.4 Linear regression analysis

For a standardized quantification of the individual neuronal encoding of punishment risk in peri-event epochs, we computed the standardized regression coefficient of the following linear regression model for each unit:

$$SC = \beta_{risk} x + \varepsilon$$

where SC denotes binned spike counts calculated in a 200 ms moving window with steps of 50 ms, $\beta_{risk}$ regression coefficients for the independent variable, blockwise punishment risk (1, shock prob. = 0; 2, shock prob. = 0.06; 3, shock prob. = 0.1), respectively. The regression coefficients were standardized by $\beta \times (S_x/S_y)$, where $S_x$, $S_y$ denote the standard deviations of independent and dependent variables, respectively.

#### 2.2.4.5 Population decoding analysis

The population-level encoding of punishment risk was quantified using the Poisson naïve Bayes classifier. In general, a decoding method works by training the classifier to 'learn' which

patterns of neuronal activity are indicative of particular task conditions. In the training phase, the association of different patterns of neuronal activity with different task conditions is learned from a subset of data (training set). In the test phase, the reliability of the association is assessed with a separate set of data (test set) based on how accurately the classifier can predict the present task conditions from the neuronal activity. For training and testing, we used a cross-validation procedure with the following steps. (1) For each unit, data from 50 trials of each risk block were taken in 200-ms window sliding in steps of 50 ms within the 4-s peri-cue and action epochs. For each of these trials, data from all units were concatenated to create a pseudo-population response vector (i.e., units that were recorded under the same conditions but in separate sessions were treated as if they had been recorded simultaneously). (2) These pseudo-population vectors are grouped into 5 splits of the sampled data, with each split containing 10 pseudo-population response vector of each risk block. (3) A classifier was trained using 4 splits of the data, and tested with the remaining split. This procedure was repeated 20 times, leaving a different split at each time (i.e., a 5-fold leave-one-split-out cross-validation was used).

Specifically, in each repetition, we have a Poisson likelihood function given by

$$P(\underline{x}_t|C_k) = \prod_{i=1}^{D} \frac{\lambda_{ki,t}^{x_{i,t}} e^{-\lambda_{ki,t}}}{x_{i,t}!}$$

where $\underline{x}_t$ is a pseudo-population vector of spike counts at $t^{th}$ sliding window within a trial, $C_k$ indicates block ID with varying risk, and thus $k$ takes on 1, 2 or 3. $i$ indicates unit label, 1 to $D$. $\lambda_{ki,t}$ is the parameter for the Poisson distribution estimated by the following.

$$\lambda_{ki,t} = \frac{1}{N_k} \sum_{n \in C_k} x_{ni,t}$$

The posterior probability for a particular risk given the spike count vector is provided by Bayes' theorem:

$$P(C_k|\underline{x}_t) = \frac{P(\underline{x}_t|C_k)P(C_k)}{P(\underline{x}_t)}$$

We have a flat prior probability, and thus $P(C_k)$ is a constant. Hence, the classifier predicts the current risk with maximum probability given the pseudo-population activity.

$$\widehat{C_k} = argmax_k P(\underline{x}_t|C_k)$$

This procedure (steps 1-3) was repeated 50 times repeatedly resampling matching numbers of units from each region (n = 100) to for a valid interregional comparison of the decoding accuracy.

#### 2.2.4.6 Gaussian-process factor analysis (GPFA)

GPFA extracts a smooth low-dimensional neural trajectory from simultaneously recorded neuronal time series data (binned spike counts). GPFA performs smoothing and dimensionality reduction in a common probabilistic framework. The GPFA model simply consists of a set of factor analyzers, one at each time bin, that are linked together in the low-dimensional state space by a Gaussian process. We provide a simple mathematical description of GPFA below. Yu et al. (2009) provides a thorough analytical and practical discussion of the GPFA model. Let $y_{:,t} \in \mathbb{R}^{q\times 1}$ be the high-dimensional vector of square-rooted spike counts recorded at time point *t = 1, . . . , T*, where $q$ is the number of simultaneously recorded single units. We extract a corresponding low-dimensional latent *neural state* $x_{:,t} \in \mathbb{R}^{p\times 1}$, at each time point, where $p$ is the dimensionality of the neural state space ($p < q$). We define a linear-Gaussian relationship between $y_{:,t}$ and $x_{:,t}$.

$$y_{:,t}|x_{:,t} \sim \mathcal{N}(Cx_{:,t} + d, R)$$

where $C \in \mathbb{R}^{q \times p}$, $d \in \mathbb{R}^{q \times 1}$, and $R \in \mathbb{R}^{q \times q}$ are model parameters to be fitted. The neural states $x_{:,t}$at different time points are linked through Gaussian processes. A separate GP is defined for each dimension of the neural state space indexed by *i = 1, . . . , p*

$$x_{i,:} \sim \mathcal{N}(0, K_i)$$

where $x \in \mathbb{R}^{1 \times T}$is the $i^{th}$ row of $x_{:,t=1,\ldots,T}$ and $K_i \in \mathbb{R}^{T \times T}$ is the covariance matrix for $i^{th}$ GP. The parameters of the GPFA model above were fitted using the expectation-maximization algorithm, which finds the model parameters that maximize the probability of the observed data. Using the learned GPFA model, we extract neural trajectories $\mathrm{E}[x_{:,:}|y_{:,:}]$ from the observed data. These low-dimensional neural trajectories can be related to the high-dimensional observed activity using the GPFA model above, which defines a linear mapping $C$ between the two spaces. Each column of $C$ defines an axis in the high-dimensional space, and the $i^{th}$ element in $x_{:,t}$specifies the location along each axis. Columns of $C$ were orthonormalized for a "PCA-like" visualization, and the neural trajectories were plotted in the orthonormalized low-dimensional space. The dimensionality was determined based on the distribution of cross-validated data likelihoods across different dimensionalities. We found that data likelihoods peaked or plateaued around the dimensionality of five in all neural populations, thus 5D was used across all populations for better comparability. We also tested other dimensionalities, and found that similar behavioral and neural correlations held at different dimensionalities. GPFA model fitting and extraction of population neural trajectories were implemented using the open-source GPFA matlab code package (Yu et al., 2009).

#### 2.2.4.7 LFP power spectra and coherence

The local field potential (LFP) power spectral densities were quantified using the chronux routine mtspecgramc (Bokil et al., 2010). Briefly, the LFP time series within the peri-event epochs were Fourier transformed in a 500 ms moving window with steps of 50 ms with the multi-taper method applied:

$$S = \frac{1}{K}\sum_{k=1}^{K}\left|\int_0^T u_k(t)x(t)e^{-2\pi i f t}\,dt\right|^2$$

where $u_k(t)$ is the multi-tapers (9 tapers were used), $x(t)$ is the LFP time series in a moving window. The baseline normalized power spectra (Z-score) were calculated using the mean and standard deviation of the baseline power spectra across trials. In addition, we inspected the trial-by-trial spectro-temporal representations of LFP time series applying the continuous wavelet transform. We confirmed that comparable representations were attained by the Fourier- and wavelet-based time-frequency analyses.

The magnitude squared coherence (MSC) between time series recorded from mPFC and VTA was calculated in the same moving window with the 9 multi-tapers applied using the chronux routine cohgramc. Briefly, the MSC was quantified as:

$$C_{xy}(f) = \frac{\left|S_{xy}(f)\right|^2}{S_x(f)S_y(f)}$$

Where $S_{xy}(f)$ is the cross spectral density of LFP time series in the two regions, and $S_x(f)$, $S_y(f)$ are the autospectral density for each region.

#### 2.2.4.8 Bivariate Granger causality analysis

To examine mutual influences (directionality) between LFP oscillations in the two regions, we quantified Granger causality between the simultaneously recorded peri-action LFP

traces (-2 to 2 s around the action occurring at time = 0). The bivariate Granger causality (G-causality) infers causality between two time series data based on temporal precedence and predictability (Barnett and Seth, 2014; Granger, 1969). That is, a variable $X_1$ 'Granger causes' a variable $X_2$ if information in the past of $X_1$ helps predict the future of $X_2$ with better accuracy than is possible when considering only information already in the past of $X_2$ itself. In this framework, two time series $X_1(t)$ and $X_2(t)$ recorded from mPFC and VTA can be described by a bivariate autoregressive model:

$$X_1(t) = \sum_{j=1}^{p} A_{11,j} X_1(t-j) + \sum_{j=1}^{p} A_{12,j} X_2(t-j) + \varepsilon_1(t)$$

$$X_2(t) = \sum_{j=1}^{p} A_{21,j} X_1(t-j) + \sum_{j=1}^{p} A_{22,j} X_2(t-j) + \varepsilon_2(t)$$

where $p$ is the model order (the maximum number of time-lagged observations included in the model), which was estimated by the Akaike information criterion. We then estimated parameters of the model; $A$ contains the coefficients of the model, and $\varepsilon_1$, $\varepsilon_2$ are residuals (prediction errors) with covariance matrix $\Sigma$ for each time series.

Once the model coefficients $A_j$ and $\Sigma$ are estimated, the spectral matrix can be obtained as:

$$S(f) = \langle X(f) X*(f) \rangle = H(f) \Sigma H*(f)$$

where the asterisk denotes matrix transposition and complex conjugation, $\Sigma$ is the noise covariance matrix, and the transfer function $H(f)$ is defined as the inverse matrix of the Fourier transform of the regression coefficients:

$$H(f) = \left(I - \sum_{j=1}^{p} A_j e^{-2\pi i k f}\right)^{-1} \qquad 0 \leq f \leq 2\pi$$

The spectral G-causality from 1 to 2 is then obtained by:

$$I_{1\to 2}(f) = -\ln\left(1 - \frac{(\Sigma_{11} - \Sigma_{21}^2/\Sigma_{22}))|H_{21}(f)|^2}{S_{22}(f)}\right)$$

The spectral G-causality measure lacks known statistical distribution, thus a random permutation method was used to generate a surrogate distribution, by which the upper bound of the confidence interval was found at $\alpha = 0.001$. This procedure was implemented using an open-source matlab toolbox, the Multivariate Granger Causality Toolbox (Barnett and Seth, 2014).

#### 2.2.4.9 LFP-Spike phase-locking analysis

To quantify the individual neuronal spike time synchrony with the local and interregional 8 Hz oscillations were quantified as follows. The mPFC and VTA LFPs during the baseline and peri-action 4-s time windows were bandpass filtered to isolate oscillations within 5 – 15 Hz frequency range. The instantaneous phase of each filtered LFP segment was determined using the Hilbert transform and each spike was assigned the phase of its contemporaneous LFP segment. The phase-locking value (PLV) of each unit was defined as the circular concentration of the resulting phase angle distribution, which was quantified as the mean resultant length (MRL) of the phase angles. The MRL is the sum of unit vectors indicating instantaneous phases of each spike occurrence normalized by the number of spikes, thus the MRLs were bound to take a value between 0 (no phase-locking) to 1 (perfect phase-locking).

$$MRL = \frac{1}{N}\left|\sum_{n=1}^{N} e^{j\Phi_n}\right|$$

where $\Phi_n$ represents the phase assigned to n$^{th}$ spike occurrence, and $N$ is the total number of spikes. Since the MRL statistic is sensitive to the number of spikes, we calculated MRL 1,000 times with 100 spikes of each unit randomly selected for each iteration, and the PLV was the

MRL averaged across all iterations. As comparing PLVs across blocks with varying levels of risk was of our central interest, PLV was computed per each block. Only the units with their peri-action spike counts within each block greater than 100 in all three blocks were included in the phase-locking analysis. Units passing the Rayleigh's z-test at $\alpha = 0.05$ were determined to be significantly phase-locked. The directionality of the LFP and spike phase relationship was inferred by a time-lagged phase-locking analysis, in which the spike times were shifted relative to the LFP time series, stepping by 4 ms within the range of -100 to 100 ms (Likhtik et al., 2014; Spellman et al., 2015). At each time lag, the PLV of each single unit and its significance were assessed, and the maximum PLV across all time lags was found for each unit. We repeated the analysis with different time lags and analysis windows, and confirmed that the results were very similar across different parameters.

#### 2.2.4.10 Statistical analysis

Parametric statistical tests were used for z-score normalized data and non-normalized data that are conventionally tested using a parametric test. Nonparametric approaches, such as conventional nonparametric tests or bootstrapping were used for a hypothesis test of data, of which statistical distribution is unknown, e.g. phase-locking values (PLVs). For all tests, the Greenhouse–Geisser correction was applied as necessary due to violations of sphericity. All statistical tests were specified as two-sided. Multiple testing correction was applied for all tests including multiple comparisons using the Bonferroni correction.

## 2.3 RESULTS

### 2.3.1 Anxiety-like behavioral changes as a function of punishment risk

Punishment risk varying across blocks induced anxiety-like aversive behavioral changes (Figure 2-1a-b), as the mean response time (RT) markedly increased as a function of risk (Figure 2-1c; GLM repeated measures, $F_{2, 32} = 24.94$, $p < 0.001$). We also measured time spent in immobility during RT, a widely used behavioral measure of anxiety in rodents, and observed a significant increase in immobile RT (Figure 2-1c; GLM repeated measures, $F_{2, 32} = 22.44$, $p < 0.001$), demonstrating that the increased RT may involve anxiety. The increase in RT could not be explained by changes in motivation for the reward, as the time for reward retrieval (reward RT) remained consistent across blocks regardless of risk (Figure 2-1c inset; GLM repeated measures, $F_{2, 32} = 2.97$, p = 0.07). Punishment risk induced a pronounced increase in the trial-to-trial variability in RT beyond the level of increase expected corresponding to the mean increase (Figure 2-1d; GLM repeated measures, $F_{2, 32} = 13.89$, $p < 0.001$). This increase in behavioral variability was associated with shock occurrences, as the RT varied as a function of the trial lag from the previous shock (Figure 2-1e), indicating that animals systematically adjusted their behavior across trials even in the same block. When animals performed the same number of trials and blocks in the absence of punishment throughout a session, namely 'no-shock control session', the mean and variance RT did not differ across blocks (Figure 2-2).

In an attempt to ensure that the risk-dependent increase in RT was pertinent to anxiety, we tested whether the anxiolytic diazepam could block the increase in RT. Systemic pretreatment of diazepam (2 mg/kg) significantly averted the RT increment in the high risk block, compared

with saline pretreatment (Figure 2-1f, left; Repeated measures ANOVA, $F_{4, 48}$ = 3.27, $p$ = 0.019; *post hoc test*, block 3, $p$ values < 0.01). Likewise, diazepam pretreatment blocked the risk-induced increase in the trial-to-trial RT variability (Figure 2-1f, right; GLM repeated measures, $F_{2, 16}$ = 0.46, p = 0.638). Diazepam or saline injected animals showed equivalent levels of reward RT (Figure 2-1f, left; Repeated measures ANOVA, $F_{4, 48}$ = 0.34, $p$ = 0.852; *post hoc test*, $p$ values > 0.51).

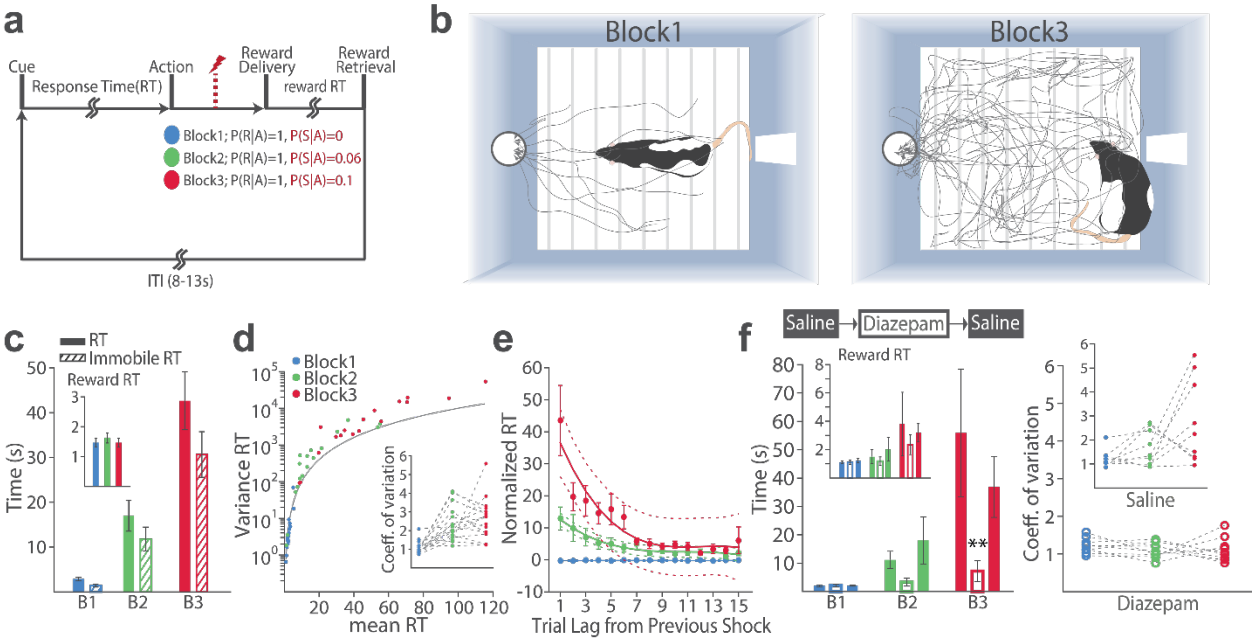


**Figure 2-1 Punishment risk induces anxiety-like changes in reward-seeking behavior.**

(a) A schematic diagram, illustrating the task design. (b) Representative behavioral trajectories in block 1 (left, 10 trials) and block 3 (right, 10 trials). (c) Significant increases in RT (filled bars) and immobile RT (slashed bars) were observed as a function of risk. (Inset) Latency from reward delivery to retrieval (reward RT) did not differ across blocks. (d) Punishment risk increased variability in RT. The gray curve indicates the expected variance RT as a function of mean RT, considering the RT as time intervals of a Poisson point process. Each dot indicates each animal's data. Note that variances of RT in block 2 & 3 appear above the gray curve. (Inset) The coefficient of

variation was significantly increased as a function of risk. (e) RT varied systematically as a function of the trial lag from the previously punished trial in risky blocks. (f) Animals performed three sessions of the task with pretreatment of saline (Day1) – diazepam (2 mg/kg) – saline (Day2). Left, Pretreatment of an anxiolytic diazepam (2 mg/kg), but not the saline injection, averted a risk-induced increase in the mean RT. **p < 0.005; post hoc test. (left inset) Injections did not influence the reward RT. Right, Diazepam pretreatment also prevented an increase in the variance RT, which was observed in saline-pretreated performance (right inset).

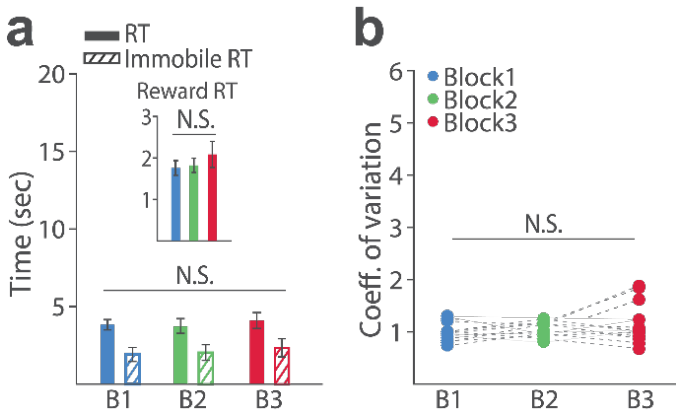


**Figure 2-2 Behavior does not change across blocks in the absence of punishment risk.**

(a) RT, immobile RT, and reward RT (inset) did not change across blocks in the absence of punishment. (b) The trial-to-trial variability in RT did not differ across blocks.

### 2.3.2 Individual neuronal encoding of punishment risk

During the task performance, total 167 mPFC and 102 VTA single units were recorded from histologically verified electrodes (Figure 2-3a). For all single unit data analyses, VTA units were classified into putative dopamine (DA, n = 55) and non-dopamine (non-DA, n = 47) subtypes

(Figure 2-4, Methods). We first examined the trial-averaged neuronal activity of mPFC, VTA DA and non-DA units to compare their general tuning properties during the cue onset, action and reward delivery. The vast majority of VTA DA units displayed phasic excitatory responses at task-event occurrences (Schultz et al., 1993), whereas non-DA and mPFC units showed weaker and temporally diffuse responses (Figure 2-3; Repeated measures ANOVA, post-cue, $F_{2, 266}$ = 22.05; peri-action, $F_{2, 266}$ = 43.78; post-reward, $F_{2, 266}$ = 48.93, $p$ values < 0.001).

We then quantified single neuronal encoding of punishment risk using a percent explained variance (ωPEV) statistic (Buschman et al., 2012), i.e. how much of the variance in a neuron's firing rate can be explained by punishment risk (Methods). To identify risk-encoding units, we compared the ωPEV statistic of the original spike trains with the ωPEV distribution of surrogate spike trains created by shuffling block labels (Methods, Figure 2-5). Representative risk-encoding mPFC, VTA DA, and non-DA units are illustrated in Figure 2-6. Substantial proportions of units in both regions (mPFC, 49 %; VTA DA, 65 %; VTA non-DA, 77 %) encoded punishment risk especially at the time of the action (Figure 2-7a, Figure 2-8). Hence, subsequent analyses focused on the peri-action epoch. A significant interaction between time and unit groups was observed in the peri-action ωPEV (Figure 2-7a; Repeated measures ANOVA, $F_{38, 5054}$ = 2.68, $p$ < 0.001), indicating distinct time-varying patterns in risk encoding by different unit groups. But the main effect of the unit group was not significant, indicating equivalent levels of peri-action encoding of punishment risk ($F_{2, 266}$ = 1.21, $p$ = 0.30).

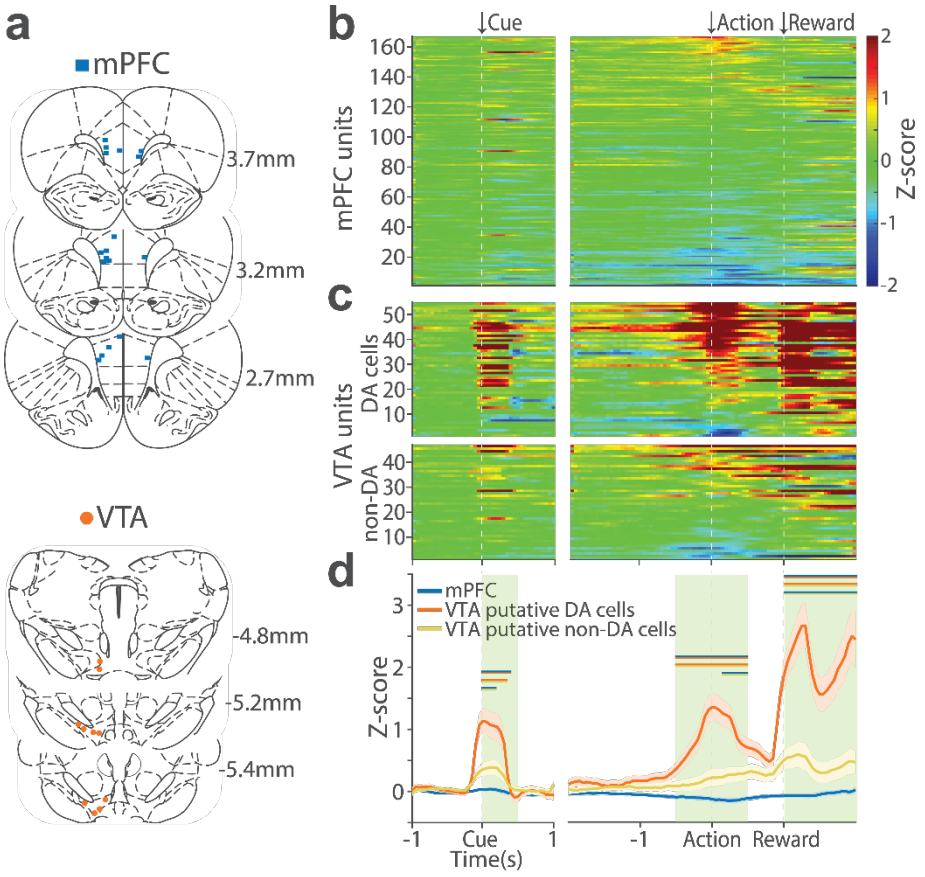


**Figure 2-3 mPFC, VTA DA and non-DA single units show distinct tuning properties at task events.**

(a) Histologically verified placements of mPFC and VTA electrodes. Rats were implanted in ipsilateral VTA and mPFC (N=10) or bilateral mPFC (N=4). (b) Baseline-normalized peri-event activity of mPFC units averaged across all trials. (c) Peri-event activity of putative DA (top) and non-DA (bottom) VTA units. (d) Peri-event activity averaged across all units of each neuronal subtype. Dual-colored bars above indicate significant pairwise differences at corresponding time bins according to the post hoc analysis ($p < 0.05$). The green shadows indicate time windows of statistical analyses.

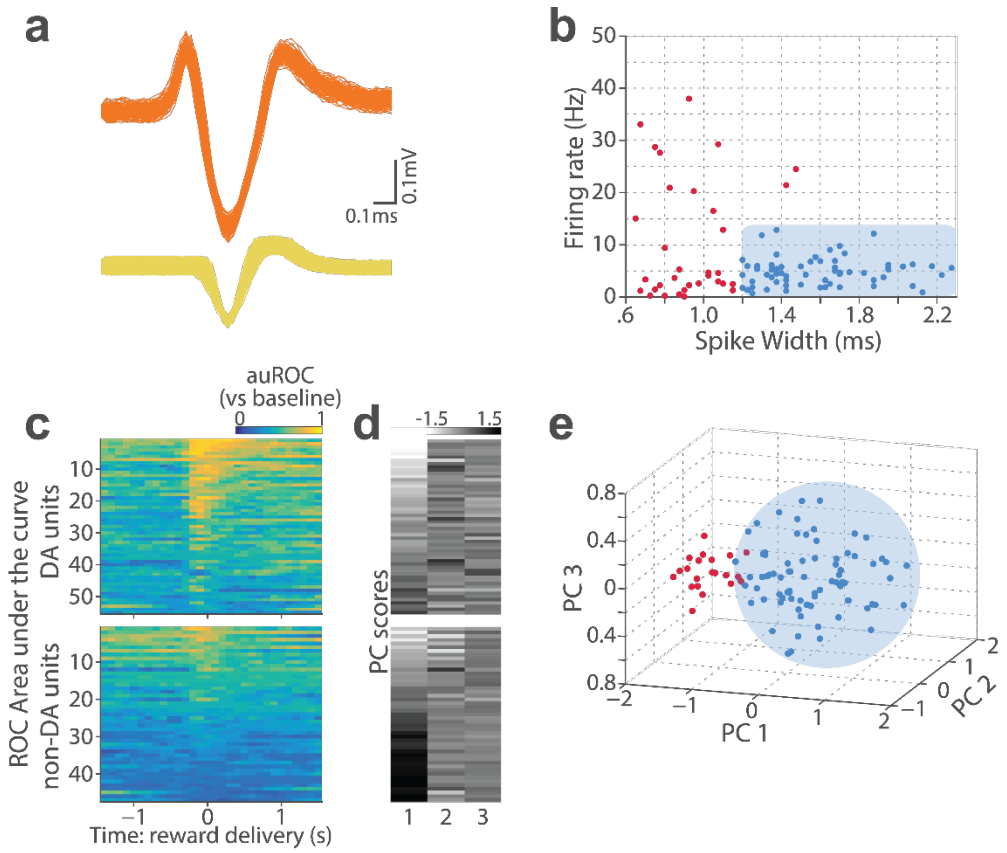


**Figure 2-4 Classification of VTA single units to putative dopamine (DA) or non-dopamine (non-DA) units.**

(a) Representative spike waveforms of a putative DA (top) and a non-DA (bottom) units. (b) Units were first classified based on their mean baseline firing rate and width of the spike waveform. Units whose mean baseline firing rate slower than 12 Hz, waveform width greater than 1.2 ms were considered to be putative DA units (blue circles). (c) To characterize each unit's reward response, ROC curves were calculated by comparing the firing-rate distributions of reward delivery vs baseline epochs. (d) Principal component analysis (PCA) was conducted on auROC values. (e) Units were mapped onto a 3-d space comprising the top three principal components. Unsupervised clustering was conducted by fitting Gaussian mixture models which yielded two clusters of units: one with phasic excitation to reward (blue circles), the other with sustained excitation or suppression to reward (red circles). Units in the former cluster were classified as putative DA units. Only the units satisfying both criteria (b) and (e) were finally labelled as putative DA units, and the rest of units were putative non-DA units.

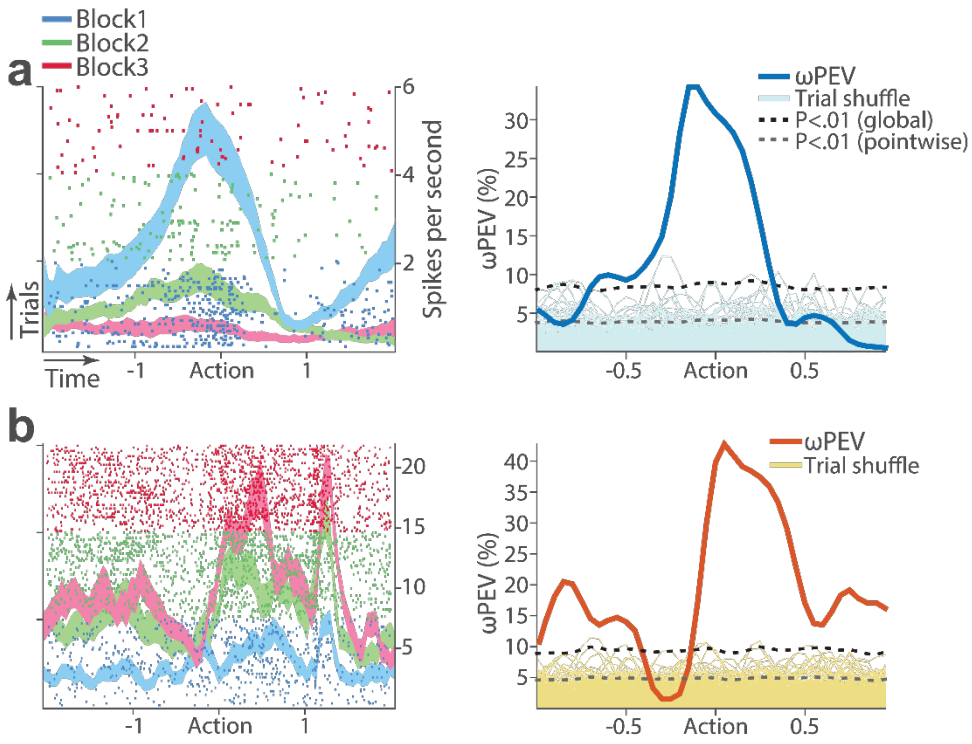


**Figure 2-5 Identification of single units discriminating their firing rates across different blocks as a function of risk.**

(a) Left, A raster plot showing a representative mPFC unit's peri-action spike activity across blocks with spike density functions of different blocks superimposed. (a) Right, To quantify each unit's encoding of risk, percent variance in the unit's firing rate explained by blockwise punishment risk (ωPEV) was calculated (Methods). To determine the global ωPEV band, trial-shuffled surrogate ωPEV distribution (light blue curves) was acquired, and the pointwise and global ωPEV bands were found from the distribution at $\alpha = 0.01$ (Methods). A unit whose ωPEV curve crosses the global band was determined as a risk-encoding unit. (b) Left, A representative VTA unit's peri-action activity across blocks. (b) Right, This VTA unit satisfied the risk-encoding criterion.

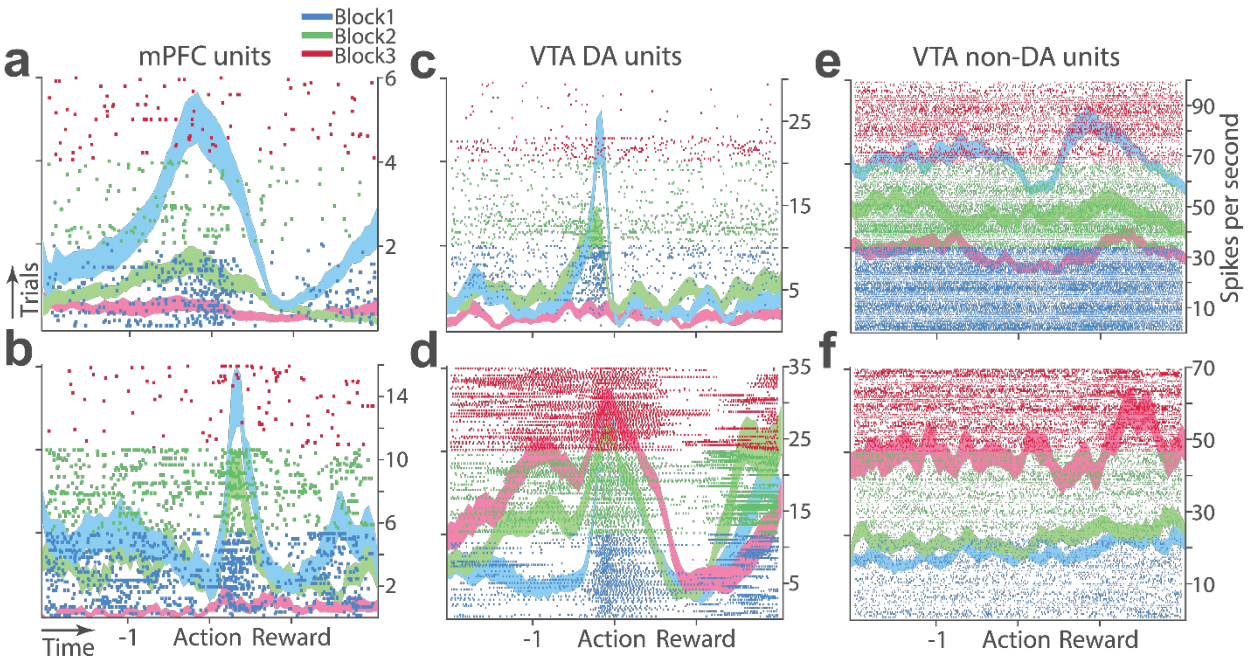


**Figure 2-6 Representative risk-encoding mPFC (a-b), VTA DA (c-d) and non-DA (e-f) single units.**

In each plot, data are for 150 trials of action (one row per trial, ticks mark spike times) with three varying levels of punishment risk (color-coded). The horizontal axis represents time around the action occurring at time = 0. Spike density functions of different blocks are superimposed as mean ± s.e.m. (shaded area). The right vertical axis indicates firing rates.

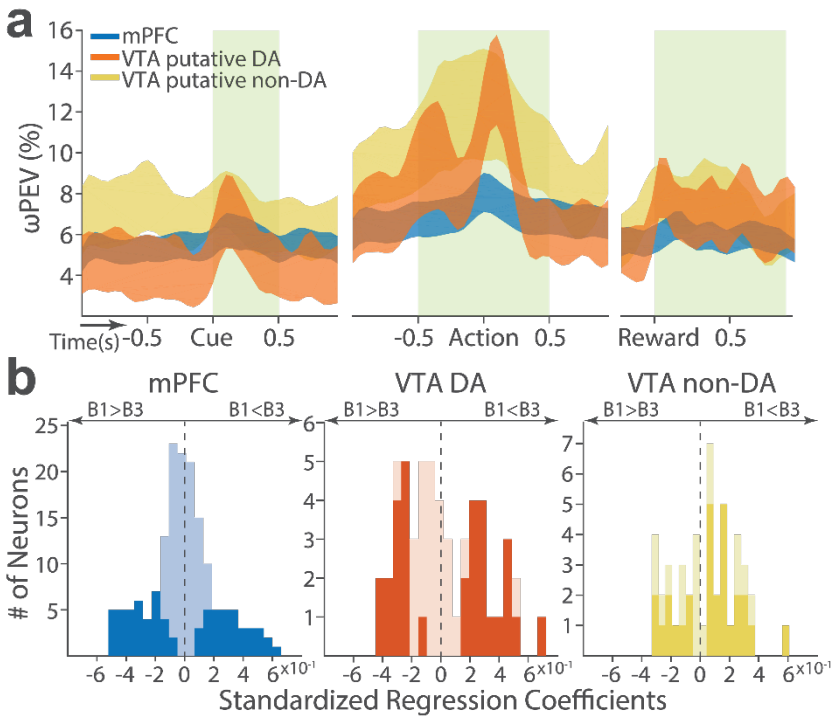


**Figure 2-7 mPFC, VTA DA and non-DA single units encode punishment risk with bidirectional activity modulation.**

(a) The mean ± s.e.m. (shaded area) ωPEV averaged across all units in each neuron group. (b) All single units are distributed across the horizontal axis based on modulation of their peri-action activity across blocks as a function of punishment risk. Standardized regression coefficients (SRC) were computed for a normalized quantification of each unit's peri-action activity modulation by punishment risk (Methods). In each distribution, units with positive or negative activity modulation as a function of risk are located in the right or left portion of the distribution. The risk-encoding units are solid-colored, while the non-encoding units are pale-colored.

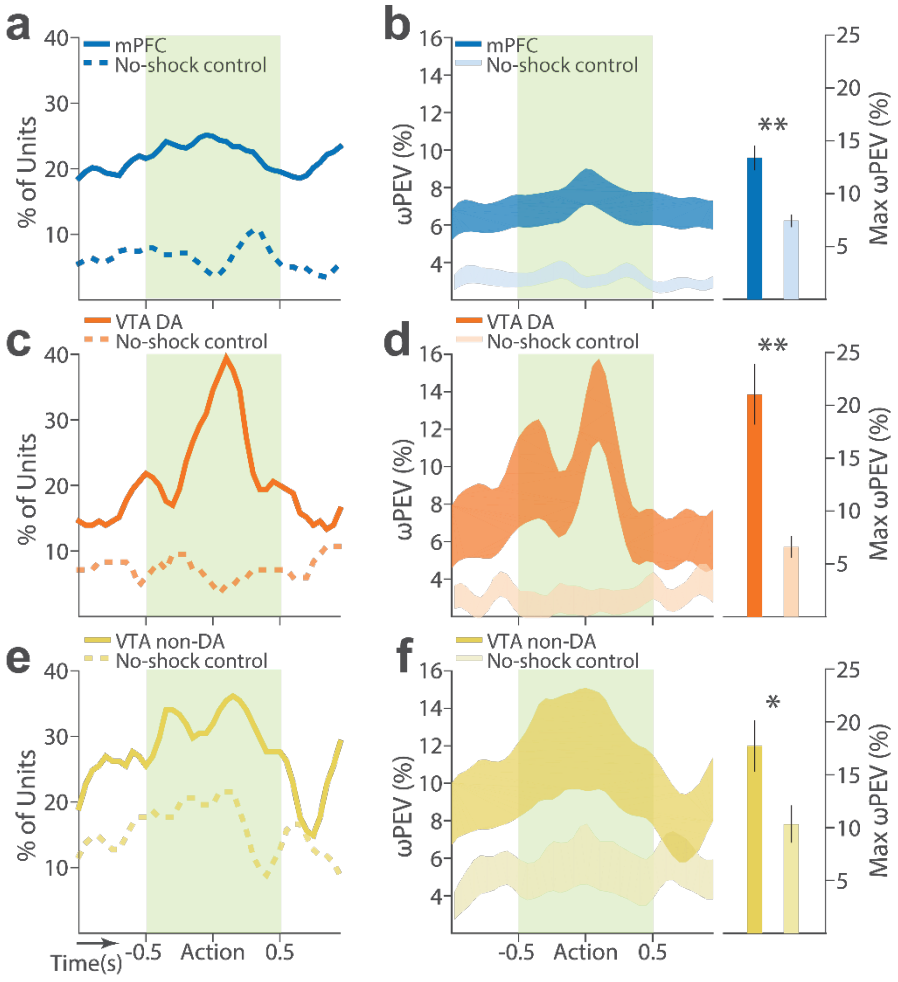


**Figure 2-8 Blockwise firing rate changes in the presence vs absence of punishment risk varying across blocks.** (a) Proportion of mPFC units showing significant firing-rate changes across blocks during the peri-action epoch in the presence vs absence (no-shock control) of punishment risk. (b) Left, Percent variance in the mPFC unit firing rates explained by the block shift (ωPEV) in the presence vs absence of punishment risk (mean ± s.e.m.). Right, Maximum peri-action ωPEV of mPFC units differed in the presence vs absence of risk (Student's t-test, $t291 = 3.81$, $p < 0.001$). (c) Proportion of VTA DA units showing significant firing-rate changes across blocks. (d) Left, ωPEV of VTA DA units in the presence or absence of risk. Right, Maximum peri-action ωPEV of VTA DA units in the presence vs absence of risk ($t81 = 4.19$, $p < 0.001$). (e) Proportion of VTA non-DA units showing significant firing-rate changes across blocks. (f) Left, ωPEV of VTA non-DA units in the presence vs absence of risk. Right,

Maximum peri-action ωPEV of VTA non-DA units in the presence vs absence of risk ($t_{74} = 2.25$, $p = 0.028$). *$p < 0.05$, **$p < 0.005$.

To further characterize individual neuronal risk-encoding schemes, we examined the sign (direction) of neuronal activity modulation as a function of risk (Methods). Equivalent fractions of mPFC, VTA DA, and non-DA units encoded punishment risk with excitatory or inhibitory activity modulation, i.e., some increased their firing rates, whereas others decreased their firing rates as a function of risk (Figure 2-7b). This indicated that the mesoprefrontal representation of punishment risk may not be simply described as activation or inhibition of one particular cell group in one region. Rather, the bi-directionality observed even within the same cell group (Figure 2-7b) indicates that distinct neuronal subgroups may encode distinct motivational properties related to punishment risk.

Punishment can exert long-lasting behavioral impacts, which may involve persistent neuronal activity modulation outlasting the task-event epochs (Cohen et al., 2015; Somerville et al., 2013). Thus, we examined whether individual units modulated their baseline firing rate during the inter-trial interval as a function of punishment risk. Consistent with previous neurophysiological studies showing stress-induced DA neuronal baseline activity (Grace, 2016; Holly and Miczek, 2016), we found that VTA DA units tended to increase their baseline firing rate in an aversive context (Figure 2-9; GLM repeated measures, $F_{2, 108} = 2.94$, $p = 0.066$). VTA non-DA and mPFC units did not significantly differ their firing rates as a function of risk (Figure 2-9; GLM repeated measures, VTA non-DA, $F_{2, 92} = 0.618$, $p = 0.484$; mPFC, $F_{2, 332} = 1.084$, $p = 0.325$).

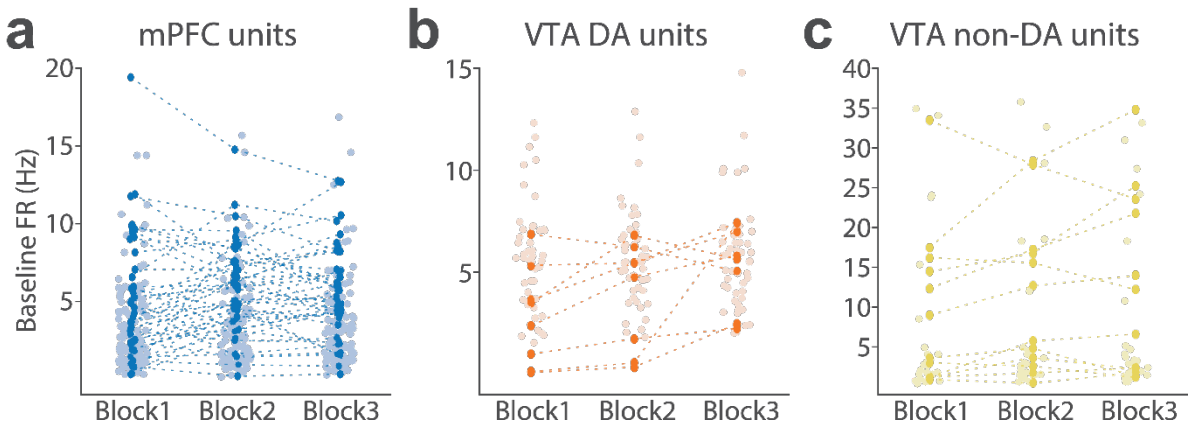


**Figure 2-9 Blockwise baseline firing rate changes across blocks.**

(a) The mean baseline firing rate within the 2-s baseline period during the inter-trial interval was calculated for each mPFC unit per block. Each dot corresponds to each mPFC unit. The mPFC units with a significant change in the baseline firing rate, according to the criterion described in Figure 2-5, are solid-colored, whereas the rest of units are pale-colored. (b) The mean baseline firing rates of the VTA DA units (b) and non-DA units (c). Conventions are same as (a).

To disentangle neuronal encoding of risk from other confounding factors that may affect blockwise changes in the neuronal activity – such as satiety, fatigue, and/or spontaneous changes over time, additional 126 mPFC and 57 VTA single units (putative DA, n = 28; putative non-DA, n = 29) were recorded during performance in the no-shock control session. During this session, much weaker blockwise changes in firing rates were observed, (Figure 2-8), indicating negligible impact of confounding factors on the neuronal encoding of risk.

### 2.3.3 Neuronal population representation of punishment risk

Given the prevalent single neuronal encoding of risk, the mPFC and VTA neuronal population activity is likely to be informative of risk in a given trial. To test this, we performed a population decoding analysis, using the Poisson naïve Bayes classifier (Methods). From both populations, blockwise punishment risk in a given trial could be decoded with high accuracies well above the chance level (33.3 %) (Figure 2-10a). Combined with the single neuronal data, these data suggest that both mPFC and VTA precisely represent the blockwise punishment risk at the single neuronal and neuronal population levels.

Our behavioral data indicated remarkable trial-to-trial variability in RT, and the variability increased as a function of risk (Figure 2-1d), meaning that the RT varied across trials even within the same block. To more rigorously test the link between the behavioral and neural data, we examined whether and to what extent the behavioral variability could be explained by the mPFC and VTA neuronal activity. At the single neuron level, we found that only small fractions of single units exhibited significant correlation between their firing rate and the RT across trials (mPFC, 10.2 %; VTA DA, 36.4 %; VTA non-DA, 25.5 %). This result indicated that inferring trial-by-trial behavior from single neuronal activity was much limited. Given this limitation, we attempted to leverage statistical power of the single-trial analysis by correlating the RT with the neural population activity. A classic approach to measure the neuronal population activity is averaging across neurons, but the bi-directionality in risk-encoding observed across individual neurons (Figure 2-7b) undermined validity of such approach. Alternatively, we identified the low-dimensional state space that captured patterns of activity co-modulation among the simultaneously recorded mPFC and VTA populations comprising ten or more single units. Trial-by-trial neural population trajectories were extracted within this state

space using a dimensionality reduction method Gaussian process factor analysis (GPFA; Methods) (Yu et al., 2009). Then we examined the correlation between the neural population trajectory and the RT across trials. The mPFC and VTA population trajectories tracked the trial-to-trial variation in RT, as the deviation (Euclidean distance) of each trial's neural trajectory from the block 1 mean trajectory was significantly correlated with the deviation of each trial's RT from the block 1 mean RT. That is, the further each trial's neural trajectory deviated from the block 1 mean trajectory, the greater the RT appeared (Figure 2-10b-e). Significant correlations were observed in all four mPFC and three VTA populations comprising 10 to 25 single units subjected to this analysis (Figure 2-10, 2-11, 2-12). We further examined the neural and behavioral correlation within each block to probe if the neural population trajectories could even track the behavioral variation within each block. As our behavioral data indicated more pronounced trial-to-trial variability in RT in the high risk block (Figure 2-1d), we focused on this block and asked whether the increased behavioral variability was correlated with the neural population trajectories. Significant correlations were observed specifically in the high risk block in two of the four mPFC populations (Figure 2-11), indicating that the neural and behavioral correlation emerged as the behavioral variability arose with risk. Similarly, significant correlations were detected in two of the three VTA populations in the high risk block (Figure 2-12).

We extracted trial-by-trial trajectories of neural population activity recorded from the no-shock control sessions. Consistent with the lack of correlation observed in the absence of risk (Block 1; Figure 2-10, 2-11, 2-12), none of the mPFC and VTA population activity showed a significant correlation with behavioral RT in the no-shock control session. These results indicate

that distinct neural population activity emerged and tracked behavior only in the presence of but not in the absence of punishment risk (Figure 2-11, 2-12).

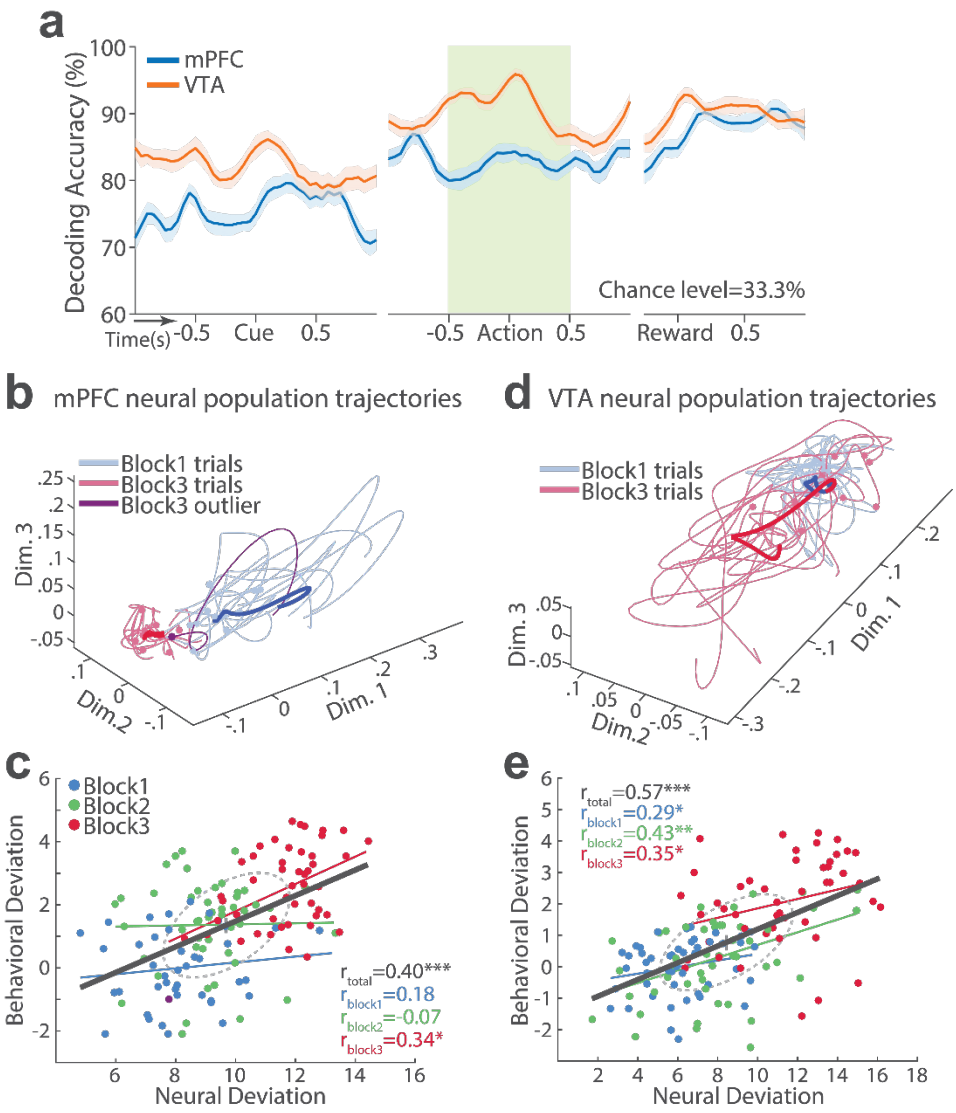


**Figure 2-10 Representation of punishment risk in mPFC and VTA neural populations.**

(a) Accuracy of decoding punishment risk (block label) from the VTA and mPFC neural populations. Decoding accuracy was calculated with a 5-fold leave-one-split-out cross-validation (Methods). (b-e) Single-trial analysis of neural population activity reveals the linkage between neural and behavioral variability. (b) Representative mPFC neural population trajectories visualized in the top three orthonormalized dimensions of the neuronal activity co-

modulation space. The dimensionality of state space was determined to be five for all populations, based on the cross-validated data likelihood (Methods). This example mPFC population comprises 16 units. Each trajectory corresponds to -0.5 to 0.5 s peri-action epoch (action occurring at time = 0). Filled circles indicate initial points of neural trajectories. For simplicity, ten trials were randomly selected per block 1 and 3. Heavy lines indicate the mean trajectory averaged across all trials in each block. The purple-colored block 3 neural trajectory represents a single trial with an outlying RT similar to a block 1 trial. (c) A scatter plot indicating behavioral deviation from the block 1 mean RT and neural deviation from the block 1 mean trajectory of the mPFC population shown in (b). RT was log transformed for proper scaling. Superimposed color-coded lines indicate regression slopes per block. The dark gray line indicates the regression slope for total trials pooled across blocks. The behavioral and neural correlation coefficients calculated on total trials and trials per block are indicated. *p < 0.05, **p < 0.005. (d) Neural population trajectories of a representative VTA population comprising 10 units. (e) A scatter plot indicating behavioral deviation from the block 1 mean RT vs neural deviation from the block 1 mean trajectory of the VTA population shown in (d).

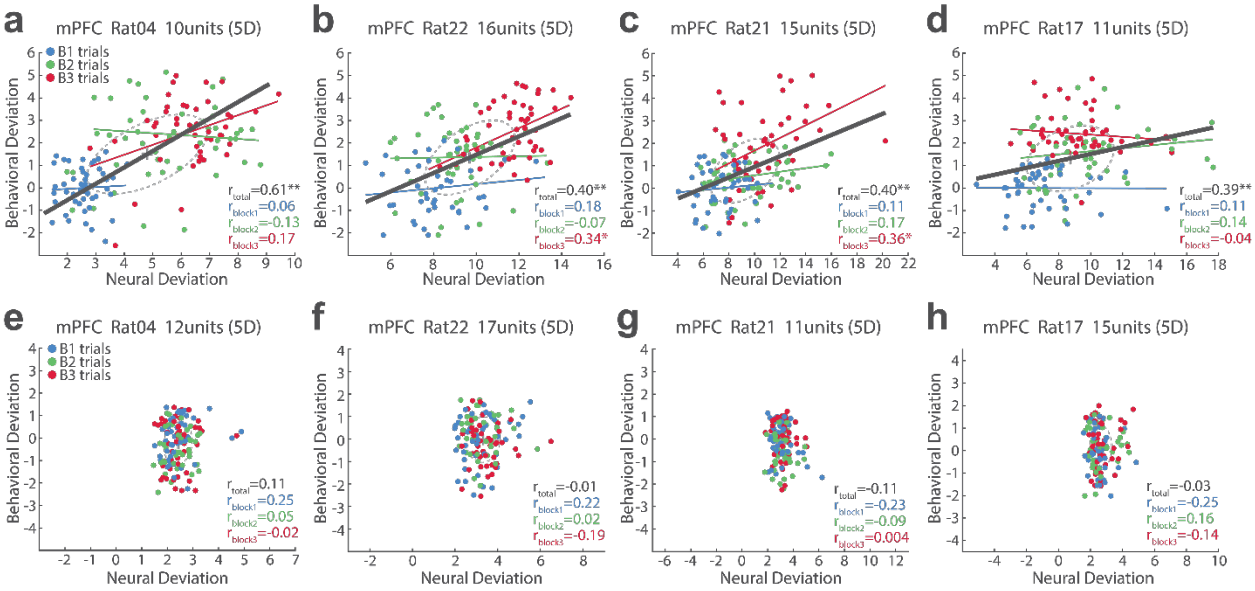


**Figure 2-11 Single-trial analysis of mPFC neural population activity reveals the linkage between neural and behavioral variability during risky reward-seeking.**

(a-d) Scatter plots represent each animal's behavioral deviation from the block 1 mean RT vs neural deviation from the block 1 mean neural population trajectory. RT was log transformed for proper scaling. In each plot, the animal's ID, the number of units comprising the neural population, and the state space dimensionality are indicated. Superimposed color-coded lines indicate regression slopes per block. The dark gray line indicates the regression slope for total trials pooled across blocks. The behavioral and neural correlation coefficients calculated on total trials and trials per block are indicated. *p < 0.05, **p < 0.005. (e-h) Data from no-shock control sessions. Note the lack of behavioral and neural correlation in the absence of risk.

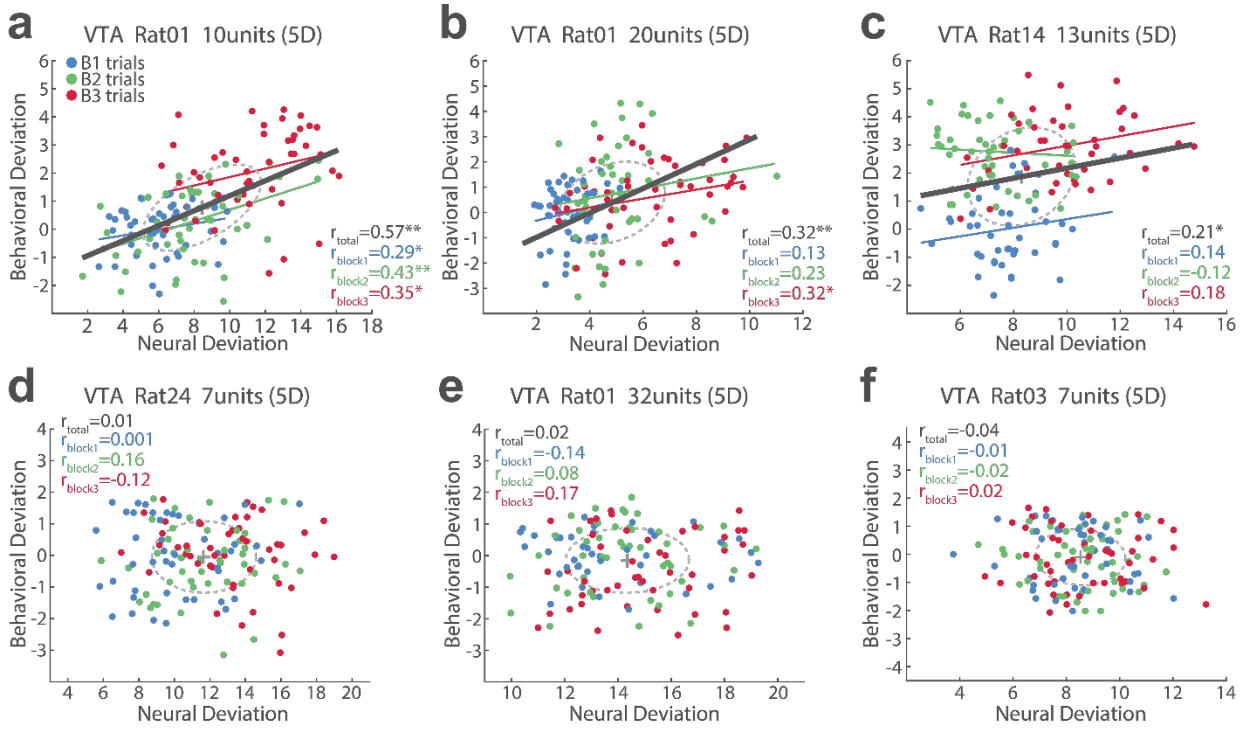


**Figure 2-12 Single-trial analysis of VTA neural population activity reveals the linkage between neural and behavioral variability during risky reward-seeking.**

(a-c) Scatter plots represent each animal's behavioral deviation from the block 1 mean RT vs neural deviation from the block 1 mean neural population trajectory. (d-f) Data from no-shock control sessions, indicating the lack of behavioral and neural correlation in the absence of punishment risk. Conventions are same as Figure 2-11.

### 2.3.4 Punishment-induced decline in the VTA and mPFC neural synchrony

At the neural circuit and network level, synchronous oscillations can provide temporal coordination among local and interregional neural groups, thereby promoting various cognitive, emotional, and motivational functions (Adhikari et al., 2010; Buschman et al., 2012; Fries, 2015; Fujisawa et al., 2008; Fujisawa and Buzsaki, 2011; Karalis et al., 2016b; Kim et al., 2012; Kim et al., 2010; Likhtik et al., 2014). We examined whether such oscillation-mediated neural synchrony subserved encoding of the instrumental action and punishment risk contingent on the action.

During risk-free performance in the block 1, LFP oscillations in the 6 to 10 Hz band specifically arose in both regions preceding and during the action (Figure 2-13a-d). For simplicity, we refer to this as 8 Hz oscillation hereafter. The 8 Hz oscillation was markedly reduced as a function of risk in both regions (Figure 2-13e-f), even though animals' motor activity was kept similar across trials due to execution of the action in the peri-action epoch. A significant interaction between risk and the frequency band was detected in LFP power during post-cue and pre-action time periods in both regions (Repeated measures ANOVA, VTA, post-cue, $F_{52,\ 1092} = 5.11$; pre-action, $F_{52,\ 1092} = 7.78$, $p$ values $< 0.001$; mPFC, post-cue, $F_{52,\ 1872} = 1.60$, $p = 0.005$; pre-action, $F_{52,\ 1872} = 2.29$, $p < 0.001$, Figure 2-13g-h). The 8 Hz oscillations appeared to be coherent between the two regions during the risk-free action, but the coherence significantly reduced as a function of risk (Figure 2-13i). A significant interaction between risk

and the frequency band was observed in LFP coherence during the pre-action period (Repeated measures ANOVA, post-cue, $F_{52, 1092} = 0.93$, $p = 0.62$; pre-action, $F_{52, 1092} = 2.45$, $p < 0.001$).

To examine the mutual influences (directionality) of the LFP time series between the two regions, we quantified Granger causal influences (GC) in the VTA-to-mPFC and mPFC-to-VTA directions (Methods). During the risk-free action in the block 1, the 8 Hz oscillation was driven by VTA, as mPFC was GC influenced by VTA significantly greater than the GC influence of the other direction (Figure 2-13j). A significant interaction between directionality and the frequency band was observed in GC coefficients in all blocks, indicating that the oscillation directionality varied across frequency bands (Figure 2-13j; Repeated measures ANOVA, Block 1, $F_{25, 700} = 2.05$, $p = 0.002$; Block 2, $F_{25, 700} = 2.38$, $p < 0.001$; Block 3, $F_{25, 700} = 5.59$, $p < 0.001$). But importantly post hoc analysis revealed significantly greater VTA-to-mPFC directionality in frequency bands including the 8 Hz in block 1, and the directionality declined in blocks 2 & 3 (Figure 2-13j). Taken together, these results suggest that VTA-driven 8 Hz oscillations entrain the mesoprefrontal circuit during the risk-free action. Decline in this entrainment may represent punishment contingent on the action, as power, coherence, and directionality of the 8 Hz oscillation declined as a function of punishment risk. Analyses of no-shock control data revealed that these risk-dependent changes in the mesoprefrontal 8 Hz oscillation were not evident in the absence of punishment risk (Figure 2-14).

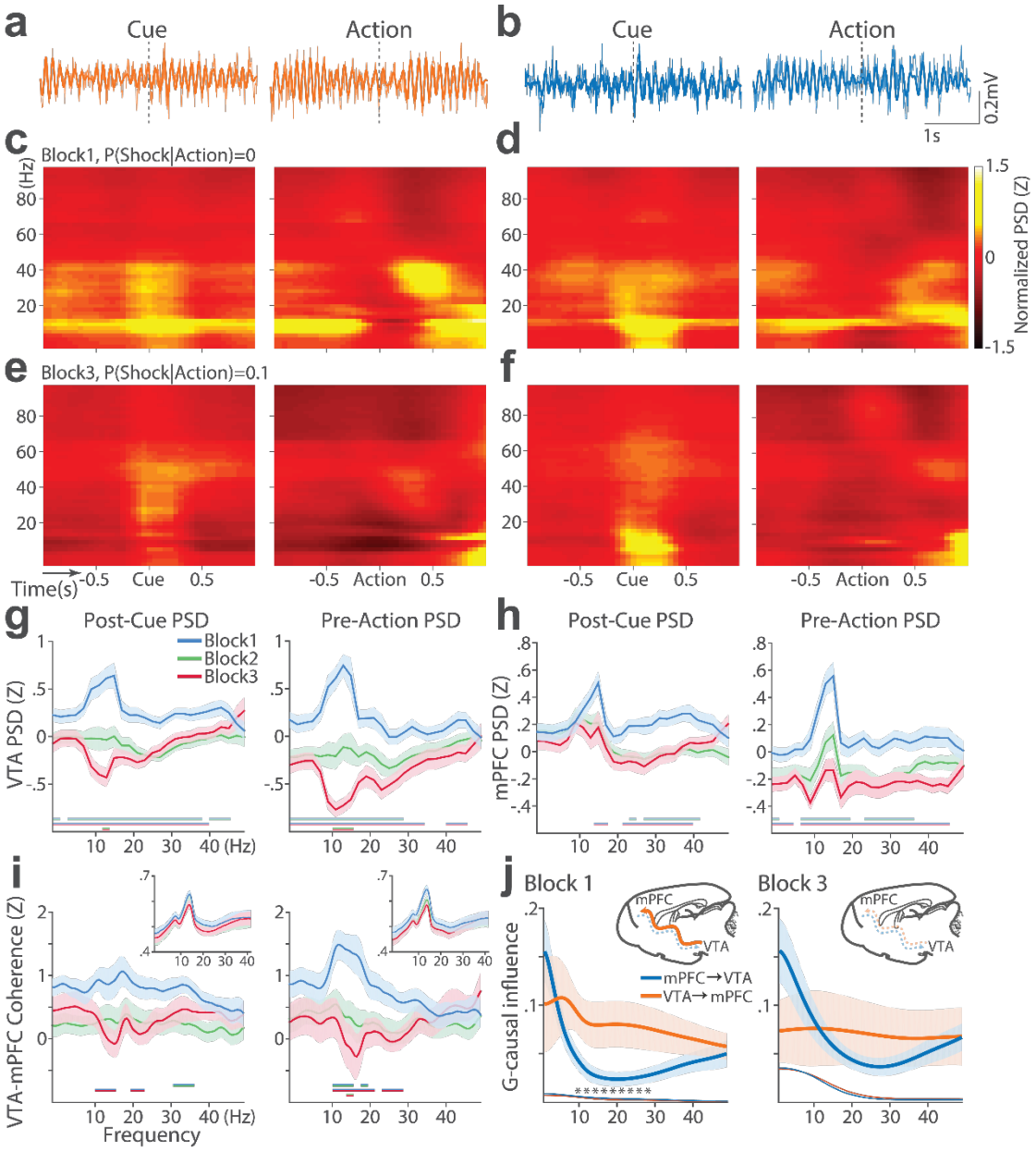


**Figure 2-13 Punishment risk declines the 8 Hz oscillation-mediated neural synchrony in the mesoprefrontal circuit.**

(a) Representative VTA peri-event LFP traces in a block 1 trial. Bandpass filtered LFP signal (heavy line) is superimposed on the raw trace (thin line). (b) Simultaneously recorded mPFC LFP traces. (c) Baseline-normalized VTA power spectral densities (PSDs) averaged across block 1 trials (left: peri-cue PSD, right: pre-action PSD). mPFC block 1 PSDs are in (d). (e) Diminished VTA 8 Hz PSD in block 3. (f) Similar diminishment observed in

mPFC 8 Hz PSD. (g) Mean ± s.e.m. (shaded area) normalized VTA PSDs of each block corresponding to 1 s post-cue (left) and pre-action (right) epochs. Dual-colored bars below indicate significant pairwise differences at corresponding frequency bins according to post hoc analyses ($p < 0.05$). (h) Normalized mPFC PSDs in post-cue (left) and pre-action (right) epochs. (i) Normalized VTA-mPFC LFP coherence in post-cue (left) and pre-action (right) epochs. Insets represent non-normalized LFP coherences of each block. (j) Granger-causality, representing mutual influences (directionality) between VTA and mPFC peri-action LFP time series in block 1 (left) & 3 (right). Blue and orange curves represent mPFC-to-VTA and VTA-to-mPFC Granger-causal influences, respectively. Shaded areas indicate s.e.m. Thin colored-lines below indicate upper bounds of confidence intervals ($\alpha = 0.001$) acquired by the random permutation resampling of time bins. An asterisk indicates significant difference between bidirectional Granger-causal influences at the corresponding frequency bin ($p < 0.05$).

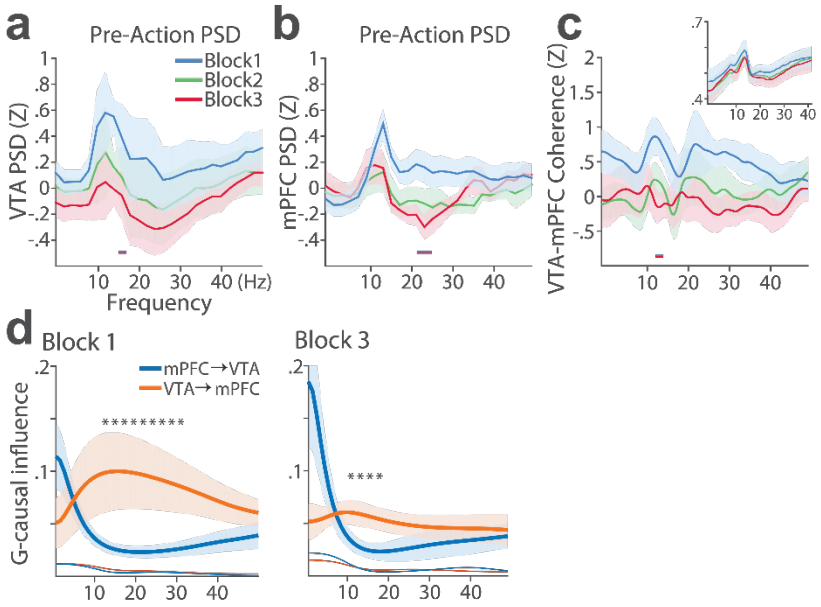


**Figure 2-14 The mesoprefrontal 8 Hz oscillations barely change across blocks in the absence of punishment risk.**

(a) Mean ± s.e.m. (shaded area) normalized VTA PSDs of each block corresponding to 1 s pre-action epoch. Dual-colored bars below indicate significant pairwise differences at corresponding frequency bins according to post hoc

analyses ($p < 0.05$). (b) Normalized mPFC PSDs. (c) Normalized VTA-mPFC LFP coherence of each block in the pre-action epoch. Insets represent non-normalized LFP coherences. (d) Granger-causality, representing mutual influences (directionality) between VTA and mPFC peri-action LFP time series in block 1 (left) & 3 (right). Blue and orange curves represent mPFC-to-VTA and VTA-to-mPFC Granger-causal influences, respectively. Shaded areas indicate s.e.m. Thin colored-lines below indicate upper bounds of confidence intervals ($\alpha = 0.001$) acquired by the random permutation resampling of time bins. An asterisk indicates significant difference between bidirectional Granger-causal influences at the corresponding frequency bin ($p < 0.05$).

### 2.3.5 Punishment-induced decline in the local and interregional LFP–spike synchrony

Synchronous oscillations can provide temporal coordination of spike activity of local and interregional neuron groups by creating rhythmic sequences of neuronal excitation and inhibition, thereby enhancing 'neuronal communication' between coherently timed neuron groups (Fries, 2015; Harris and Gordon, 2015). The presence of such LFP-mediated spike timing coordination was examined by measuring phase-locking of the neuronal spike activity to the local and interregional 8 Hz oscillations in the peri-action epoch (Methods).

When probed within each region, substantial proportions of VTA (37 %) and mPFC (23 %) single units that were subjected to the phase-locking analysis (Methods) were significantly phase-locked to the local 8 Hz oscillation in the risk-free block 1 according to the Rayleigh z-test for non-uniformity of the spike phase distribution (Figure 2-15). Consistent with the temporally specific increase in 8 Hz spectral power (Figure 2-13c-d), the phase synchrony specifically arose during the action from the baseline level in the phase-locked units in both regions (Figure 2-15a & d; Signed-rank test, *p* values < 0.001). Enhanced phase-locking but to a lesser degree was observed even in units that failed the Rayleigh's test (Figure 2-15a & d; Signed-rank test, *p*

values < 0.001), indicating widespread influence of the 8 Hz oscillation on the local neuronal spike timing. The temporal relationship (directionality) between the spike outputs and the local 8 Hz oscillation was examined using a time-lagged phase-locking analysis (Likhtik et al., 2014; Spellman et al., 2015). The spike-LFP phase-locking was quantified using spike times lagged relative to the local or interregional LFP to infer the directionality in the LFP-spike interaction (Methods). We found that in block 1 greater proportions of units appeared to be phase-locked with negative time lags. The vast majority of phase-locked units (VTA, 74 %; mPFC, 67 %) had their maximum phase-locking values (PLVs; Methods) with a negative lag (Figure 2-15b & e; Signed-rank test, $p$ values < 0.005). These indicated entrainment of spike timing by preceding cycles of the oscillation, i.e. directionality from the 8 Hz oscillation to spike activity. To examine the modulation of LFP-spike phase-locking by punishment risk, we compared the PLVs across different blocks. A trend toward reduction in PLV was found in block 3 compared with block 1 in mPFC (Figure 2-15c; Signed-rank test, $p$ = 0.077), and a significant reduction was found in VTA (Figure 2-15f; $p$ = 0.006). Likewise, the proportion of phase-locked units declined in block 3 compared with block 1 in both regions (Figure 2-15b & e; Chi-square test, mPFC, $\chi^2_1$ = 3.25, $p$ = 0.071; VTA, $\chi^2_1$ = 4.31, $p$ = 0.038). We examined VTA DA and non-DA neuronal phase-locking separately. Greater fraction of DA units (45 %) appeared to be phase-locked compared with non-DA units (23 %) in block 1 (Figure 2-15g; Chi-square test, $\chi^2_1$ = 5.04, $p$ = 0.025). The DA neuronal PLV in block1 significantly declined as a function of risk in block 2 & 3 (Figure 2-15h; Signed-rank test, $p$ values < 0.01), by contrast, the non-DA neuronal PLV did not differ across blocks ($p$ values > 0.43). These indicated that the punishment-induced reduction in the VTA neuronal phase-locking was predominated by the DA neuronal asynchrony.

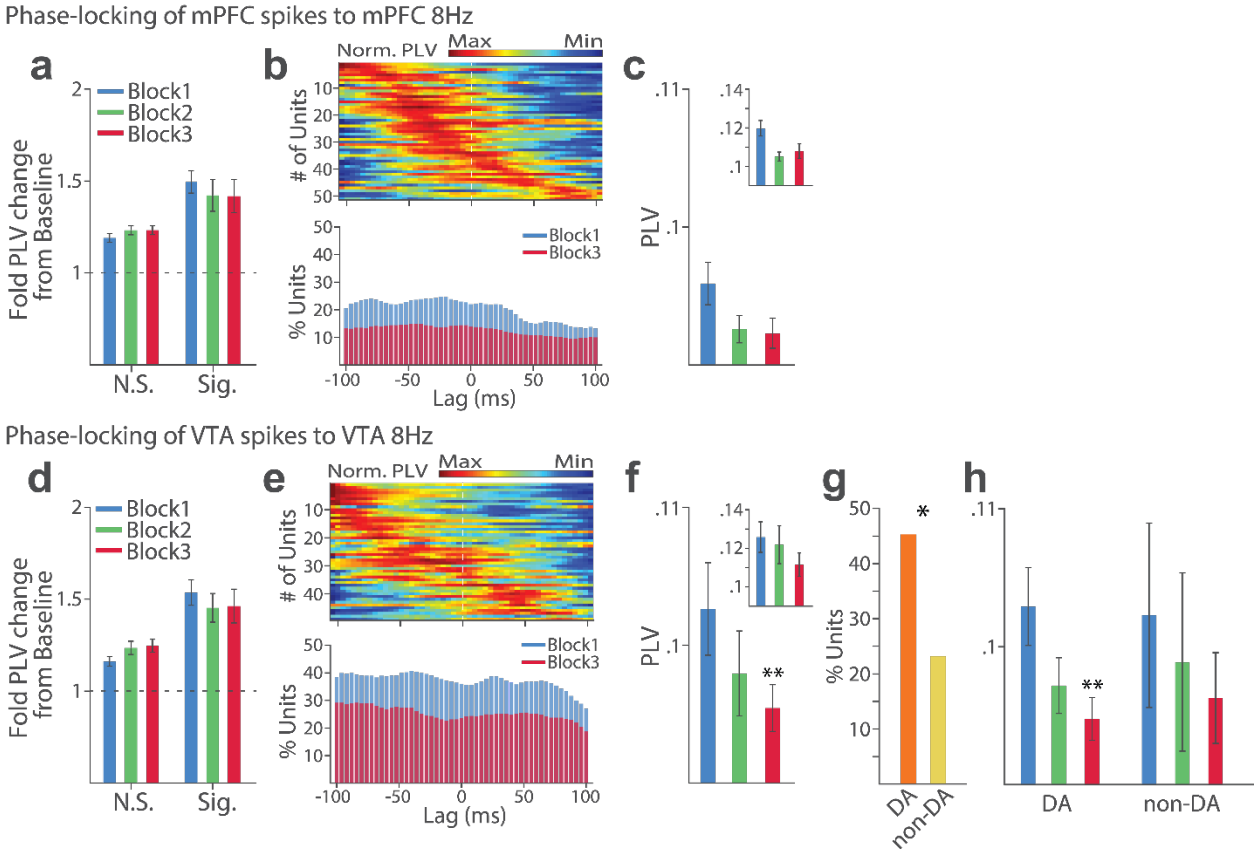


**Figure 2-15 Punishment risk declines mesoprefrontal neuronal synchrony to the local 8 Hz oscillation.**

(a-c) Modulation of mPFC neuronal synchrony to the mPFC 8 Hz oscillation by risk. (a) Fold change from baseline in the strength of the neuronal phase-locking during peri-action epoch in units that passed Rayleigh z-test (Sig.) and rest of the units (N.S.). (b) Top, Normalized PLVs in block 1 across a range of lags for all phase-locked mPFC units, aligned by peak lag. Bottom, Percentage of significantly phase-locked mPFC units in block 1 vs 3 across a range of lags. (c) Mean ± s.e.m. PLVs across different blocks. Inset, PLVs including significantly phase-locked units only. (d-h) Modulation of VTA neuronal synchrony to the VTA 8 Hz oscillation. (d) Fold change from baseline in the strength of the neuronal phase-locking. (e) Top, Normalized PLVs in block 1 for all phase-locked VTA units. Bottom, Percentage of significantly phase-locked VTA units. (f) Mean ± s.e.m. PLVs across different blocks. (g) Percentage of phase-locked VTA DA vs non-DA units. (h) PLVs of VTA DA and non-DA units plotted separately.

Next we examined the interregional LFP-spike phase-locking between VTA and mPFC. Based on the Granger causal influence indicating VTA-to-mPFC directionality in 8 Hz oscillations, we anticipated stronger mPFC neuronal synchrony to the VTA 8 Hz than that of the other direction. Consistent with this, we found that a substantial proportion of mPFC units (31 %) were phase-locked to the VTA 8 Hz oscillation in block 1. A representative mPFC unit with significant phase-locking is shown in Figure 2-16a-b. The interregional spike-phase synchrony emerged specifically during the action compared with the baseline (Figure 2-16c, Signed-rank test, $p$ values < 0.001). We examined directionality of the LFP-spike synchrony using the time-lagged phase-locking analysis. In block 1, the majority of phase-locked units had their peak PLVs with a negative lag (Figure 2-16d; Signed-rank test, $p$ = 0.066). Likewise, greater proportions of phase-locked units were observed on negative lags (Figure 2-16d). In addition, the mean PLV across negative time lags appeared to be greater than that of the positive lags (Figure 2-16e; Signed-rank test, $p$ = 0.023). These indicate mPFC neuronal entrainment to preceding VTA 8 Hz oscillatory cycles, i.e. VTA-to-mPFC directionality. When compared across blocks, the mPFC neuronal entrainment by the VTA 8 Hz declined as a function of risk (Figure 2-16e-g, Signed-rank test, $p$ = 0.003). As the degree of phase-locking diminished, the VTA-to-mPFC directionality also was obscured (Figure 2-16d-e). We also examined the VTA neuronal phase-locking to the mPFC 8 Hz. The degree of phase-locking appeared to be much weaker regardless of punishment risk in both DA and non-DA units, corroborating the VTA-to-mPFC directionality in the 8 Hz-mediated spike phase modulation (Figure 2-17).

In sum, we found a coherent 8 Hz oscillation temporarily synchronized the VTA-mPFC neural circuit during the risk-free action. This synchrony declined as a function of punishment risk. Analyses of no-shock control data showed unchanging mesoprefrontal synchrony across

blocks in the absence of punishment risk (Figure 2-18, 2-19), suggesting the mesoprefrontal asynchrony as a specific circuit state representing punishment contingent on the action.

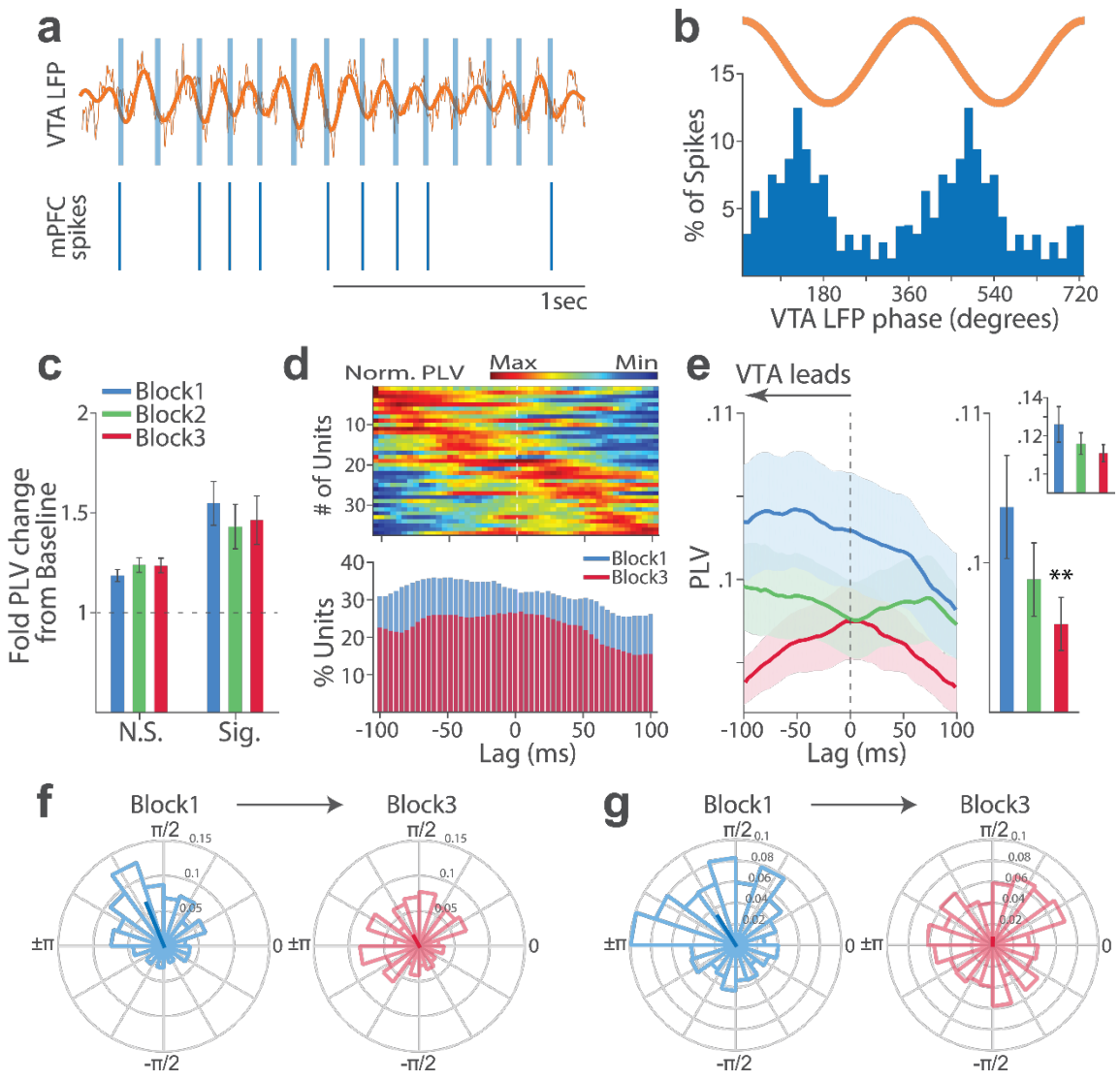


**Figure 2-16 Punishment risk declines mPFC neuronal synchrony to the VTA 8 Hz oscillation.**

(a) Top, Example raw (thin line) and bandpass filtered (heavy line) VTA LFP traces. Bottom, Neuronal spikes of a simultaneously recorded mPFC unit. This unit's preferred phase is indicated with light blue columns superimposed on LFP traces. (b) Distribution of spike-phase angles of the example mPFC unit relative to the VTA 8 Hz oscillation (Rayleigh's $p < 0.001$). (c) Fold change from baseline in the strength of mPFC neuronal phase-locking (PLV) during

the peri-action epoch in units that passed Rayleigh z-test (Sig.) and rest of the units (N.S.). PLVs were quantified by averaging 1,000 mean resultant lengths (MRLs) of the circular phase angle distribution comprising 100 resampled spikes at each iteration (Methods). (d) Top, Normalized PLVs in block 1 across a range of time lags for all phase-locked mPFC units, aligned by peak lag. Bottom, Percentage of significantly phase-locked units in block 1 vs 3 (e) Left, PLVs calculated with different time lags applied to spike trains relative to LFP time series. Right, Mean ± s.e.m. PLVs of all units across different blocks. Inset, PLVs including significantly phase-locked units only. (f-g) Each polar plot represents the distribution of spike-phase angles of an example mPFC unit in block 1 vs 3. To quantify the circular concentration of phase angles, we calculated the MRL indicated as a superimposed bar on each polar plot.

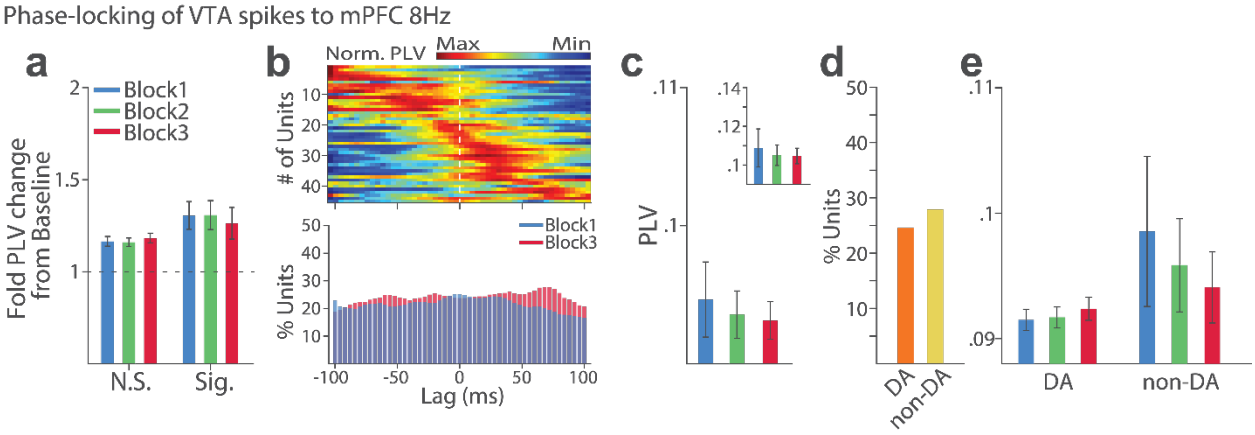


**Figure 2-17 VTA single units show weak phase synchrony to the mPFC 8 Hz oscillation.**

(a) Fold change from baseline in the strength of the neuronal phase-locking. (b) Top, Normalized PLVs in block 1 for all phase-locked VTA units. Bottom, Percentage of significantly phase-locked VTA units. (c) Mean ± s.e.m. PLVs across different blocks. (d) Percentage of phase-locked VTA DA vs non-DA units. (e) PLVs of VTA DA and non-DA units plotted separately.

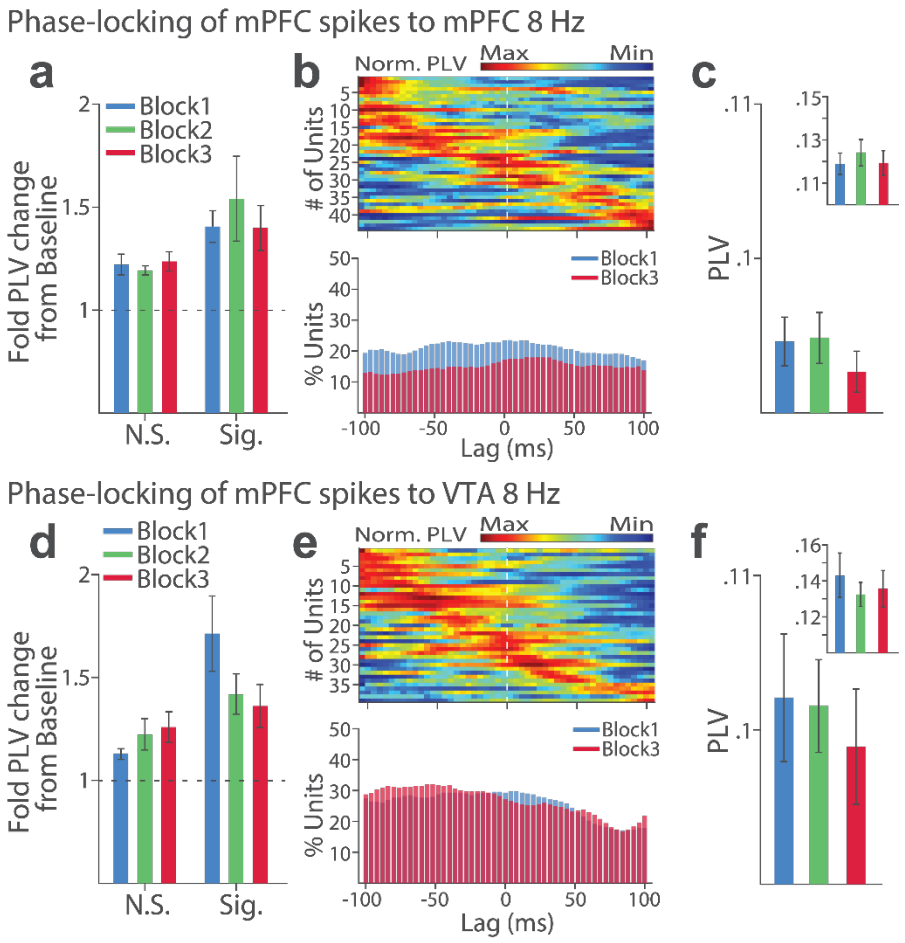


**Figure 2-18 mPFC neuronal synchrony to mPFC and VTA 8 Hz oscillations barely changes across blocks in the absence of punishment risk (No-shock control).**

(a-c) mPFC neuronal phase-locking to the mPFC 8 Hz oscillation. (a) Fold change from baseline in the strength of the neuronal phase-locking during peri-action epoch in units that passed Rayleigh z-test (Sig.) and rest of the units (N.S.). (b) Top, Normalized PLVs in block 1 across a range of time lags for all phase-locked mPFC units, aligned by peak lag. Bottom, Percentage of significantly phase-locked mPFC units in block 1 vs 3 across a range of lags. (c) Mean ± s.e.m. PLVs across different blocks. Inset, PLVs including significantly phase-locked units only. (d-f) mPFC neuronal phase-locking to the VTA 8 Hz oscillation. Conventions are same as above.

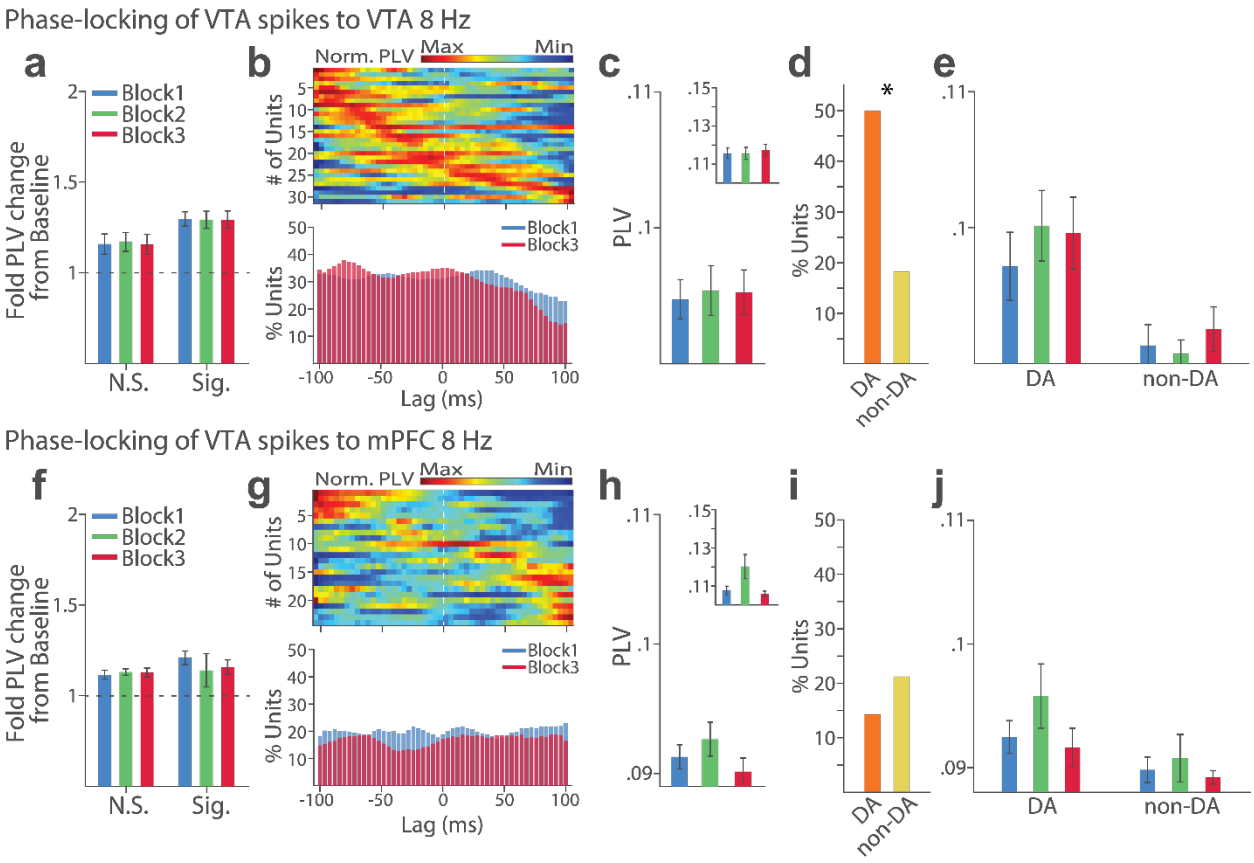


**Figure 2-19 VTA neuronal synchrony to VTA and mPFC 8 Hz oscillations barely changes across blocks in the absence of punishment risk (No-shock control).**

(a-e) VTA neuronal phase-locking to the VTA 8 Hz oscillation. (a) Fold change from baseline in the strength of the neuronal phase-locking during peri-action epoch in units that passed Rayleigh z-test (Sig.) and rest of the units (N.S.). (b) Top, Normalized PLVs in block 1 across a range of time lags for all phase-locked mPFC units, aligned by peak lag. Bottom, Percentage of significantly phase-locked mPFC units in block 1 vs 3 across a range of lags. (c) Mean ± s.e.m. PLVs across different blocks. Inset, PLVs including significantly phase-locked units only. (d) Percentage of phase-locked VTA DA vs non-DA units. (e) PLVs of VTA DA and non-DA units plotted separately. (f-j) VTA neuronal phase-locking to the mPFC 8 Hz oscillation. Conventions are same as above.

## 2.4 DISCUSSION

To unravel the VTA and mPFC neural representation of punishment risk contingent on a goal-directed behavior, we engaged animals in a risky reward-seeking task, wherein an instrumental action constantly procured a reward but probabilistically led to punishment. The majority of VTA and mPFC neurons encoded risk of punishment by modulating their firing rates as a function of risk. Likewise, risk of punishment at a given trial could be accurately decoded from both VTA and mPFC neuronal population activity. Further, the trial-by-trial neural population trajectories were significantly correlated with the trial-to-trial behavioral variability. These results demonstrate pronounced spike-rate mediated coding of punishment risk by the VTA and mPFC individual neurons and neuronal populations. At the neural circuit level, we found that punishment risk induced asynchrony between the two regions, as the coherent theta oscillation that emerged during the risk-free instrumental actions significantly declined as a function of risk. Together these findings suggest that the neural circuit comprising VTA and mPFC utilizes multiple layers of coding schemes including spike-rate and LFP-mediated neural synchrony codes to represent punishment risk contingent on a goal-directed behavior.

### 2.4.1 Individual neuronal encoding of punishment risk

Using a novel behavioral paradigm, we could model and systematically measure the anxiety-like changes in reward-seeking actions as a function of punishment risk contingent on the action. We demonstrated that the vast majority of individual VTA and mPFC neurons encoded punishment risk by modulating their firing rates. The individual neuronal encoding was most pronounced at

the time of the action, compared to the other task events, suggesting that the risk-encoding neurons represented contingency between the action and punishment.

Equivalent proportions of risk-encoding neurons in both regions encoded punishment risk by increasing or decreasing their peri-action firing rates. The sign (direction) of a neuron's response to punishment may inform its function in motivational control. While heterogeneous response patterns have been widely observed in PFC neuronal encoding of punishment (Kobayashi et al., 2006; Matsumoto et al., 2007; Seo and Lee, 2009; Ye et al., 2016), active debates are ongoing whether VTA DA neurons encode punishment with excitatory vs inhibitory responses (Bromberg-Martin et al., 2010; Schultz, 2016). The conventional theory and data suggest that the canonical RPE-coding DA neurons respond to appetitive vs aversive events with opposite signs by excitation and inhibition, respectively (Joshua et al., 2008; Matsumoto and Hikosaka, 2009; Schultz, 1998). We found that a subset of VTA DA neurons conformed to this pattern. These neurons responded to the risk-free (purely appetitive) action with phasic excitation, which was inhibited as a function of punishment risk. By contrast, a sizable proportion of DA neurons showed excitatory encoding of punishment risk, i.e., they treated appetitive and aversive components in the same direction, and responded to punishment risk with further excitation. Previous studies reported a subpopulation of DA neurons showing similar excitatory responses to appetitive and aversive stimuli (Brischoux et al., 2009; Joshua et al., 2008; Matsumoto and Hikosaka, 2009; Valenti et al., 2011). An integrating theory suggests that such dichotomous (bidirectional vs unidirectional) DA neuronal encoding of appetitive and aversive events may reflect different DA neuron groups conveying distinct motivational signals of an event (Bromberg-Martin et al., 2010). Punishment is an event of negative valence associated with avoidance, but of high salience deserving prioritized attention, and both aspects

of punishment need to be represented for a proper behavioral coping. Our observation of bidirectional encoding of punishment by equivalent proportions of VTA DA, non-DA, and mPFC neurons suggests that different neuron groups may convey distinct motivational properties of punishment.

### 2.4.2 Neuronal population encoding of punishment risk

We examined the population-level encoding of punishment risk in a neuronal population state space that captured patterns of activity co-modulation among the simultaneously recorded mPFC or VTA neurons on a trial-by-trial basis. This approach was motivated by the following reasons. First, we observed that different neuron groups represented punishment risk with bidirectional and time-varying activity modulations. This suggests that punishment may not be signaled simply as activation or inhibition of one specific type of neurons at one particular time point in the VTA-mPFC circuit. Rather, our data suggest that punishment should be represented as a net result of heterogeneous and time-varying activity modulations in the population of neurons. In this regard, simply averaging across neurons, time or trials may lead to significant loss of information. Second, we observed that animals varied their behavior trial-to-trial even within a block of the same degree of risk, and the behavioral variability was elevated as a function of punishment risk. Explaining the behavioral variability with the neural data may establish a stronger association between the behavioral and neural data. But we found that individual neurons were limited in representing the trial-to-trial behavioral variability. Thus, we intended to leverage the statistical power of the single-trial analysis by correlating the behavioral data with the neuronal population activity (Cunningham and Yu, 2014).

By examining the neural population trajectories, we confirmed that punishment risk was represented as distinct trial-by-trial neural population trajectories in both regions. Distinct trajectories manifested in a behaviorally relevant manner, as the trial-by-trial neural population trajectories were significantly correlated with the trial-to-trial behavioral variability in RT in all VTA and mPFC populations. Furthermore, in some neural populations the correlations with RTs appeared to be significant even when measured within each block of same risk. The behavioral and neural association at the population level was observed, even though the majority of single neurons failed to track the trial-to-trial RT variability. These findings suggest that the neuronal population activity tracked the punishment-based behavioral variation on a single-trial basis.

### 2.4.3 The degree of VTA-mPFC neural synchrony varies with punishment risk

At the neural circuit level, we observed that coherent theta oscillations synchronized the VTA and mPFC specifically during risk-free actions, effectively phase-modulating the neuronal spike activity in the two regions. Analyses of the temporal relationship indicated that the neural synchrony arose in the VTA-to-mPFC direction. That is, the VTA driven bottom-up theta oscillation entrained the mesoprefrontal LFPs and neuronal spike activity during the action in the absence of punishment risk. The theta oscillation preferentially entrained DA neurons but much fewer non-DA neurons in the VTA. Considering the phasic excitatory responses of the DA neurons during the action, the theta-oscillation-mediated neural synchrony may promote the phase-coupling between VTA DA and mPFC neurons specifically during the risk-free action. As the synchrony declined as a function of punishment risk, the phase-coupling might also collapse, resulting in a distinct pattern of DA transmission in the VTA-mPFC synapses during the risky action.

The mechanism underlying the theta rhythmogenesis is not clear yet. However, our data showing preferential DA neuronal phase-locking suggest the link between DA neuronal activity and the theta oscillation. In line with this, previous studies suggested that the DA neurotransmission is critical for theta oscillations in PFC. Blockade of D1 receptors in mPFC diminished theta oscillations (Parker et al., 2014). On the other hand, local infusion of dopamine in mPFC enhanced theta oscillations as well as the theta coherence between mPFC and hippocampus (Benchenane et al., 2010). In addition, theoretical models suggest that bursting of the VTA dopaminergic input onto the PFC may synchronize cortical oscillators (Buhusi and Meck, 2005). These evidences suggest that the theta oscillation mediated by DA neuronal activity and DA transmission in the mPFC may synchronize the VTA and mPFC during the risk-free reward-seeking actions.

When considering interregional LFP signals, it should be noted that field potentials in one brain region can be volume conducted through the brain tissue, and some LFP signals can be recorded far away from the source (Buzsaki et al., 2012). We demonstrated LFP-spike synchrony via phase-locking of the spike activity to both local and interregional 8 Hz oscillations. This argues against the possibility that the oscillation-mediated neural synchrony shown here is an artifact due to the volume conduction of the LFP oscillation occurring elsewhere. First, because neuronal spike activities are not subject to volume conduction artifacts, in addition the presence of LFP-spike phase-locking within each region show local relevance of the LFPs (Adhikari et al., 2010; Buzsaki et al., 2012). In addition, the theta-oscillation-mediated neural synchrony observed here may involve other mesocorticolimbic brain structures implicated in a reward-seeking behavior. In this regard, it is likely that the 8 Hz oscillation may be transmitted from VTA to mPFC indirectly via another brain region. This possibility can be hardly ruled out, unless

one monitors all possible connectivity simultaneously. However, our observation that a substantial proportion of mPFC neurons displayed a significant phase-locking to the VTA 8 Hz suggests that the neural synchrony may be mediated via the mesoprefrontal circuit.

The VTA-mPFC neural synchrony was predominantly mediated by the 8 Hz oscillation, which is distinguished from the 4 Hz oscillation in mPFC reported by recent studies during fear-conditioned freezing in synchrony with the amygdala (Dejean et al., 2016; Karalis et al., 2016a; Likhtik et al., 2014). Considering the distinct behavioral states associated with the 8 Hz vs 4 Hz oscillations in mPFC, these findings together suggest that the mPFC may be entrained by distinct bands of theta oscillations in appetitive vs aversive states. The fast vs slow mPFC theta oscillations may occur in preferential synchrony with VTA and amygdala in appetitive vs aversive states, thereby the bottom-up information transfer from the two subcortical regions can be routed depending on the behavioral context. This scenario would predict that the 8 Hz-mediated mesoprefrontal synchrony would diminish in the presence of punishment risk, whereas 4 Hz oscillation may arise in the mPFC. In accord with this, our results showed that the mesoprefrontal 8 Hz-mediated synchrony significantly declined as a function of risk. We did not observe the emergence of 4 Hz oscillation presumably because animals in our task engaged in instrumental actions unlike the fear conditioned animals that generated freezing for the most part. Entrainment of a neural circuit with varying frequency oscillations as a function of a task variable has been widely observed in sensory cortical circuits (Bosman et al., 2012; Jia et al., 2013). Such frequency modulation, along with the power modulation, could promote selection and binding of task-relevant neuronal ensembles to give rise to a functional neural network (Fries, 2015). Likewise, our data may reflect the rise and fall of coherent VTA and mPFC

neuronal ensembles that may promote a flexible control of instrumental behavior as a function of punishment risk.

In a broader perspective, the neural synchrony mediated by different theta bands in distinct behavioral states may also implicate neuron groups in the other mesocorticolimbic structures such as amygdala, nucleus accumbens and lateral habenula that are critical for appetitive and aversive behaviors. Mounting evidence suggests that distinct VTA and mPFC neuron groups within the same region selectively respond to appetitive vs aversive events (Lammel et al., 2012; Ye et al., 2016). Importantly, these studies have shown that the neuron groups differentially tuned for appetitive vs aversive events display discrepant patterns of input-output connectivity within the mesocorticolimbic system (Lammel et al., 2012; Ye et al., 2016). This projection specificity may be the foundation for the selective recruitment of distinct neuron groups in distinct-valence experiences. However, the anatomical connectivity alone may not be sufficient to bind the appetitively or aversively tuned neuron groups into a functional neural network in a timely manner. In this regard, the neural synchrony mediated by coherent oscillations may play a key role for the rise and fall of the functional neural networks depending on the behavioral context. While our data may provide a partial demonstration, future studies with simultaneous recording of multiple mesocorticolimbic structures would ultimately address the hypothesis that the neural synchrony mediated by distinct oscillations subserve the brain-wide formation of appetitive vs aversive neural networks in a behaviorally and timely relevant manner.

### 2.4.4 Conclusion

Signaling risk and its contingency on a stimulus and/or an action is a fundamental problem the brain needs to resolve to promote adaptive behavior and survival. Previous studies have implicated the mesoprefrontal neural circuit in this process by indicating general activation of this neural circuit or by stimulating this neural circuit resulting in aversive behavior. Our data further extend these findings by revealing dynamic coding schemes of the mesoprefrontal neural circuit in representing punishment and risk-based aversive behavioral modulation. In the clinical perspective, overcoming an excessive aversive behavior in the absence of commensurate threat is thought to be the key therapeutic goal in treating pathological anxiety. Our data suggest that the mesoprefrontal circuit can be a promising target for a circuit-based intervention. Particularly, recovering the synchronous theta oscillations in this circuit can be a viable approach with currently available tools for deep brain stimulation.

# 3.0 IMPACT OF ANXIETY ON FLEXIBLE RULE-BASED COGNITIVE CONTROL OF GOAL-DIRECTED BEHAVIOR AND ITS PFC NEURONAL CORRELATES

## 3.1 INTRODUCTION

Anxiety can be an adaptive reaction to stressful or unpredictable life events but it produces adverse cognitive effects that impede ongoing behavior and contribute to clinical manifestation of anxiety disorders (Bishop, 2007; Eysenck et al., 2007). Anxiety also is one of the more debilitating symptoms of psychiatric disorders including post-traumatic stress disorder, obsessive-compulsive disorder, mood disorders, schizophrenia and autism (Hamilton et al., 2014; Luthi and Luscher, 2014; Owens et al., 2005; Ruglass et al., 2014; Solomon et al., 2008). In addictive disorders, for example, co-morbidity with anxiety, as well as the anxiety associated with drug withdrawal during abstinence, are major contributing factors to relapse (Luthi and Luscher, 2014; Ruglass et al., 2014).

Human behavioral and imaging investigations have described a complex impact of anxiety on prefrontal cortex (PFC)-related cognitive functions including deficits in flexible control of behavior (Bishop, 2007; Eysenck et al., 2007; Shin et al., 2001). Multiple models have been proposed for proper coping or pathological response to anxiety (Adhikari, 2014; Ouimet et al., 2009; Robinson et al., 2013) and stress (Arnsten, 2009; Hains and Arnsten, 2008). However,

the impact of anxiety on spontaneous and phasic activity of PFC neuronal ensembles during cognitive-behavioral performance is largely unknown.

Animal electrophysiological studies of PFC neurons during anxiety have focused primarily on fearful or avoidance behaviors (Adhikari et al., 2010, 2011; Burgos-Robles et al., 2009; Sotres-Bayon et al., 2004). While these studies have informed us about the representation of fear-related events such as freezing behavior, anxiety is not limited to a rapid neuronal or behavioral event, but often is an enduring state that is sustained for many minutes to hours. More importantly, the negative impact of anxiety extends beyond an aversive feeling and influences ongoing goal-directed behaviors that utilize cognitive and affective processing at the service of cognitive flexibility.

We sought to determine the impact of a sustained anxiety state on PFC neural processing of a behavior that involved cognitive flexibility. The anxiety state was induced by a pharmacological model with excellent clinical validity. Specifically, extensive literature indicates that inverse agonists of allosteric benzodiazepine binding sites in $GABA_A$ receptors, such as FG7142, produce anxiety-like physiological, neurochemical and behavioral effects in rodents (Evans and Lowry, 2007), primates (Murphy et al., 1996a; Murphy et al., 1996b; Ninan et al., 1982) and humans (Dorow, 1987). We combined this experimental model of anxiety with unit recording in two subregions of the PFC with particular importance for cognitive control and emotional regulation: the dorsomedial and orbitofrontal PFC (dmPFC and OFC) (Darrah et al., 2008; Durstewitz et al., 2010; Floresco et al., 2008; Lee, 2013; Likhtik et al., 2014; Schoenbaum et al., 2009; Stefani and Moghaddam, 2005). We assessed the impact of FG7142 on spontaneous activity of dmPFC and OFC neurons while rats freely moved in their home cage during wake cycle and while they engaged in a rewarded extradimensional set-shifting task. The task, similar

to other rodent set-shifting tasks, required rats to guide their instrumental behavior based on two rules involving distinct perceptual dimensions, and switch between the rules. This particular task has been well characterized (Darrah et al., 2008; Floresco et al., 2008) and was selected for its feasibility for multiple extradimensional shifts within each session with electrophysiological recordings.

We found that the anxiogenic treatment induced sustained suppression of the spontaneous activity of subpopulations of dmPFC and OFC neurons. During task performance, this treatment produced modality-specific behavioral impairment that correlated with reduced recruitment of dmPFC, but not OFC, neurons that encode conflict related actions.

## 3.2 METHODS

### 3.2.1 Subjects and surgical procedure

Male Sprague Dawley rats (~400 g, Harlan) were singly housed on a 12 h light/dark cycle (lights on at 7 p.m.). All data were collected during the dark cycle. Animals were not previously exposed to any drugs or behavioral training. Microelectrode arrays were implanted in the dmPFC and contralateral OFC or bilateral dmPFC (home cage; n = 11, set-shifting task; n = 8 rats) of isoflurane-anesthetized rats, and secured with dental cement for chronic recording. The following coordinates (Paxinos and Watson, 1998) were used (relative to bregma): dmPFC (home cage) = 3.0 mm anterior, 0.7 mm lateral, 2.2 mm ventral from skull; dmPFC (set-shifting task) = 3.0 mm anterior, 0.7 mm lateral, 4 mm ventral; OFC (home cage and set-shifting task) =

3.0 mm anterior, 3.3 mm lateral, 4.5 mm ventral. Recording sessions began after one week of postoperative recovery. At the completion of all recordings, rats were anesthetized with 400 mg/kg i.p. chloral hydrate and perfused with saline and 10 % buffered formalin. Coronal slices of PFC were collected from each brain and cresyl-violet stained. Placements of electrode arrays were confirmed via light microscope. All procedures were in accordance with the National Institute of Health's Guide to the Care and Use of Laboratory Animals, and were approved by the University of Pittsburgh Institutional Animal Care and Use Committee.

### 3.2.2 Experimental design

#### 3.2.2.1 Home-cage recording

In a home cage recording experiment, single-unit activity was recorded from a freely moving rat in a clear polycarbonate home cage with bedding. After 30 min of baseline recording, each rat received an i.p. injection of FG7142 (5 or 10 mg/kg in vehicle) or 1.0 ml/kg vehicle (one drop tween 80 in 10 ml distilled water). Neuronal activity was recorded for 120 min after injection. The order of injections was randomized across rats with at least 3 days of washout period between injections.

#### 3.2.2.2 Set-shifting task

In a set-shifting experiment, a rat received an i.p. injection of vehicle, 5 or 10 mg/kg FG7142. Ten minutes were allowed after the injection before placing the rat in the operant chamber. After a 3 min habituation period in the chamber, the task was initiated. The order of injection was randomized for each rat with at least 3 days of washout period before the next injection.

### 3.2.3 Training and testing of the set-shifting task

Rats were placed on a restricted diet of 13g of food/rat/day with free access to water to maintain approximately 85 % of their free-feeding weight. Rats were trained on an extra-dimensional set-shifting task that requires instrumental action according to two discrimination rules, each involving a distinct perceptual dimension, spatial position and a light cue (Figure 3-2a). For training parameters and detailed characterization of this task, see Darrah et al (2008). Both perceptual dimensions in this task involve a light cue presented at one of the two cue ports. Performance according to the 'Light' discrimination rule (light rule) requires a nose poke to the illuminated cue port, regardless of its spatial location for a reward pellet (Figure 3-2a). Performance according to the 'Side' discrimination rule (side rule) requires a nose poke to the cue port at a designated spatial location (valid side; left or right), regardless of illumination (Figure 3-2a). In side rule trials, the light cue was presented in the pseudo-randomly selected side to ensure that the cue was presented at each side no more than two consecutive trials. Rats were trained on an initial rule (dimension) to a performance criterion of ten consecutive correct (rewarded) responses, and then immediately switched to the alternate rule.

After pre-training, rats were trained daily on the set-shifting task, being required to shift their response patterns between the light and side rules. Each session consisted of four sets. The first set was pseudo-randomly assigned with either light or side rule. After ten consecutive correct responses, the next set with the alternate rule commenced. Set-shifting was not explicitly signaled, thus rats had to learn it by trial and error based on delivery or omission of the reward. A successful training session consisted of 4 sets completed in 90 min. For the counterbalancing of the poke direction, the light cue was not presented in the same port more than twice. In addition, each session included two side rule sets using right and left ports as the valid side, thus

the side rule trials included equivalently mixed right- and left-poking trials. After establishing stable baseline performance (at least 3 consecutive successful sessions), rats were subjected to electrode implantation surgery. The first recording was initiated only after the recovery of the stable baseline performance.

In each trial, a correct response was rewarded with a sugar pellet, while an incorrect response was not rewarded. Occurrence of an incorrect response reset the number of consecutive trials to zero. Immediately after each response, the food trough in the opposite wall of the chamber was illuminated, regardless of the accuracy of response, until rats poked to the trough to end the trial. After 10 s inter-trial interval, the next trial was initiated as the light cue was turned on.

### 3.2.4 Electrophysiology

Single unit activity was recorded simultaneously via bilateral eight-channel Teflon-insulated stainless steel 50 μm microwire arrays (NB Laboratories, Denison, TX). Unity-gain junction field effect transistor headstages were attached to a headstage cable and commutator nonrestrictive to the animals' movement. Signals were amplified via a multichannel amplifier (Plexon, Dallas, TX). Spikes were bandpass filtered between 220 Hz and 6 kHz, amplified 500× and digitized at 40 kHz. Single unit activity was then digitally high-pass filtered at 300 Hz and LFP were low-pass filtered at 125 Hz. Threshold crossing spike waveforms were stored for offline analysis. Single units were sorted using the Offline Sorter software package (Plexon). Single unit activity was further analyzed only if the unit displayed a stable waveform throughout the recording session. To prevent analysis of the same unit recorded on different channels, we examined cross-correlograms. If a unit presented a peak of activity at the time of the reference

unit's firing, only one of the two was further analyzed. Because each animal was allowed at least 3 days of washout between recording sessions, we treated units recorded in different sessions as different units despite the fact that the same unit may have been serially recorded. This approach allowed for the most conservative assessment of unit identity. Units meeting these criteria were used in all single unit analyses. We did not exclude putative fast-spiking interneurons from our samples. Only 1.9 % of total units displayed the mean firing rates higher than 20 Hz.

### 3.2.5 Neural data analysis for the home cage recording

Analyses of single unit data were conducted with Matlab (MathWorks) and SPSS statistical software (IBM). The drug-free baseline period was 27 min consisting of 9 × 3-min bins, and the post-injection period was 108 min of 36 × 3-min bins. Each unit's activity in the baseline and post-injection periods was Z-score normalized using the mean and the standard deviation of the baseline firing rate. Differences in baseline firing rate between dose groups were assessed with the Kruskal–Wallis test. Two-way repeated-measures ANOVA was used to assess the effects of dose, time period and their interaction on the population activity. Post hoc analyses with Bonferroni correction were used for between- and within- dose group comparisons subsequently. For all tests, the Greenhouse–Geisser correction was applied as necessary. All statistical tests were specified as two-sided.

To examine how the FG7142-induced inhibitory effect on population activity was manifested in individual units, each unit was classified based on modulation of its post-injection activity. For classification, the upper and lower bounds of the 95 % confidence interval of the normalized activity was used (Homayoun and Moghaddam, 2007). Units crossing the upper or lower bound in 3 consecutive 3-min bins were classified into the 'Activated' or 'Inhibited'

subgroup respectively. Units that satisfied both criteria in different time bins were grouped as 'Bidirectional.' The remaining units were labeled as 'No-change.' The distribution of units in these subgroups was compared between dose groups using the fisher's exact test. All α levels were set to 0.05.

### 3.2.6 Behavioral data analysis for the set-shifting task experiment

All behavioral performance measures – the numbers of trials to criterion, errors, percent of correct trials and reaction time – were quantitated including all corresponding trials. For all eight rats, a binomial test (one-tailed) was used to examine whether each rat performed the task significantly above the chance level. One-way ANOVA was used to assess the dose effect on total trials and time to complete the task. Two-way repeated-measures ANOVA was used to examine the effect of dose, rule and their interaction on the number of trials to criterion, the number of errors, the percent of correct trials, and the reaction time for action or food trough entry. Post hoc tests utilized the Bonferroni procedure.

### 3.2.7 Neural data analysis for the set-shifting task experiment

#### 3.2.7.1 Baseline and peri-action activity analysis

To examine how FG7142 affected the baseline neuronal activity during task performance, the firing rate of each unit was measured within the 3 s window beginning 3.5 s before each trial onset, averaged across trials, and compared across dose groups. To assess the individual neuronal activity within peri-action time periods, each unit's firing rate was computed in 50 ms bins within the peri-action windows (-2 to 2 s relative to the action occurring at time = 0). The firing

rate of each unit was averaged across trials. The trial-averaged firing rate of each unit was Z-score normalized to that of its baseline period. Units were categorized as 'Activated' or 'Inhibited' within pre- (-2 to 0 s) and post-action (0 to 2 s) relative to the action occurring at time = 0 periods, if their average normalized activity contained two or more consecutive 50 ms bins with $Z > 1.96$ or $Z < -1.96$, respectively. The remaining units were categorized as 'No-change.' These criteria were validated using a bootstrap analysis on the baseline period (a 2 s window beginning 2.5 s before the trial onset) of each unit. For each unit, the baseline window was randomly sampled with replacement 10,000 times. The proportion of 2 s windows that resampled activity reached the significance criteria is a measure of the expected false-positive rate for that unit during any 2 s window. The expected false-positive rate was $\alpha = 0.0023$. Differences in the distribution of neuronal responses (activated, inhibited or no-change) between dose groups were assessed with Fisher's exact test. The normalized population activity in the pre- or post-action period was compared across dose groups, using one-way ANOVA.

#### 3.2.7.2 Linear regression analysis

A multiple linear regression model was used to investigate how each unit encoded task-relevant information. The following multiple linear regression model was used:

$$Spike\ Count\ = \beta_0 + \beta_1 \mathrm{TR(t)} + \beta_2 \mathrm{R(t)} + \beta_3 \mathrm{R(t-1)} + \beta_4 \mathrm{D(t)} + \beta_5 \mathrm{D(t-1)} + \beta_6 \mathrm{RT(t)}$$

where TR(t) represented the task rule on trial t (0 if light, 1 if side), R(t) is the response outcome on trial t (1 if correct, 0 if incorrect), R(t-1) is the previous response outcome on trial t-1 (1 if correct, 0 if incorrect), D(t) is the poke direction on trial t (1 if right, 0 if left), D(t-1) is the poke direction on trial t-1 (1 if right, 0 if left), RT(t) is the reaction time on trial t (1 if high, 0 if medium, -1 if low latency, for each animal). To investigate the neural representation of the task rule specifically in CF trials, we used a slightly modified regression model (below) in which we

selected CF trials in both side and light rule sets, and then examined the encoding of CF trials of one rule, relative to the trials of the other rule.

$$Spike\ Count\ = \beta_0 + \beta_1 \mathrm{TR(t; CF)} + \beta_2 \mathrm{R(t)} + \beta_3 \mathrm{R(t-1)} + \beta_4 \mathrm{D(t)} + \beta_5 \mathrm{D(t-1)} + \beta_6 \mathrm{RT(t)}$$

where TR(t; CF) represented CF trials of one rule (1) and all trials of the other rule (0), and all the other terms were represented identically as in the above regression model. Initial trials of each set were excluded from the regression analysis to ensure that rats were aware of the set-shifting. Both correct and incorrect trials after the 5$^{th}$ correct response of each set were included. The regression analysis was conducted for the spike count of each unit, in a window of 1-s width that slides in steps of 0.2 s within the range of 2 s before and after the instrumental action. Units that had 1) three or more consecutive or 2) four or more sliding windows with significant coefficients ($p < 0.05$, based on the t-test) for each covariate ($\beta_1$ to $\beta_6$) during the peri-action time period of interest were considered to encode the corresponding variable. The stringency of this criterion was verified by calculating the false-positive rate when the regression was performed on bootstrap resampled trials (1,000 samples; the expected false-positive rate < 0.05). To compare the proportions of units signaling trial types, current or previous response outcome between dose groups, Fisher's exact test was used.

To investigate how the dmPFC neural representation of the task rule evolved from early to late phases of a set, trials in each session were divided into two subsets, one comprising the 1$^{st}$ half of the trials in each set and the other comprising the 2$^{nd}$ half of the trials. We then quantified the neuronal selectivity for the two rules using a sliding receiver operating characteristic (ROC) analysis (Figure 3-8c). The area under the ROC curve was utilized as an index of neuronal selectivity. A value of 0.5 was indicative of no selectivity between two conditions, whereas a value of 1 was interpreted as complete discriminability. ROC values were calculated with a

sliding 0.4 s window in 0.2 s steps. The peak ROC values in the pre-action period were used for comparison. A ROC analysis also was applied to the rule-encoding dmPFC units to quantify their discriminability of the rule in side CF and light CF trials (Figure 3-10c).

#### 3.2.7.3 Population decoding analysis

After examining the individual neuronal encoding of task variables, we quantified the population level coding using a Poisson naïve Bayes classifier. In general, this decoding method works by training the classifier to "learn" which patterns of neural activity are indicative of particular task conditions (e.g., which is the current rule). In the training phase, the association of different patterns of neural activity with different task conditions is learned from a subset of data (training set). In the test phase, the reliability of the association is then assessed with a separate set of data (test set) based on how accurately the classifier can predict the present task conditions.

For training and testing, we used a cross-validation procedure with the following steps. (1) For each neuron, data from 20 trials were randomly selected for each of the 2 conditions (e.g. light and side rules). For each of these trials, data from all neurons were concatenated to create a pseudo-population response vector (i.e., neurons that were recorded under the same conditions but in separate sessions were treated as if they had been recorded simultaneously). (2) These pseudo-population vectors are grouped into 20 splits of the sampled data, with each split containing one pseudo-population response vector for each task condition. (3) A classifier was trained using 19 splits of the data, and tested with the remaining split. This procedure was repeated 20 times, leaving a different split at each time (i.e., a 20-fold leave-one-split-out cross-validation was used) (Meyers et al., 2012). This procedure (steps 1-3) was repeated 50 times for each 200-ms window sliding in steps of 50 ms within the 4-s peri-action period.

Specifically in each repetition, we have a Poisson likelihood function given by

$$P(\underline{x}_t|C_k) = \prod_{i=1}^{D} \frac{\lambda_{ki,t}^{x_{i,t}} e^{-\lambda_{ki,t}}}{x_{i,t}!}$$

where $\underline{x}_t$ is a pseudo-population vector of spike counts at $t^{th}$ sliding window within a trial, $C_k$ indicates a particular rule (side or light) or a response outcome (correct or incorrect response), and thus $k$ takes on either 1 or 2. $i$ indicates unit label, 1 to $D$. $\lambda_{ki,t}$ is the parameter for the Poisson distribution estimated by the following:

$$\lambda_{ki,t} = \frac{1}{N_k} \sum_{n \in C_k} x_{ni,t}$$

The posterior probability of a particular rule or an outcome given the spike count vector is provided by Bayes' theorem:

$$P(C_k|\underline{x}_t) = \frac{P(\underline{x}_t|C_k)P(C_k)}{P(\underline{x}_t)}$$

We assumed a flat prior probability, and thus $P(C_k)$ is a constant. Hence, the classifier predicts the task condition with maximum probability given the pseudo-population activity.

$$\widehat{C_k} = argmax_k P(\underline{x}_t|C_k)$$

The result of population decoding analysis was quantified as the percentage of correctly predicted test splits, which we termed as "decoding accuracy." The mean and standard deviation of decoding accuracy were calculated across the scores of 50 re-sampling procedure.

To examine whether there are dynamic temporal patterns in the dmPFC neuronal signaling of the task rule, i.e. do the neurons encode the task rule differentially at different times, we ran a temporal-cross-training analysis (Meyers et al., 2012) (Figure 3-9c-e). In this analysis, a classifier is trained with data from one time point and then tested on data from different trials

that were taken either from the same time period or a different time period, using the same steps (1-4) described above.

### 3.2.8 Behavioral testing on the elevated plus maze

Although numerous previous reports have established the anxiogenic effects of FG7142 (Atack et al., 2005; Cole et al., 1995; Pellow and File, 1986), we assessed the effect of FG7142 versus vehicle on the elevated plus maze (EPM) to ensure that a similar effect is replicated in our hands. Ten minutes after injection, rats were transported into the testing room and placed on the center of the EPM with their heads facing an open arm. The experimenter then left the room and the rat's behavior was video recorded for 5 min. The EPM consisted of two open arms (45 × 10 cm) with transparent 1-cm-high edging, and two closed arms (45 × 10 × 48 cm) diverging from a common central platform (10 × 10 cm) elevated 90 cm above the floor. Video records were analyzed using an automatic video tracking software (ANY-maze, Stoelting, Wood Dale, IL) to quantify (1) time spent in the open arms, closed arms or center platform, (2) number of entries made into open and closed arms and (3) total distance traveled on the maze. These measures were compared between vehicle and FG7142-injected groups using independent-samples t test.

## 3.3 RESULTS

### 3.3.1 Inhibitory effect of FG7142 on PFC neuronal population activity

In total, 138 dmPFC and 184 OFC units were recorded from histologically verified electrodes of 11 freely behaving rats in home cages (Figure 3-1a); the mean baseline firing rate before administration of drug was 5.67 ± 0.50 Hz in dmPFC and 4.47 ± 0.35 Hz in OFC. There was no difference in these levels across dose groups in either subregion (Kruskal–Wallis test, dmPFC; $\chi^2_2 = 3.32$, $p = 0.19$, OFC; $\chi^2_2 = 2.03$, $p = 0.36$).

We examined the impact of doses of FG7142 (5 and 10 mg/kg) that produces physiological, neurochemical and cognitive deficits (Evans and Lowry, 2007; Mikkelsen et al., 2005; Murphy et al., 1996b; Pehrson et al., 2013) without inhibiting the animals' motor abilities. Treatment with FG7142 (10 mg/kg i.p.) reduced the spontaneous firing rate of subpopulations of dmPFC and OFC units (Figure 3-1b-e). We quantified the impact of FG7142 on both population activity (Z-score) and on individual units. For the latter, units that fired significantly below or above pre-injection baseline in 3 consecutive 3-min bins were classified as 'Inhibited' and 'Activated.' Units that were both inhibited and activated were classified as 'Bidirectional.' The remaining units were classified as 'No-change.' In the dmPFC, a significant interaction between dose group and time period was observed (Two-way repeated measures ANOVA, $F_{2, 135} = 8.58$, $p < 0.001$). Both 5 and 10 mg/kg doses of FG7142 suppressed population activity compared to baseline or vehicle (Figure 3-1f; post hoc test, $p$ values < 0.01). A substantial proportion of units inhibited, whereas fewer units increased or bidirectionally modulated their firing rates. The distribution of units in inhibited, activated and bidirectional subgroups was significantly different

from that of vehicle units (Figure 3-1g; Chi-square test, 5 mg/kg; $\chi^2_3 = 10.61$, $p = 0.014$, 10 mg/kg; $\chi^2_3 = 17.51$, $p = 0.0006$). OFC population activity was suppressed by FG7142 in a similar manner. A significant interaction between dose group and time period was detected (Two-way repeated measures ANOVA, $F_{2, 179} = 8.39$, $p = 3.0 \times 10^{-4}$). FG7142 at 5 mg/kg significantly suppressed population activity compared to baseline or vehicle (Figure 3-1h; post hoc test, $p$ values < 0.0001). A significant suppression was observed compared to that of the baseline (post hoc test, $p = 0.009$), as well as a trend toward suppression compared to that of vehicle injection (post hoc test, $p = 0.07$) after 10 mg/kg injection. A substantial proportion of units inhibited their activity, and the distribution of inhibited, activated and bidirectional subgroups was significantly different from that of vehicle units (Figure 3-1i; Chi-square test, 5 mg/kg; $\chi^2_3 = 17.42$, $p = 0.0006$, 10 mg/kg; $\chi^2_3 = 9.56$, $p = 0.023$). In both dmPFC and OFC, we verified that the interactions between dose group and time period were significant, when examined using the raw firing rates without Z-score normalization (Two-way repeated measures ANOVA, dmPFC; $F_{2, 135} = 3.16$, $p < 0.05$, OFC; $F_{2, 179} = 10.21$, $p < 1.0 \times 10^{-4}$). Similarly in both regions, we observed significant suppression of the raw population activity from the baseline after 5 or 10 mg/kg injection of FG7142 (post hoc test, $p$ values < 0.003).

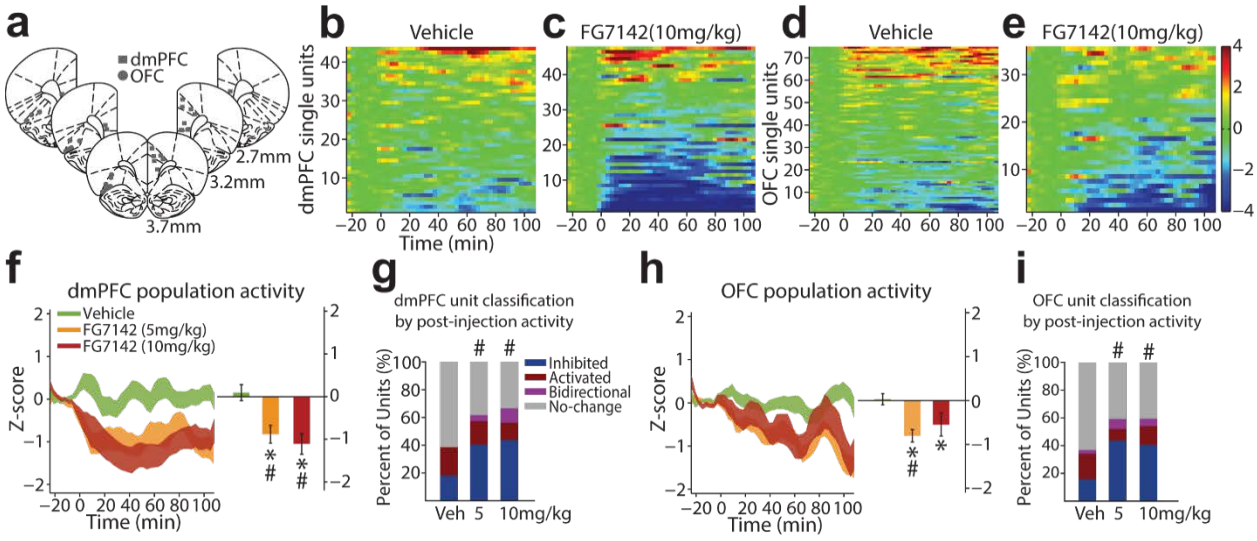


**Figure 3-1 Modulation of PFC single unit and population activity by FG7142.**

(a) Histologically verified placements of dmPFC (squares) and OFC (circles) electrodes used for home cage and set-shifting task recording. (b-c) The baseline-normalized activity (Z-score) of all dmPFC single units before and after vehicle (b) or 10 mg/kg FG7142 (c) injection. Baseline activity is normalized to zero, and injection occurred at time = 0. Each row depicts activity of an individual unit arranged by direction and magnitude of activity change. The number of units (n) and rats (N); vehicle n = 44, N = 8; 5 mg/kg n = 47, N = 7; 10 mg/kg n = 47, N = 7. (d-e) The baseline-normalized activity of all OFC single units; vehicle n = 76, N = 9; 5 mg/kg n = 71, N = 10; 10 mg/kg n = 37, N = 8. (f) Left, The normalized dmPFC population activity before and after FG7142 or vehicle injection, displayed as mean ± standard error (shaded area). Right, The mean population activity averaged across the entire post-injection period. Asterisks and number signs (#) indicate statistically significant difference compared to pre-injection baseline and vehicle, respectively. Error bars indicate standard errors. FG7142 injection led to suppression of the population activity, compared to the pre-injection baseline or the vehicle control. (g) Proportion of dmPFC units classified based on the post-injection activity. A number sign indicates significant difference in the distribution of classified units, compared to the vehicle. Increased proportions of FG7142 injected units were classified as inhibited compared to vehicle units. (h) The normalized OFC population activity and the mean population activity during the post-injection period. (i) Proportion of OFC units classified based on the post-injection activity.

### 3.3.2 Impact of FG7142 on set-shifting task performance

We investigated changes in dmPFC and OFC neural correlates that may underlie alterations in cognitive behavior in anxiety. Rats were trained in an operant set-shifting task (Darrah et al., 2008). This task demands a high cognitive load and requires rule-based control of instrumental behavior by requiring rats to discriminate between two rules, each involving a distinct perceptual dimension: spatial location and a light stimulus (Figure 3-2a). Thus the task requires rats to form associations between a stimulus, a response and an outcome for each rule, and then flexibly switch between the two rules based on the response outcome. Animals were trained before electrode implantation to successfully perform 3 consecutive extradimensional shifts per test session, with sets pseudo-randomized for each session. Stable baseline performance (3 consecutive successful sessions) was reached in 18 ± 3.0 training sessions. Performance remained consistent after the surgical implantation of electrode arrays (Total trials; One-way ANOVA, $F_{1, 14} = 0.44$, $p = 0.52$, Total time; One-way ANOVA, $F_{1, 14} = 0.53$, $p = 0.48$, The number of trials to criterion; Two-way repeated measures ANOVA, $F_{1, 14} = 1.74$, $p = 0.21$, The number of errors; Two-way repeated measures ANOVA, $F_{1, 14} = 1.58$, $p = 0.23$).

Systemic injection of FG7142 did not impede the ability of animals to engage in, and to complete the set-shifting task. Animals performed well above the chance level (binomial test, $p$ values $< 2.32 \times 10^{-7}$) and did not display overt performance impairment. The number of total trials required to complete the task, i.e., to perform three consecutive extradimensional shifts, was similar across vehicle and dose groups (Figure 3-2b; One-way ANOVA, $F_{2, 21} = 1.28$, $p = 0.30$). Total time taken to complete the task also was not significantly different across groups (Figure 3-2b; One-way ANOVA, $F_{2, 21} = 1.91$, $p = 0.17$). This allowed us to move forward with

analyzing specific aspects of rule-dependent performance without confounding effects of the anxiogenic treatment producing motor and indiscriminate cognitive impairments. We then compared the number of trials to criterion (10 consecutive correct trials) in the light- and side-rule sets across dose groups. A significant interaction between dose and rule was found, as rats that received FG7142 reached the criterion with fewer trials in the light rule, but with more trials in the side-rule sets compared to when they received vehicle injection (Figure 3-2c; Two-way repeated measures ANOVA, $F_{2, 21} = 4.26$, $p = 0.028$, post hoc test, 10 mg/kg, $p = 0.012$). The rule-dependent modulation of performance was echoed in the number of errors. A significant interaction between dose and rule was found with the number of errors in side-rule sets increasing, and that of the light-rule sets decreasing after FG7142 injection (Figure 3-2d; Two-way repeated measures ANOVA, $F_{2, 21} = 5.93$, $p = 0.009$; post hoc test, 10 mg/kg, $p < 0.001$). Similar numbers of trials to criterion and errors were detected in the side- and light-rule sets during performance after vehicle injection (post hoc test, vehicle, $p$ values > 0.21).

Performance during the side-rule sets was further subtyped based on correspondence between illuminated and correct side (Figure 3-2a bottom right). Specifically, in approximately half of the pseudo-randomly selected side-rule trials, the correct choice was the illuminated side [non-conflict (NCF) trials], whereas the incorrect choice side was illuminated in the rest of the trials [conflict (CF) trials]. Trials in the light-rule set also were subtyped based on correspondence between illuminated and previously correct side (Figure 3-2a bottom left). In about half of the light-rule trials, a light cue was presented in the previously correct side (NCF trials), whereas the light cue was presented in the previously incorrect side in the other half of the trials (CF trials). A significant effect of trial type was found on the percent correct, indicating distinct performance depending on trial types (Figure 3-2e; Two-way repeated measures

ANOVA, $F_{3, 63} = 172.15$, $p < 1.0 \times 10^{-4}$). As expected, animals' performance was more prone to errors in CF trials compared to NCF trials especially during the side-rule trials (Figure 3-2e; post hoc test, $p$ values < 0.032). Treatment with FG7142 significantly modified the error rates in the side CF trials. A significant interaction between dose and trial type was found ($F_{6, 63} = 4.05$, $p = 0.002$), and post hoc analysis revealed that the percent correct in the side-rule CF trials was lower during performance after 10 mg/kg injection, compared to that of vehicle injection (Figure 3-2e; post hoc test, $p = 0.049$). Percent correct in light CF trials was higher than that of side CF trials, and did not differ across dose groups (Figure 3-2e; post hoc test, $p$ values > 0.18). Performance in NCF trials was equivalent (side rule) or even greater (light rule) after FG7142 injection. Collectively, these performance patterns indicate that anxiety induces a response bias toward the light cue, leading to increased distractibility by the irrelevant cue in the side rule, but equivalent or even enhanced performance in light-rule trials. Reaction time (RT), the latency from the cue onset to the action (nose poke), also was measured separately for each trial type. In all trial types, RT trended toward a dose-dependent increase, but did not significantly differ across dose groups (Figure 3-2f; Two-way repeated measures ANOVA, post hoc test, $p$ values > 0.06). The latency for reward retrieval was similar across dose groups, indicating that the increase in RT is not associated with indiscriminate changes in locomotion or motivation for reward (Two-way repeated measures ANOVA, post hoc test, $p$ values > 0.9).

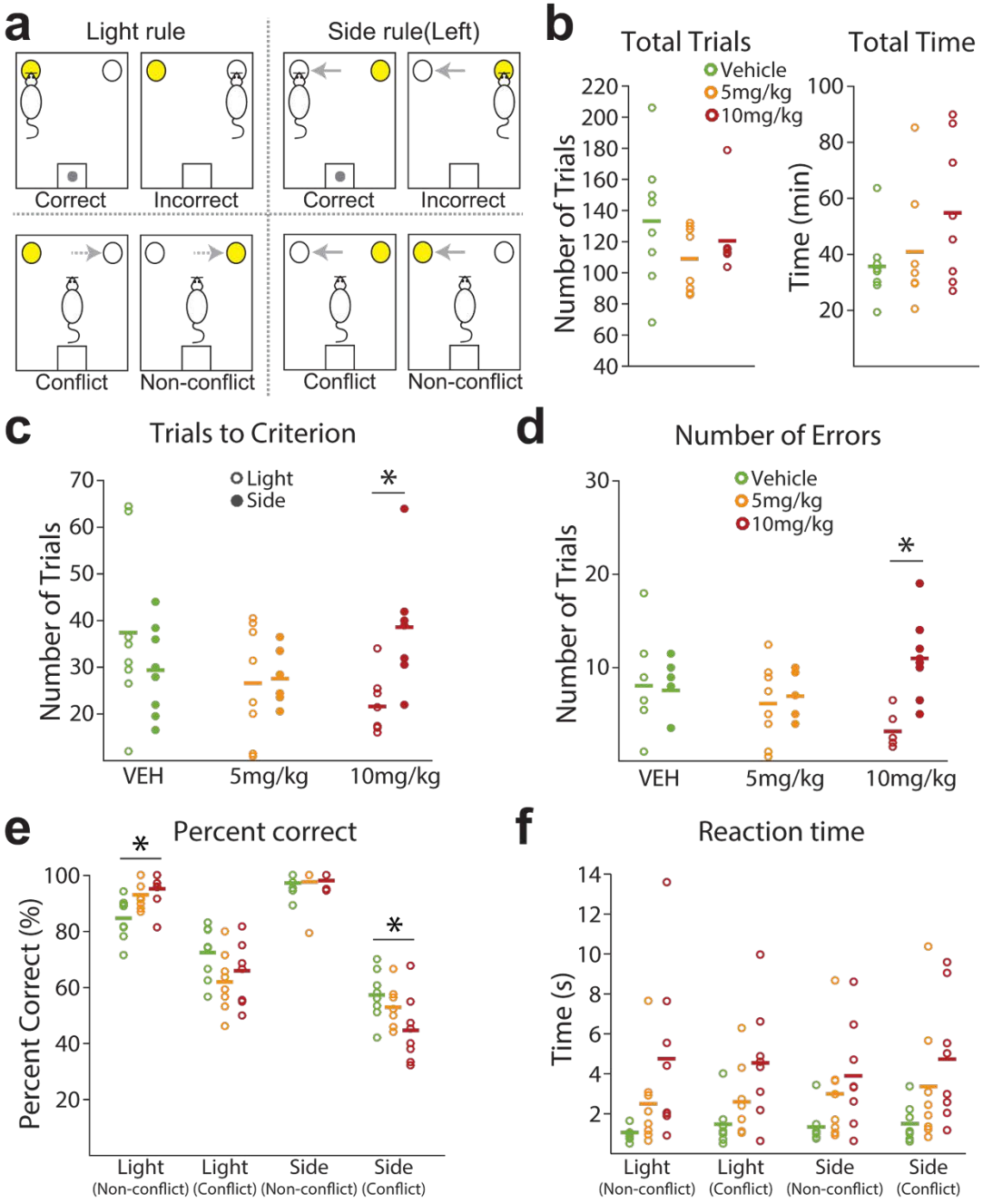


**Figure 3-2 Modulation of set-shifting task performance by FG7142.**

(a) Top left, Example correct performance in the light rule, where a nose poke to the illuminated port is rewarded. Bottom left, Light-rule trials were subtyped to conflict or non-conflict trials, based on correspondence between illuminated and previously valid side indicated with dotted arrows. Top right, Example correct performance in the side rule, where a nose poke to the valid side (e.g. the left port) is rewarded, regardless of illumination. Bottom right,

Side-rule trials were subtyped to conflict or non-conflict trials, based on correspondence between illuminated and valid side indicated with solid arrows. (b) The number of total trials and total time to complete the task were equivalent across dose groups. Each circle represents an individual data point. A horizontal bar indicates the mean of each dose group. (c) The number of trials to reach the set-shifting criterion (10 consecutive correct trials) in light- and side-rule sets was displayed for each dose group. (d) The number of errors in light and side rule sets was displayed for each dose group. An asterisk indicates a significant difference in the number of trials to the criterion or errors between light- and side-rule sets. (e) Distinct choice accuracy was observed in different trial types. All rats were more prone to errors in conflict trials. Such error propensity was more pronounced under the side rule, especially in the 10 mg/kg treated rats. Asterisks indicate significant difference compared to the vehicle treated rats. (f) The RT from the cue onset to the action trended toward a dose-dependent increase in all trial types.

### 3.3.3 Impact of FG7142 on neural correlates of set-shifting task performance

The PFC neural correlates of task performance in response to FG7142 were analyzed at individual neuronal and population levels, based on single unit activity recorded from histologically verified electrodes in dmPFC and OFC (Figure 3-1a). We first quantified the baseline firing rate and the baseline-normalized peri-action activity across all trials. The time of action was identified by the detection of an entry to the nose-poke port, and all pre- or post-action neuronal activity was aligned to timing of the port entry. Consistent with the home cage recording result, dmPFC units in FG7142 treated groups had lower baseline firing rates compared to the vehicle treated units (Figure 3-3d; One-way ANOVA, $F_{2, 188} = 5.90$, $p = 0.003$). However, the trial-averaged normalized activity (Figure 3-3e; One-way ANOVA, $F_{2, 188} = 0.82$, $p = 0.44$) and the fraction of activated units (Figure 3-3f; Chi-square test, $p$ values > 0.07) within the pre- or post-action period did not differ across dose groups.

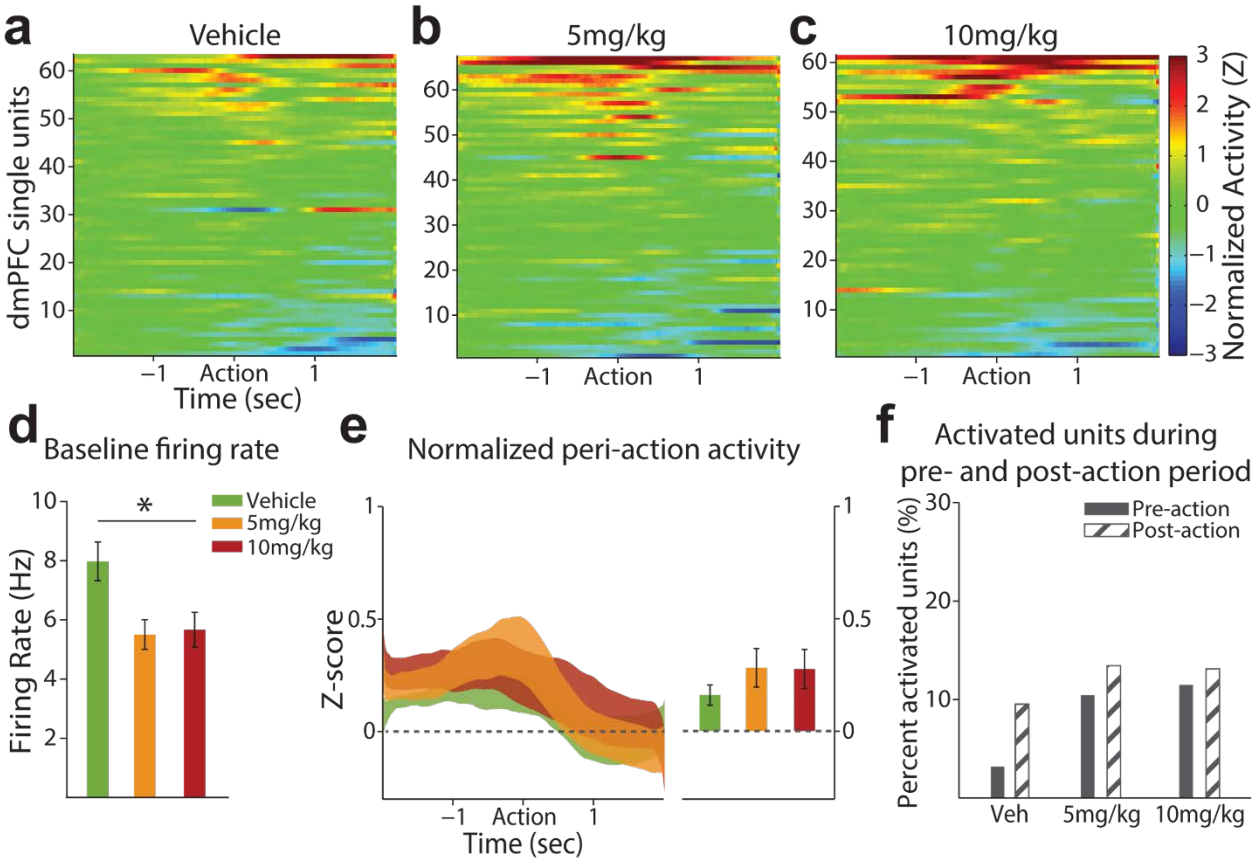


**Figure 3-3 dmPFC peri-action neuronal activity during the set-shifting task.**

(a-c) The baseline-normalized peri-action activity of vehicle or FG7142 treated units with the action occurring at time = 0, aligned to the time of the nose poke detected by the beam break at the cue port. dmPFC units tended to start modulating their activity preceding the action. The number of units (n) and rats (N); vehicle n = 63, N = 8; 5 mg/kg n = 67, N = 8; 10 mg/kg n = 61, N = 7. (d) The mean baseline firing rates of FG7142 injected units, measured during inter-trial intervals, were significantly lower than vehicle units, consistent with the effect observed in home cage recording. Error bars indicate standard errors. An asterisk indicates statistically significant difference compared with vehicle. (e) Left, The normalized population activity during the peri-action period is displayed as mean ± standard error (shaded area). Right, The mean population activity within the 2-s pre-action period. (f) The percentages of units classified as 'Activated' in pre- and post-action periods were not significantly different across dose groups. Few units were classified as 'Inhibited.'

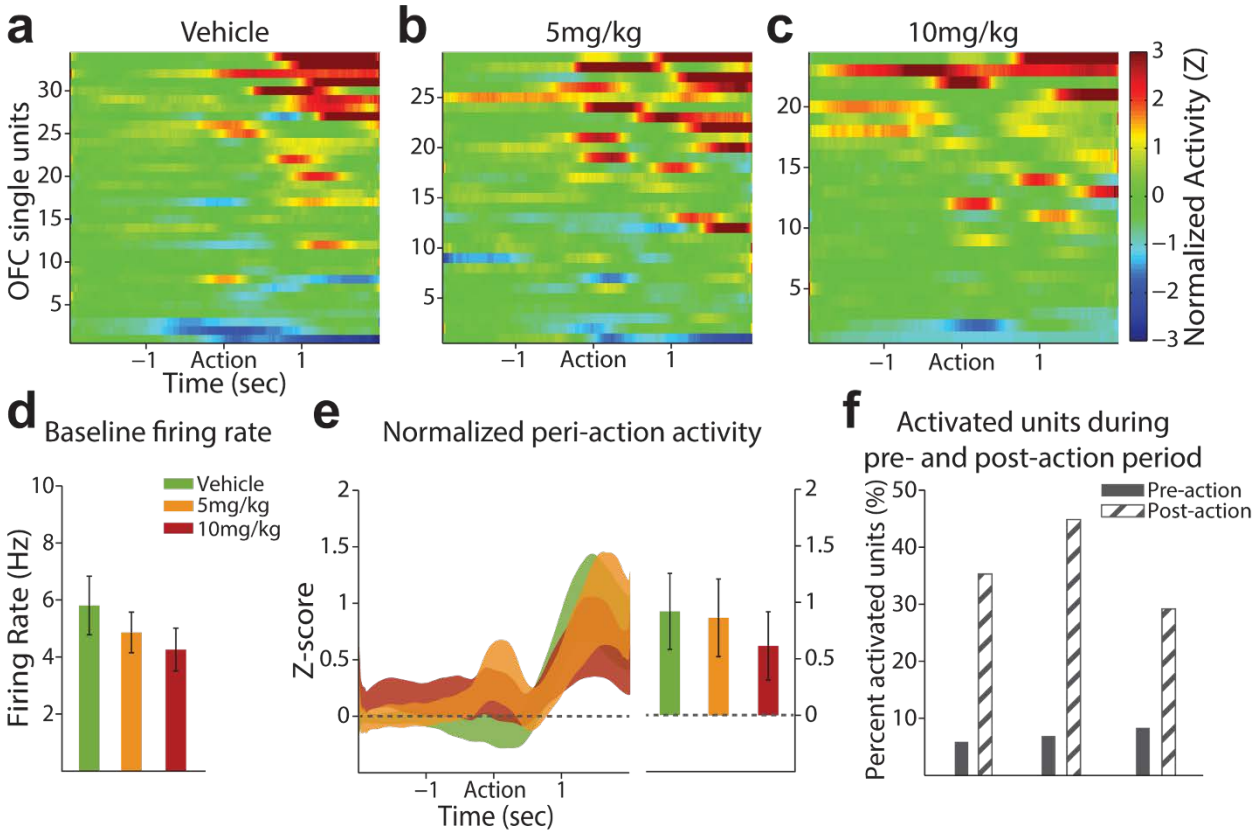


**Figure 3-4 OFC peri-action neuronal activity during the set-shifting task.**

(a-c) The baseline-normalized peri-action activity of vehicle or FG7142 treated units with the action occurring at time = 0. OFC units tended to modulate their activity during the post-action period. The number of units (n) and rats (N); vehicle n = 34, N = 5; 5 mg/kg n = 29, N = 5; 10 mg/kg n = 24, N = 4. (d) The mean baseline firing rate of FG7142 exposed units was numerically lower than vehicle units, consistent with the effect observed during home cage recording. Error bars indicate standard errors. (e) Left, The normalized population activity during the post-action period is displayed as mean ± standard error (shaded area). Right, The mean population activity within the 2-s post-action period. (f) The percentages of units classified as 'Activated' in pre- and post-action periods did not significantly differ across dose groups. Few units were classified as 'Inhibited.'

In OFC, a non-significant reduction in the baseline firing rate was observed in FG7142 treated units (Figure 3-4d; One-way ANOVA, $F_{2, 84} = 0.78$, $p = 0.46$). This contrasted the significant reduction observed during home cage recording and may be due to the impact of context (operant box vs. home cage) on the baseline spontaneous activity of OFC neurons, or the difference in the statistical power given the different sample sizes. Unlike dmPFC units, and as expected, OFC units responded more robustly during the post-action (outcome) period (Figure 3-4a-c). This post-action OFC response was not affected by FG7142, as similar trial-averaged normalized activity (Figure 3-4e; One-way ANOVA, $F_{2, 84} = 0.14$, $p = 0.87$) and fraction of activated units (Figure 3-4f; Chi-square test, $p$ values > 0.24) were observed across dose groups.

We then examined the individual neuronal encoding of various task-relevant variables, such as the rule, current and previous response outcomes, poke direction and RT, using a multiple linear regression model (Methods). We first examined the neuronal encoding of the response outcome of previous and current trials, which are the two critical features for the outcome-based guidance of behavior during the task. With all predictive variables accounting for variability in neuronal activity, some dmPFC and OFC units encoded the response outcome of the previous and/or the current trial especially during the pre- and post-action period, respectively, consistent with the literature (Strait et al., 2014; Sul et al., 2010) (Figure 3-5 & 3-6). Encoding of the previous response outcome was neither region-specific nor affected by FG7142 (Figure 3-5a-b & Table 3-1; Chi-square test, $p$ values > 0.08). To test how reliably the previous response outcome could be decoded at the population level, we carried out a decoding analysis with the entire dmPFC population of each dose group, using a linear classifier (Methods). The response outcome of the previous trial could be decoded from the dmPFC population well above the chance level across the peri-action period in all dose groups (Figure 3-5c-d). Greater

proportions of dmPFC and OFC units encoded the response outcome of the current trial, particularly in the post-action period, regardless of vehicle or FG7142 injection (Figure 3-6a-b & Table 3-1; Chi-square test, *p* values > 0.10). The classifier generated a highly accurate decoding of the current response outcome, especially during the post-action period, consistent with the individual neuronal encoding (Figure 3-6c-d). In summary, substantial dmPFC and OFC units encoded previous and/or current response outcome, but this encoding was not significantly affected by the anxiogenic manipulation, suggesting that the trial-to-trial signaling of the response outcome were intact in anxiety.

The regression analysis also indicated that FG7142 treatment did not influence the fraction of units encoding previous and current poke direction in dmPFC (Previous direction: vehicle, 17 %; 5 mg/kg, 12 %; 10 mg/kg, 11 %, Current direction: vehicle, 25 %; 5 mg/kg, 31 %; 10 mg/kg, 20 %) and OFC (Previous direction: vehicle, 6 %; 5 mg/kg, 21 %; 10 mg/kg, 13 %, Current direction: vehicle, 15 %; 5 mg/kg, 31 %; 10 mg/kg, 29 %). Similar lack of effect was observed in units that encoded the RT for the action in dmPFC (vehicle, 17 %; 5 mg/kg, 12 %; 10 mg/kg, 11 %) and OFC (vehicle, 6 %; 5 mg/kg, 21 %; 10 mg/kg, 13 %).

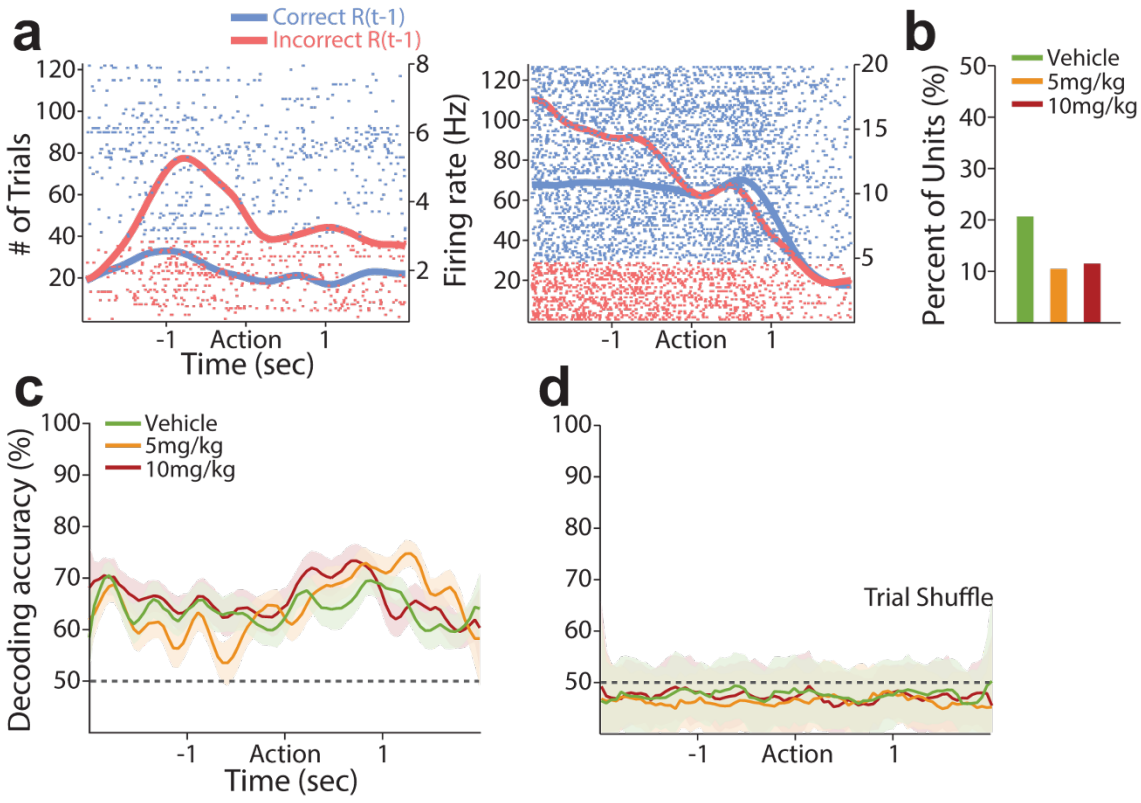


**Figure 3-5 dmPFC encoding of the previous response outcome – R(t-1).**

(a) Spike raster plots of two example dmPFC units encoding the previous response outcome during the pre-action period. Each row represents each trial, and each tick mark denotes a spike. The horizontal axis represents time before and after the action occurring at time = 0. The left vertical axis indicates the number of trials, and the right vertical axis indicates the firing rate. The spike density functions for previously correct and incorrect trials estimated with a Gaussian kernel ($\sigma$ = 100 ms) are superimposed in each raster plot. (b) Proportions of vehicle, 5 and 10 mg/kg exposed units encoding the previous response outcome were not significantly different (n = 13, 7, 7, respectively). (c) Representation of the previous response outcome in the dmPFC population, measured by the decoding accuracy of a linear classifier. Each color-coded line indicates the decoding accuracy for the previous response outcome in each dose group (vehicle, 63; 5 mg/kg, 67; 10 mg/kg, 61 units), displayed as mean ± standard deviation (shaded area) across 50 re-samplings. The black dotted line indicates the level of decoding expected by chance. (d) Shuffling the trial ID quenched the decoding accuracy for the previous response outcome to around the chance level.

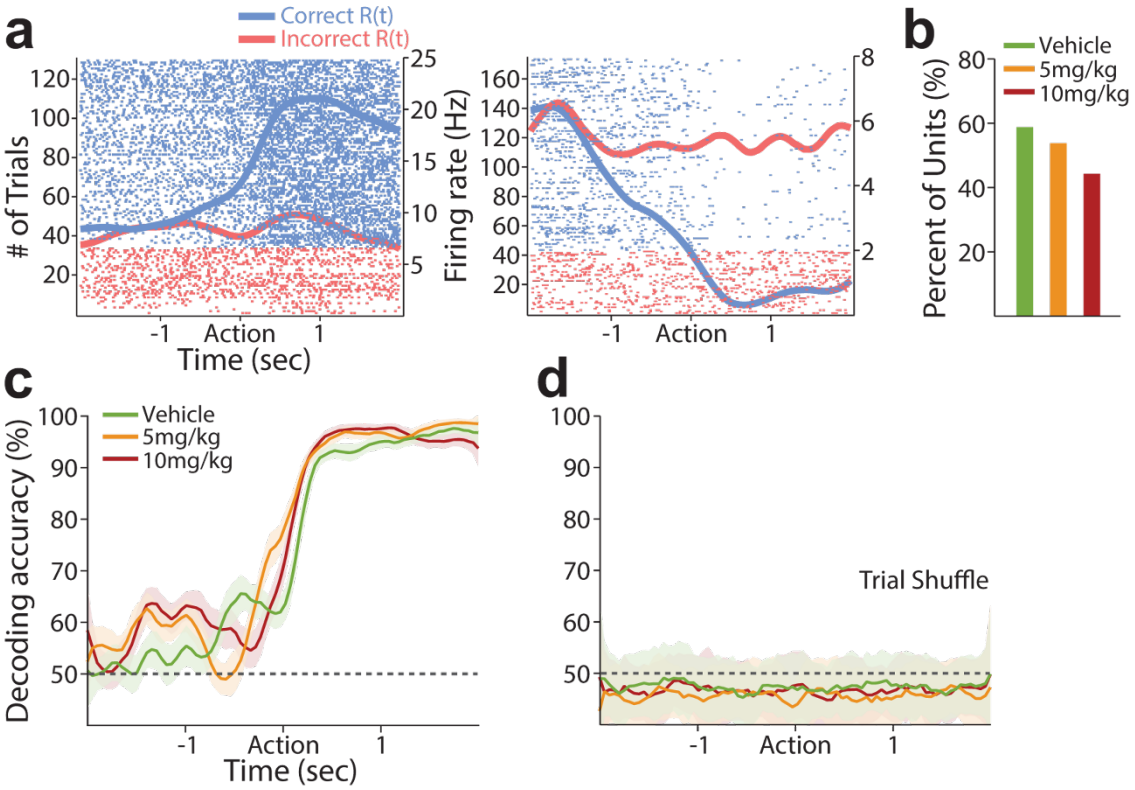


**Figure 3-6 dmPFC encoding of the current response outcome – R(t).**

(a) Spike raster plots of two example dmPFC units that encoded the current response outcome during the post-action period. (b) Proportions of vehicle, 5 and 10 mg/kg exposed units encoding the current response outcome were similar (n = 37, 36, 27, respectively). (c) The decoding accuracy for the current response outcome was highly accurate during the post-action period in all dose groups. (d) Trial-shuffling extinguished the decoding accuracy for the current response outcome to around the chance level.

OFC encoding of set-shifting task variables

| | Vehicle | 5 mg/kg | 10 mg/kg |
|---|---|---|---|
| R(t-1), Previous response outcome | 11 (32%) | 7 (24%) | 3 (13%) |
| R(t), Current response outcome | 22 (65%) | 19 (66%) | 14 (58%) |
| D(t-1), Previous poke direction | 2 (6%) | 6 (21%) | 3 (13%) |
| D(t), Current poke direction | 5 (15%) | 9 (31%) | 7 (29%) |
| RT(t), Reaction time | 2 (6%) | 6 (21%) | 3 (13%) |
| TR(t), Task rule | 10 (29%) | 5 (17%) | 6 (25%) |
| TR(SiCF), Task rule (Side CF vs. Light) | 7 (20%) | 4 (14%) | 4 (17%) |
| TR(LiCF), Task rule (Light CF vs. Side) | 4 (12%) | 4 (14%) | 6 (25%) |

**Table 3-1 The number and percentage of OFC single units encoding each task variable, according to the multiple linear regression analyses (Methods).**

Equivalent proportions of OFC units encoded each task variable, as none of the examined variables differ significantly across dose groups.

We next analyzed the neural representation of the task rule. For this, we focused on the encoding during the pre-action period because it is the temporal window that immediately precedes the action, and thus encoding within this window may guide the action. A substantial fraction of vehicle-treated dmPFC units, as exemplified in Figure 3-7, encoded the rule in the pre-action period (Figure 3-8a). The anxiogenic treatment significantly reduced the proportion of rule-encoding units (Figure 3-8a; Chi-square test, $\chi^2_1 = 5.11$, $p = 0.02$). The standardized regression coefficients (SRC) for the task rule covariate of all rule-encoding and non-encoding units are shown across the peri-action time period in Figure 3-8b. The neural representation of the task rule may gradually evolve after shifting, as the animals initially try to figure out the valid rule by trial-and-error, and finally attain the rule in the later phase of the set. We tested this by

comparing the degrees of neural discriminability based on the rule in the two subsets of data comprising the 1st half and the 2nd half trials of each set, using a sliding ROC analysis (Methods). We found that the vast majority of the rule-encoding dmPFC units in the vehicle (19/24 units, Paired t-test, $t_{23}$ = 3.35, $p$ = 0.003) and the 5 mg/kg (15/21 units, Paired t-test, $t_{20}$ = 3.69, $p$ = 0.001) groups showed enhanced selectivity in the late compared to the early phase of a set (Figure 3-8c). The emerging ROC values from the 1st to 2nd half of trials corresponded to low and high behavioral accuracy (Figure 3-8d; Overall percent correct: 66 % and 87 %), demonstrating the association between emerging neural representation of the rule and growing behavioral accuracy. The emerging pattern of rule selectivity was weakened after animals received the 10 mg/kg dose (Figure 3-8c; 7/12 units, Paired t-test, $t_{11}$ = 1.34, $p$ = 0.21), even when the behavioral choice accuracy appeared high in the 2nd half (Figure 3-8d).

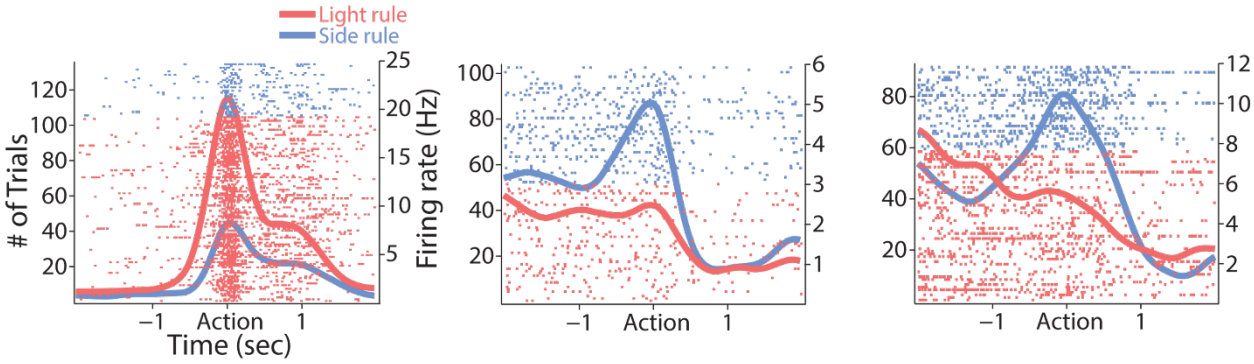


**Figure 3-7 Example dmPFC units encoding the task rule during the pre- and post-action periods.**

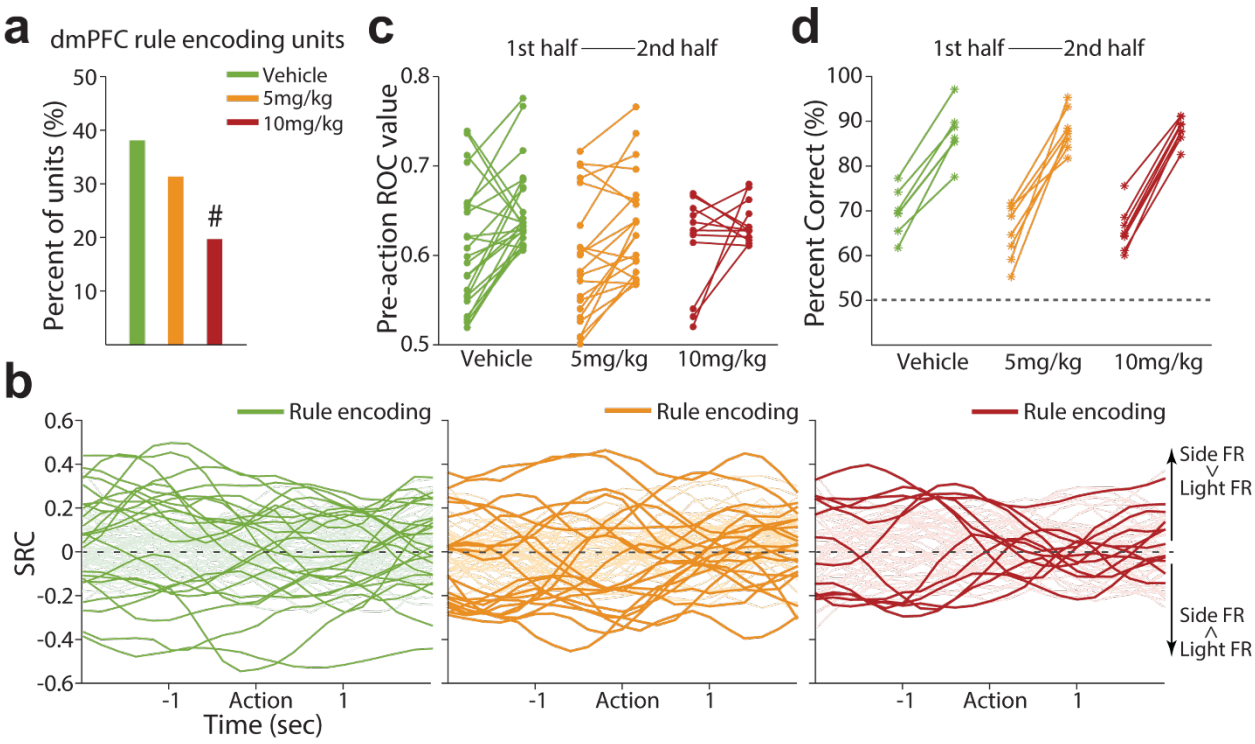


**Figure 3-8 dmPFC neuronal representation of the task rule.**

(a) The bar plot illustrates the proportion of dmPFC units encoding the rule during the pre-action period (vehicle, 24; 5 mg/kg, 21; 10 mg/kg, 12 units). The number sign indicates a significantly different proportion of encoding units compared to that of the vehicle units. (b) Standardized regression coefficients (SRC) for the task rule covariate of the multiple linear regression model are plotted. Dark-colored lines indicate SRCs for rule-encoding dmPFC units in each dose group, whereas light-colored lines indicate SRCs for the non-encoding units. Positive-valued SRCs indicate greater firing rates (FRs) in the side rule compared to the light rule, whereas negative-valued SRCs indicate greater firing rates in the light rule. (c) The degrees of neural discriminability based on the rule were examined in the two subsets of data comprising the 1st half and the 2nd half trials of each set, using a ROC analysis. For each dose group, the left and right filled circles indicate the pre-action ROC values of the 1st and the 2nd half trials of the rule-encoding units. An emerging trend of rule selectivity was observed from 1st to 2nd half trials, which was blunted in the 10 mg/kg treated units. (d) The percentage of correct choices for the 1st half (left asterisks) and the 2nd half (right asterisks) trials of each animal is indicated for a comparison with the ROC data.

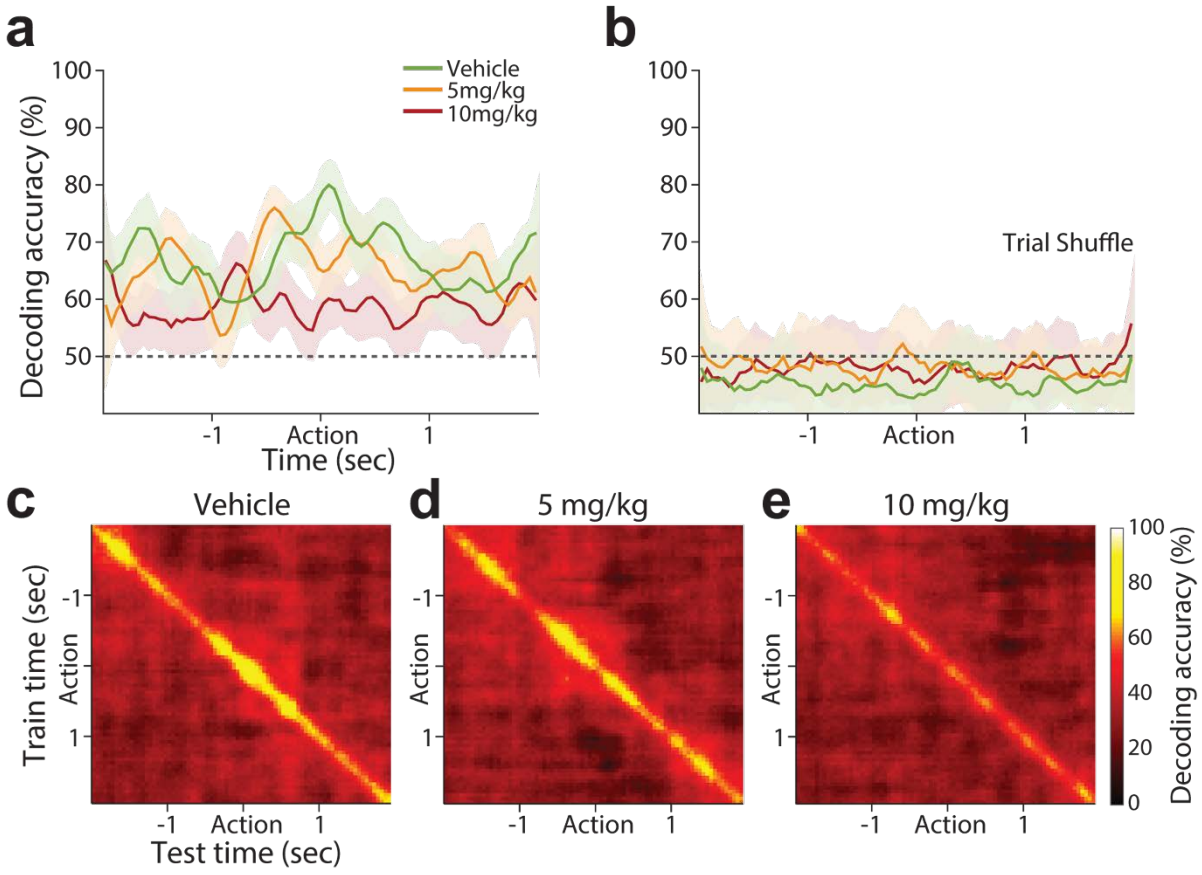


**Figure 3-9 Representation of the task rule in the dmPFC population, measured by the decoding accuracy of a linear classifier.**

(a) Each color coded line indicates the decoding accuracy of each dose group (vehicle, 63; 5 mg/kg, 67; 10 mg/kg, 61 units), displayed as mean ± standard deviation (shaded area) across 50 re-samplings. FG7142 injection, especially 10 mg/kg, is associated with lower decoding accuracy across the peri-action period. The black dotted line indicates the level of decoding expected by chance. (b) Shuffling the trial ID quenched the decoding accuracy to around the chance level. (c-e) Results from training a classifier at one time period (vertical axis) and testing the classifier at a different time period (horizontal axis) for decoding the task rule (temporal-cross-training analysis). High classification accuracy was observed from the vehicle population (c), only when the classifier was trained and tested using data from around the matching time periods, which indicates that dynamic patterns of neuronal activity convey task-rule information at different time points. A comparable result was seen from the 5 mg/kg population (d), but not from the 10 mg/kg population (e).

Reduced individual neuronal rule representation should be associated with diminished encoding of the rule at the population level. We corroborated this using the linear classifier. The classifier decoded the task rule corresponding to current trials with high accuracy from the vehicle population, but with far lower accuracy from the 10 mg/kg population, indicating that the anxiogenic manipulation was associated with reduced rule representation by the dmPFC population (Figure 3-9).

We next investigated the impact of the anxiogenic treatment on neural representation of the task rule in CF trials. We identified the CF trials in either side- or light-rule sets (Figure 3-2a), and then examined the encoding of CF trials of one rule, relative to the trials of the other rule, using a multiple linear regression model (Methods). Examples of individual dmPFC units that encoded side CF trials relative to light-rule trials are shown in Figure 3-10a. Figure 3-10b illustrates that the proportion of side-CF trial encoding dmPFC units was significantly reduced by 10 mg/kg FG7142 compared to vehicle (Chi-square test, $\chi^2_1 = 5.83$, $p = 0.016$). This is consistent with the behavior data (Figure 3-2e) showing increased error propensity in side CF trials at this dose. Fewer rule-encoding units were found in CF trials of the light rule, regardless of the dose (Figure 3-10b; Chi-square test, $p$ values $> 0.39$), which is consistent with the comparable performance across dose groups observed in these trials (Figure 3-2e). The difference between the fractions of rule-encoding units in side CF and light CF trials may reflect differential degrees of rule representation between these trials, i.e. more robust rule representation may be observed in side CF than light CF trials. To test this, we applied a ROC analysis to the rule-encoding dmPFC units identified earlier without subdivision of CF and NCF trials (Figure 3-8a) and quantified their discriminability of the rule for side CF and light CF trials (Methods). We found that greater numbers of rule-encoding dmPFC units in the vehicle (15/24

units, Paired t-test, $t_{23} = 2.36$, $p = 0.027$) and the 5 mg/kg (14/21 units, Paired t-test, $t_{20} = 2.28$, $p = 0.034$) groups showed enhanced discriminability in the side CF than light CF trials (Figure 3-10c). This difference was dampened in 10 mg/kg treated units (6/12, Paired t-test, $t_{11} = 0.91$, $p = 0.38$) (Figure 3-10c). Thus, the dmPFC neural representation of the task rule in CF trials was more pronounced under the side rule, where the conflicting light stimulus was presented explicitly and continuously throughout a set. The reduction of this representation by the anxiogenic treatment may underlie its effect on increased error propensity and performance bias.

Weaker task-rule representation was observed in the OFC, as fewer proportions of rule-encoding OFC units were found, without a significant difference across dose groups (Table 3-1; Chi-square test, $p$ values > 0.25). Likewise, the OFC rule representation in CF trials was not evident, and was not affected by anxiety (Table 3-1; Chi-square test, $p$ values > 0.18). These suggest that, unlike dmPFC neurons, OFC neurons do not encode anxiety-induced changes in rule-based task performance.

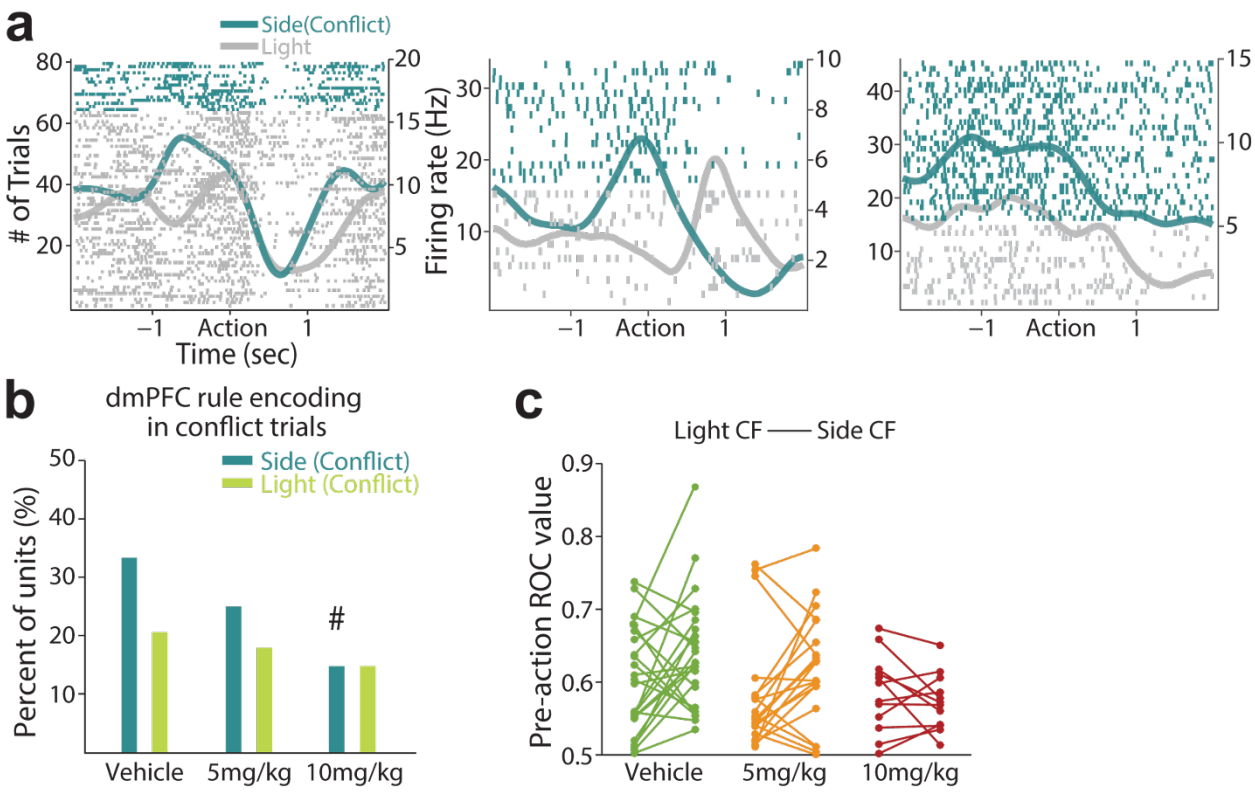


**Figure 3-10 dmPFC neuronal encoding of the task rule, examined specifically in conflict trials.**

(a) The spike raster plots of example dmPFC units that discriminatively represented side (conflict) and light trials during the pre-action period. Format same as spike raster plots above. (b) The bar plot illustrates the proportion of dmPFC rule-encoding units in side CF (vehicle, 21; 5 mg/kg, 18; 10 mg/kg, 9 units) and light CF (vehicle, 13; 5 mg/kg, 12; 10 mg/kg, 9 units) trials during the pre-action period. The proportion of rule-encoding units in side CF trials decreased in a dose-dependent manner. The number sign indicates a significantly different proportion of encoding units compared to that of the vehicle units. (c) The neural discriminability of light CF or side CF trials, relative to the trials of the other rule was quantified using a ROC analysis. Each line segment represents an individual rule-encoding unit's ROC value for the light CF trials (left filled circle) and the side CF trials (right filled circle).

### 3.3.4 FG7142 effect on anxiety-like behavior and locomotion measured on the elevated plus maze

Consistent with previous reports (Atack et al., 2005; Cole et al., 1995; Evans and Lowry, 2007; Pellow and File, 1986), FG7142 induced an anxiety-like state when measured using the elevated plus maze (EPM) (Figure 3-11a-b). Rats placed on the EPM after injection of FG7142 showed significantly fewer entries (Figure 3-11c; Independent t-test, $t_{12}$ = 3.03, $p$ = 0.01) and reduced time (Figure 3-11d; Independent t-test, $t_{12}$ = 3.01, $p$ = 0.02) spent in open arms, compared to vehicle injected rats. The total distance traveled on the maze did not differ significantly between vehicle and FG7142 injected groups (Figure 3-11e; Independent t-test, $t_{12}$ = 1.93, $p$ = 0.08), thus the anxiety-like behavior was not attributed to an overt deficit in locomotion.

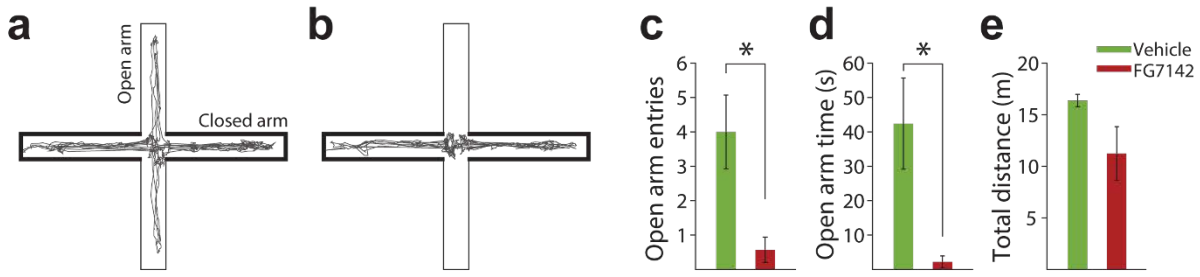


**Figure 3-11 Anxiogenic effect of FG7142 measured on the elevated plus maze.**

(a-b) A representative trajectory of a vehicle (a) or 10 mg/kg FG7142 (b) injected rat. (c) The number of open arm entries. (d) Time spent in the open arms. (e) Total distance traveled on the maze. The number of rats (N); vehicle N = 7; 10 mg/kg N = 7. Error bars indicate standard errors. An asterisk indicates statistically significant difference compared with vehicle.

## 3.4 DISCUSSION

Anxiety has been studied extensively as a stand-alone construct in laboratory animals (e.g., Adhikari et al., 2010, 2011; Calhoon and Tye, 2015; Milad and Quirk, 2012). The results have contributed to our understanding of the brain circuits that are altered in anxious and fearful animals. Detrimental impacts of human anxiety, however, extend well beyond a general aversive "fearful" state and involve disruption of ongoing goal-directed behaviors that are necessary for day-to-day functioning. A critical example is disruption of PFC-mediated cognitive functions such as flexible shifting to new behavioral strategies or overcoming distracting stimuli (Bishop, 2007; Eysenck et al., 2007). Here we sought to fill a fundamental void in the literature by addressing how a background state of anxiety influences encoding of flexible decision making by PFC neurons. We used a clinically relevant experimental model of anxiety while recording from dmPFC and OFC neurons of rats at wakeful rest or while they were engaged in an extradimensional set-shifting task. We find that anxiety engrosses a substantial number of spontaneously active PFC neurons and, more importantly, leads to diminished representation of conflict-related action by dmPFC neurons in correlation with behavioral impairment.

### 3.4.1 The challenge of modeling sustained anxiety in behaving animals

Anxiety is a construct in Research Domain Criteria (RDoC) of NIMH's Strategic Plan and a debilitating symptom of most psychiatric disorders. Anxiety generally is not a rapid neuronal "event" but a "state" that may be sustained for many minutes to hours. In a real-life situation, the impact of anxiety extends beyond its general aversive state and impairs ongoing behaviors that

utilize cognitive and affective processing. The neurodynamic nature of this impairment has been difficult to address, in part, because previous electrophysiological studies focused on fear conditioning and avoidance paradigms as a potential measure of anxiety. While these studies have revealed a role for PFC in regulating freezing and avoidance behaviors (Burgos-Robles et al., 2009; Milad and Quirk, 2002), they cannot reveal how the PFC neural correlates of cognitive and motivated behavioral events are modulated by anxiety.

To study anxiety-related PFC neural processing during cognitive and motivated behaviors, it would be ideal to produce a sustained state of anxiety in animals that does not prevent their task performance. We used a pharmacological model of sustained anxiety that has excellent cross-species validity. Inverse agonists of allosteric benzodiazepine binding sites in $GABA_A$ receptors produce an anxiogenic state (Evans and Lowry, 2007). This is an "old" approach, with one of the initial studies (Ninan et al., 1982) reporting a behavioral syndrome in rhesus monkeys that mimicked physiological and affective features of human anxiety. While these drugs produce freezing or may have pro-convulsive properties at very high doses, their symptomatic impact at moderate doses is relatively specific in the context of anxiety, in that behavioral and perceptual effects unrelated to anxiety (such as hallucination) are not reported. A well-characterized drug in this class is FG7142, which has been shown to produce PFC-mediated cognitive deficits (Murphy et al., 1996a), as well as anxiety-related cardiovascular, and neurochemical effects in humans and laboratory animals (Evans and Lowry, 2007). This approach provided a practical tool for studying the impact of sustained anxiety on cognitive task performance.

### 3.4.2 Effects of anxiety on spontaneous PFC neuronal activity

Anxiety induced by FG7142 suppressed dmPFC and OFC population activity. This effect contrasts the increase in PFC firing rate shown previously in traditional rodent models of anxiety (Adhikari et al., 2011). Our findings, however, are consistent with human imaging studies that have reported reduced activation of PFC in patients with anxiety disorders (Phelps et al., 2004; Shin et al., 2001). These data further suggest that the 'hypofrontality' commonly associated with a general state of anxiety is caused by suppression of the spontaneously active PFC neurons.

Anxiogenic compounds including FG7142 decrease the chloride flux via $GABA_A$ receptors, which should produce a direct excitatory effect on firing rate of single neurons. The observed inhibitory influence, therefore, suggests the involvement of networks of GABA interneurons and multiple inhibitory processes mediated by them (White et al., 2000). Alternatively, similar to stress, indirect mechanisms such as activation of noradrenergic or dopaminergic projections to the PFC may be involved (Arnsten, 2000; Gamo et al., 2015; Goldstein et al., 1996; Reinhard et al., 1982). DA recently has been implicated in mediating anxiety-like behaviors (Lammel et al., 2012). Selective activation of DA release in mPFC by the fiber photometry had anxiogenic effects in mice (Gunaydin et al., 2014). A hyper-reactive mesoprefrontal circuit was associated with clinical anxiety in humans (Cha et al., 2014). Consistent with PFC activation of DA release being anxiogenic, FG7142 produces a sustained increase in DA release selectively in the PFC (Bradberry et al., 1991b; Murphy et al., 1996a). Importantly, the time course of increase in DA release is similar to the duration of PFC neuronal inhibition we observed (Bradberry et al., 1991b). Post-synaptic effects of DA on PFC neurons are primarily inhibitory (Gorelova et al., 2002; Seamans et al., 2001; Sesack and Bunney, 1989), thus the anxiety-induced reduction in PFC neuronal activity may be mediated, in part, by

selective activation of DA release in PFC. Of note, high levels of dopamine D1 or noradrenergic alpha-1 receptor stimulation, similar to the impact of FG7142, reduce PFC neuronal firing in monkeys (Arnsten, 2009).

### 3.4.3 Modality specific deficits in set-shifting task performance

The dose of the anxiogenic compound used here did not prevent animals from successfully completing trials in the set-shifting task. This allowed us to unveil selective and clinically relevant anxiety-induced deficits in rule-shifting behavior. A critical aspect of our task was that it included multiple extradimensional shifts within each session. Animals had been well trained with the discrimination rules as well as shifting between them before the test session, thus the task was sensitive to measure the flexible switching between rules based on the action-outcome contingency. FG7142 injected rats readily shifted from the side to the light rule, as evidenced by fewer errors and trials to criterion in the light rule. However, when shifting to the side rule, increased errors were observed during what we coined “conflict trials” (i.e. trials where light was presented in the incorrect side). This selective deficit suggests impaired capacity to disengage from the previously relevant sensory dimension, especially when the outmoded cue was visible. This deficit is consistent with increased perseverative errors after acute stress in rodents (Butts et al., 2013) and monkeys (Murphy et al., 1996a; Murphy et al., 1996b), and perseverative behavioral patterns in patients with anxiety-related disorders (Eysenck et al., 2007; Purcell et al., 1998).

Our observation further suggests that the detrimental impact of anxiety on rule shifting is modality specific and especially vulnerable when a shift is required in the presence of previously

relevant sensory stimuli. From a broader standpoint, these behavioral findings indicate that anxiety may bias decision making to a sensory-based process that is less flexible and more prone to visual and other sensory distractors. These findings, therefore, support the notion that, under anxiety, behavioral selection is skewed by salient environmental stimuli at the expense of flexible top-down guided choices.

### 3.4.4 Neuronal encoding of deficits in behavioral rule shifting in anxiety

The baseline firing rates of dmPFC and OFC neurons were similarly inhibited by the anxiogenic treatment during home cage recording and task performance. During task performance, varying degrees of neuronal encoding of the response outcome, choice direction, and RT were observed in both regions, and signaling of these variables involving a trial-to-trial processing was not significantly affected by anxiety. In contrast, the dmPFC neural representation of task rules was selectively diminished. Encoding the task rule is a higher-order process that involves representation of relationships among the task-relevant cues, actions and outcomes. Thus, our finding suggests that the higher-order processing, subserved by dmPFC, may be particularly susceptible to anxiety.

Further analyses of the neural representation of the task rule revealed dynamic aspects of the dmPFC rule encoding and its vulnerability to anxiety. First, the rule representation gradually evolved after the set-shifting. This growing representation is unlikely to be an epiphenomenon of the enhanced correct choices or increased ‘confidence’ in choice because equivalent enhancement in behavioral accuracy was observed in both rules. Thus, the growing rule-representation may contribute to the gradual improvement in choice accuracy. This emerging

pattern in the rule representation collapsed in anxiety, suggesting that this component of rule representation is vulnerable to anxiety. Second, we observed that dmPFC rule representation was different in side vs. light CF trials. This can be attributed to the fact that conflict arises more explicitly in the side rule due to the continuous presence of the salient light cue. The rule representation in the side CF trials was disrupted in anxiety in correlation with increased performance errors. Collectively, these data indicate that the anxiety-related alterations in task performance are associated with deteriorated dmPFC representation of the task rule.

Our analyses revealed that fewer proportions of OFC, compared to dmPFC, neurons signaled rule-relevant information. The majority of OFC neurons modulated their activity in the post-action period when the response outcome was presented, suggesting specialized roles of dmPFC and OFC in encoding distinct information during a rewarded and complex cognitive task, i.e., task rule vs. response outcome, consistent with previous literature (Bissonette et al., 2008; Dias et al., 1997; McAlonan and Brown, 2003). It should be underscored that these findings do not discount a role for OFC in mediating other adverse effects of anxiety.

### 3.4.5 Conclusion

The model of anxiety used here has been validated in humans and monkeys. While this model is different from conventional rodent models of anxiety, the fact that the type of cognitive deficits and the hypofrontality associated with this model parallel observations in the human anxiety literature, enhances the clinical relevance of our electrophysiology and computational results. These results provide mechanistic insight for how anxiety diminishes rule-based guidance of behavior, leading to performance bias, and increased error propensity in decision making under

conflict. They also single out encoding of actions by PFC neurons as particularly vulnerable to anxiety.

# 4.0 GENERAL DISCUSSION

## 4.1 SUMMARY AND INTERPRETATION OF MAIN FINDINGS

This dissertation study sought to delineate the neural basis of cognitive and motivated behavioral changes in anxiety. To this end, we first investigated the VTA and mPFC neural encoding of instrumental action in simple and complex behavioral tasks in a "normal" state – i.e., a non-anxious state. Then, we examined how the neural encoding was altered in association with behavioral changes in anxiety. The following is a summary and interpretation of the main findings.

### 4.1.1 The impact of anxiety on simple instrumental behavior

The negative effects of anxiety are characterized in part by profound deficits in reward-related behavioral domains such as anhedonia and aberrant reward-associated perception (Russo and Nestler, 2013). To investigate the neural basis of anxiety-related disruptions in reward-related behavior, we trained animals to engage in a simple instrumental action leading to a food reward with varying degrees of punishment risk contingent on the action. Animals exhibited anxiety-like behavioral changes as a function of punishment risk. The neurophysiological data suggest that the VTA-mPFC neural circuit reflects these punishment-based anxiety-like behavioral changes

using multiple coding schemes at the single neuronal, neural population, and neural circuit levels.

#### 4.1.1.1 A novel task that elicits punishment-based anxiety-like behavior

A neuro-mechanistic study on behavioral impact of anxiety needs to isolate a neural activity related to a specific behavior, then monitor how it varies as a function of anxiety. Commonly used Pavlovian paradigms such as the classical fear conditioning, although relevant when studying the neural basis of aversive conditioning, do not involve performance of goal-directed behavior. Therefore, we designed a new task in which animals engage in reward-motivated instrumental action with varying risk of punishment (Figure 2-1). This paradigm provided a systematic quantification of punishment-based aversive behavioral changes, represented by: 1) increase in the mean RT, and 2) increase in the trial-to-trial variability in RT as a function of risk. We confirmed that these behavioral changes were pertinent to anxiety, since a systemic pretreatment with the anxiolytic diazepam reversed the behavioral effects. Importantly, the behavioral changes were specific to the action on which punishment was contingent, as the reward retrieval and consumption occurring after the action were not affected. This corroborates that the behavioral changes were based on contingency of punishment on the action, not due to changes in general motivation and/or mobility. Collectively, these results validate our behavioral paradigm as a model to study behavioral and neurophysiological impact of anxiety.

#### 4.1.1.2 Individual neuronal encoding of action in a non-anxious state

We first examined individual neuronal response profiles in the absence of punishment risk. The majority of VTA and mPFC neurons responded to one or more task events – cue onset,

action, and/or reward delivery – indicating the involvement of the mesoprefrontal neural circuit in the instrumental behavior. When compared across different cell types, VTA DA neurons exhibited phasic excitatory response at task events, whereas non-DA and mPFC neurons displayed weaker and more temporally diffuse responses. The prominent task-related excitatory neuronal responses in DA neurons are consistent with the notion that midbrain DA neurons play a key role in initiating and executing a motivated behavior toward reward (Aberman and Salamone, 1999; Jin and Costa, 2010; Mingote et al., 2005; Wassum et al., 2012).

#### 4.1.1.3 Theta-oscillation-mediated VTA-mPFC neural synchrony in a non-anxious state

We found that coherent theta oscillations around the frequency band of 8 Hz emerged and synchronized the VTA-mPFC neural circuit specifically during preparation and generation of the action in the absence of punishment risk. Granger-causality analysis revealed VTA-to-mPFC directionality of the 8 Hz oscillation. The VTA-driven 8 Hz oscillation provided temporal coordination of neuronal spike activity in both regions, as substantial proportions of the individual neurons tended to emit a spike at a preferred phase of the 8 Hz oscillation. This is one of the first observations suggesting that LFP-mediated neural synchrony may promote neural communication between VTA and mPFC during motivated behavior (Fujisawa and Buzsaki, 2011).

LFP-based neural synchrony, especially when mediated by a low-frequency oscillation, is thought to be a network-wide phenomenon that may involve two or more brain areas even at a distance (Fries, 2015; Kopell et al., 2000). Thus, it is likely that the 8 Hz-mediated neural synchrony we demonstrated may involve other mesocorticolimbic areas, such as the NAc, dorsal striatum, amygdala, and hippocampus that are critically involved in appetitive behavior – i.e., the brain's reward network. This hypothesis could be addressed by simultaneous recording from

these regions in future studies. If this were the case, it would suggest that 8 Hz-mediated network-wide neural synchrony may facilitate neural communication across groups of neurons throughout the network, promoting appetitive behaviors leading to reward.

#### 4.1.1.4 Individual neuronal encoding of punishment-based anxiety-like behavior

We found that the vast majority of VTA and mPFC single neurons of all cell types encoded punishment risk by modulating their firing rates. Individual neuronal encoding appeared to be most pronounced at the time of the action, compared with other task events, suggesting that the majority of individual neurons represented the contingency between the action and punishment.

When neuronal encoding properties were closely examined, distinct temporal and directional tuning properties were observed in a region- and cell-type specific manner. Similar to their action-evoked responses in general, we found that VTA DA neurons exhibited phasic encoding around the time of action, whereas VTA non-DA and mPFC neurons displayed temporally diffuse encoding. These results suggest that VTA and mPFC neurons are collectively capable of representing the behavioral impact of punishment on both short and extended timescales (Cohen et al., 2015; Somerville et al., 2013).

The sign (direction) of neuronal responses to aversive events is thought to carry information about the motivational properties of an event. While heterogeneous response patterns have been commonly observed in PFC neuronal encoding of punishment (Kobayashi et al., 2006; Matsumoto et al., 2007; Seo and Lee, 2009; Ye et al., 2016), active debates are ongoing particularly with regard to the VTA DA neuronal response properties: in particular, whether they encode punishment with excitatory vs inhibitory responses (Bromberg-Martin et al., 2010; Schultz, 2016). Mounting evidence indicates that, in fact, distinct DA neuron groups

encode punishment with excitatory or inhibitory responses (Brischoux et al., 2009; Joshua et al., 2008; Matsumoto and Hikosaka, 2009; Valenti et al., 2011). In other words, some DA neurons – including the typical RPE-coding neurons – treat rewarding and aversive events with opposite signs, while others treat them with the same sign. An integrative theory suggests that this dichotomy in DA neuronal encoding may reflect distinct motivational signals conveyed by distinct DA neuron groups to code the motivational value vs the salience of an event (Bromberg-Martin et al., 2010; Schultz, 2016). Punishment is an event of negative value associated with avoidance, but it also has high salience deserving prioritized attention, and both aspects need to be encoded to ensure an adaptive behavioral response. Our observation of bidirectional encoding of punishment by equivalent proportions of VTA DA, non-DA, and mPFC neurons suggest that the VTA-mPFC neural circuit conveys distinct motivational properties of punishment.

#### 4.1.1.5 Neural population encoding of punishment-based anxiety-like behavior

Given the prevalent individual neuronal encoding of punishment, VTA and mPFC neurons as a population would be expected to convey a high level of information about punishment risk. Indeed, we could accurately decode risk from the activity of the VTA and mPFC neural populations, corroborating the individual neuronal representation of punishment risk.

Our behavioral data indicated remarkable trial-to-trial behavioral variability in RT, and the variability increased as a function of risk. To establish a more robust association between the behavioral and neural data, we examined to what extent the behavioral variability could be explained by the neural data. We initially found that individual neurons were limited in representing the trial-to-trial behavioral variability. However, we found that much more reliable inference of trial-by-trial behavior was possible from joint activity of the simultaneously

recorded neural populations: the neural population activity states (trajectories) varied systematically in correlation with the behavioral RT across trials. Importantly, in many cases, the trial-by-trial neural population trajectories could track the trial-to-trial behavioral variability even within the same block – especially in the high-risk block, where the highest degree of behavioral variability was observed. These findings suggest that VTA and mPFC neural population activity tracked anxiety-induced behavioral variation on a single-trial basis.

#### 4.1.1.6 Desynchronization of the VTA-mPFC circuit in anxiety

At the circuit level, the VTA-mPFC neural synchrony we observed, which was mediated by a VTA-driven 8 Hz oscillation during risk-free actions, declined as a function of punishment risk. The power, coherence, and directionality of the 8 Hz oscillation diminished in both areas. Likewise, the phase-locking of mPFC and VTA neuronal spike activity to the VTA-driven 8 Hz oscillation significantly diminished as a function of punishment risk. These results suggest that punishment-based anxiety may involve a deficit in the functional network of neuron groups, linked via 8 Hz-mediated neural synchrony, that emerges in an appetitive behavioral state. In an aversive and anxiogenic state, distinct neuron groups that preferentially process punishment and aversive behavior may emerge, possibly with synchrony mediated by an oscillation at a distinct frequency band. Consistent with this hypothesis, recent studies have demonstrated that a slower oscillation (4 Hz) synchronized mPFC and amygdala, which may reflect the formation of an "aversive" neural network (Dejean et al., 2016; Karalis et al., 2016b).

### 4.1.2 Impact of anxiety on PFC-mediated flexible cognitive control of behavior

Anxiety has been associated with detrimental effects on PFC-mediated cognitive control of behavior in complex task situations wherein rule-based decision-making and/or flexible shift to a new strategy are required. By examining the prefrontal neural correlates of extradimensional set-shifting in a sustained state of anxiety, we found that cognitive inflexibility – i.e., inability to shift to a new task rule – was associated with disrupted neuronal encoding of task rules in dmPFC, but not OFC, as well as sustained suppression of the spontaneous PFC neuronal activity.

#### 4.1.2.1 Impact of anxiety on set-shifting task performance

The most pronounced behavioral impact of anxiety was difficulty in shifting to a new rule: as the animals treated with the anxiogenic FG7142 displayed impaired ability to shift to a new rule – i.e., cognitive inflexibility. Animals treated with the anxiogenic drug were specifically impaired when shifting from the light rule to the side rule; most errors were committed in conflict trials, wherein the light stimulus was presented on the invalid side. It is important to note that the anxiogenic-treated animals readily shifted from the side rule to the light rule. In general, the anxiogenic-treated animals tended to select the cue port with the light stimulus regardless of the rule. Therefore, we concluded that anxiety biased animals' action toward the light stimulus. Such behavioral bias may not be problematic in the absence of conflict, but it may be detrimental when a choice is required against the bias; i.e., when a choice based on a different perceptual dimension is required in the presence of conflict due to the irrelevant stimulus – i.e., a distractor. From a broader standpoint, these behavioral findings indicate that anxiety may bias decision making toward a sensory-based "bottom-up" process that is less flexible and more prone to distractions by irrelevant visual and other sensory distractors.

These findings, therefore, support the notion that, under anxiety, action selection is skewed by salient environmental stimuli at the expense of flexible top-down guided choices. It is important to note that such anxiety-related behavioral bias may be beneficial in hazardous and unpredictable situations when detection of potential threats and reflexive responses are required, wherein reflective, rule-based behavioral guidance may not be feasible.

#### 4.1.2.2 PFC neural correlates of set-shifting

Cognitive flexibility – operationalized as flexible set-shifting in our study – involves a higher-order process requiring PFC neural encoding of multiple task-relevant variables such as the task rule and the response outcome signaled by delivery or omission of reward. A task rule comprises a permutation of relevant cues, actions, and outcomes; it defines an effective action leading to a desired outcome given the environmental stimuli at the moment. Once the action is executed, a neural representation of the outcome provides either a positive or negative reinforcement, allowing animals to retain the current rule or shift to an alternative rule in subsequent trials. We found that substantial proportions of dmPFC and OFC single neurons encoded the two critical task covariates – the task rule, and the response outcome of the previous and current trials. The single-neuronal encoding was corroborated by highly accurate decoding of the task variables achieved at the neural population level. Comparing PFC subregions, we found that dmPFC neurons tended to encode the task rule more robustly before and during the time of action, whereas OFC neurons displayed stronger encoding of the response outcome following the action, suggesting specialized roles subserved by the dmPFC and OFC for cognitive flexibility.

#### 4.1.2.3 Impact of anxiety on PFC neuronal baseline activity

The anxiogenic perturbation induced sustained suppression of dmPFC and OFC neuronal activity. The inhibitory effect of the anxiogenic was commonly observed in animals freely behaving in a home cage or performing the set-shifting task in an operant chamber. Such "hypofrontality" is consistent with human neuroimaging studies reporting reduced activation of the PFC in patients with anxiety disorders (Phelps et al., 2004; Shin et al., 2001). It is also consistent with studies showing stress-induced structural plasticity, such as general atrophy of dendrites and loss of spines that may lead to reduced excitatory tone in the PFC (Russo and Nestler, 2013; Shansky et al., 2009).

Mechanistically, anxiety-related PFC neuronal suppression is likely to be attributed to the increased prefrontal DA transmission due to activation of the mesoprefrontal circuit. Converging lines of evidence point to this DA hypothesis. First, rodent and non-human primate studies have consistently demonstrated that the anxiogenic compound (FG7142), similar to other types of stressors, increased the DA concentration in PFC (Abercrombie et al., 1989; Bradberry et al., 1991a; Moghaddam et al., 1990; Thierry et al., 1976). Likewise, hyper-reactive mesoprefrontal circuit was associated with clinical anxiety in humans (Cha et al., 2014). Second, the mesoprefrontal VTA DA neurons receive preferential input from the LHb, a brain area that selectively responds to aversive behavioral states. Accordingly, stimulation of VTA DA terminals in the PFC induced anxiety-like behavior (Gunaydin et al., 2014). Finally, the post-synaptic effects of DA on PFC neurons are known to be complex, but primarily inhibitory when examined *in vivo* (Gorelova et al., 2002; Seamans et al., 2001; Sesack and Bunney, 1989). Thus, the anxiety-induced reduction in PFC neuronal activity may be mediated, in part, by selective activation of dopamine release in PFC.

#### 4.1.2.4 Impact of anxiety on the PFC neural correlates of set-shifting

We next investigated how the anxiogenic perturbation affected PFC neuronal encoding of task-relevant variables in task performing animals. The most pronounced impact of the anxiogenic was a significant decline in the dmPFC (but not OFC) neuronal encoding of the task rule preceding the action, suggesting that dmPFC-mediated rule-based action selection is disrupted in anxiety. The impaired dmPFC rule encoding was demonstrated as reduced proportion of rule-encoding neurons, as well as declined accuracy in decoding the task rule from the dmPFC neural population activity. By contrast, dmPFC and OFC neuronal encoding of task covariates reflecting animals' trial-by-trial behavior – such as the response outcome, direction, and latency – remained intact when the system was perturbed by administration of the anxiogenic drug. Together these findings suggested susceptibility of the dmPFC neuronal encoding of the task rule to the anxiogenic perturbation.

Disrupted dmPFC neuronal encoding of the task rule has been also demonstrated as the lack of the emerging neuronal selectivity between rules which was observed when animals learned set-shifting across trials in the absence of the anxiogenic perturbation. To associate this reduced dmPFC neural representation of the task rule with the specific behavioral deficit observed in conflict trials during the light-to-side rule shift, we further examined dmPFC neuronal rule discriminability specifically in conflict vs non-conflict trials. From the neural data recorded in the absence of anxiogenic perturbation, we observed that dmPFC neurons discriminated their firing activity compared with that of the other rule, which may be required to direct their behavior in the presence of the conflict. The anxiogenic perturbation diminished dmPFC neuronal rule discriminability in the conflict trials during the light-to-side shift, which

was consistent with the specific behavioral impairment in these trials – i.e., conflict trials in the side rule.

Taken together, these results suggest that dmPFC neuronal encoding of the task rule was susceptible to the anxiogenic perturbation, leading to errors specifically when the rule-based guidance of behavior is required due to the presence of explicit distractors. The critical question is why the neuronal encoding of the task rule is specifically vulnerable to anxiogenic perturbation. We currently have an incomplete answer to this. Encoding the task rule is a higher-order process that involves the representation of relationships among the task-relevant cues, actions, and outcomes, unlike the encoding of other task covariates that could be processed on a trial-by-trial basis. PFC neuronal encoding of a construct comprising complex cognitive-perceptual structures may involve fine-tuned ensemble activity of numerous neurons, which might be more susceptible to perturbations. Thus, our findings suggest that the higher-order processing subserved by dmPFC may be particularly vulnerable to anxiety.

## 4.2 THE NEURAL BASIS FOR THE BEHAVIORAL IMPACT OF ANXIETY

In this section, we discuss how our findings relate to and further advance our current understanding of the neural basis of anxiety and behavioral its impact. Our data suggest that the neural basis of behavioral effects of anxiety may not be described simplistically as activation or inhibition of one specific type of neurons at one particular time point. Rather, the results suggest that anxiety affects both spontaneous and task-related activity of single neurons, neural populations, and network-level neural oscillations in the VTA-mPFC circuit, leading to aberrant cognitive and motivational processing.

### 4.2.1 Current models explaining the behavioral impact of anxiety

For the recent decades, converging data have supported the hypothesis that mood disorders, including anxiety and depression, are characterized in part by a loss of excitatory and inhibitory PFC control over subcortical structures that process reward and punishment, such as the amygdala and, ventral and dorsal striatal areas, leading to aberrant affective and cognitive behaviors (Calhoon and Tye, 2015; Luthi and Luscher, 2014; Russo and Nestler, 2013; Tovote et al., 2015). This anomalous PFC control has been associated with changes in spontaneous and task-related PFC neural functioning (Arnsten, 2015; Maren and Holmes, 2016). Likewise, structural changes such as stress-induced synaptic plasticity, atrophy of neuronal dendrites and, loss of spines have suggested reduction of the excitatory tone in PFC (Liu et al., 2012; Shansky et al., 2009). In this framework, the VTA-mPFC circuit comprises a critical node, since stress-induced activation of the mesoprefrontal circuit, as well as a sustained increase in the PFC DA tone, have both been associated with anxiety-related disruptions in PFC neural functioning (Arnsten, 2009; Hains and Arnsten, 2008).

While this simplistic model remains conceptually valid, a more integrative and updated model needs to be synthesized, as our understanding of the PFC and mesocorticolimbic neural bases for cognitive, motivational, and affective processing has grown rapidly. Most importantly, mounting evidence has demonstrated that the PFC comprises highly heterogeneous neuron groups that encode different task events with distinct patterns of activity (Matsumoto et al., 2007; Pinto and Dan, 2015; Seo and Lee, 2009; Ye et al., 2016). In fact, such heterogeneity – i.e., mixed selectivity – has been suggested as a key computational property that is essential for cognitive functions of the PFC (Ma et al., 2014; Rigotti et al., 2013). We reason that this

heterogeneous patterns of neuronal response, under “normal” or anxious conditions would be best revealed when an animal is cognitively and affectively engaged within a task.

Functional heterogeneity observed in mesocorticolimbic brain areas is often associated with anatomical input-output connectivity, such that neurons that are similarly tuned for a task variable are more likely to be connected to each other (Lammel et al., 2011; Lammel et al., 2012). In addition to anatomical connectivity, enormous evidence has shown that functional connectivity may arise in association with a task-related construct in the form of neuron-to-neuron interaction and/or network-wide interaction through coherent oscillations (Adhikari et al., 2010; Buschman et al., 2012; Fries, 2015; Fujisawa et al., 2008; Fujisawa and Buzsaki, 2011; Karalis et al., 2016b; Kim et al., 2012; Kim et al., 2010; Likhtik et al., 2014). Such circuit- or network-level neural phenomena may only be revealed through the simultaneous monitoring of two or more neural structures from task performing animals. Therefore, we focused on how specific neural functioning was modulated by an anxiogenic perturbation with simultaneous recording from the VTA-mPFC neural circuit or different PFC subregions.

### 4.2.2 Synthesizing an advanced model to explain the behavioral impact of anxiety

Some of our findings are in partial agreement with the classic model for the PFC and mesoprefrontal role in the representation of anxiety. Numerous studies have suggested that the VTA-mPFC circuit preferentially responds to stressors and the resultant anxiety. Neurophysiological studies have shown that subpopulations of VTA DA neurons tend to increase their firing rates in response to aversive stimuli (Barik et al., 2013; Brischoux et al., 2009; Holly and Miczek, 2016; Thierry et al., 1976; Valenti et al., 2011; Zweifel et al., 2008). Meanwhile, neurochemical studies have shown elevation of DA concentration in the PFC in response to

stressful and anxiogenic manipulations (Abercrombie et al., 1989; Bradberry et al., 1991b; Moghaddam et al., 1990). It should be noted that many of these results was obtained while animals were anesthetized or freely behaving without task performance, corresponding to the baseline period in our experiments. Indeed, our baseline neuronal activity data were consistent with these previous findings (Figure 2-9). We found VTA DA neurons displayed elevated baseline firing rates in anxiety; on the other hand, we observed sustained suppression of baseline PFC neuronal activity by the anxiogenic treatment (Figure 3-1). Thus, the classic view on the mesoprefrontal representation of anxiety may fit the overall basal circuit state of anxiety: hyper- and hypo-activity of VTA DA neurons and PFC neurons, respectively. However, when we examined task-related neuronal activity under the anxiety condition, we observed highly heterogeneous modulations of neuronal activity. We believe that interpreting these heterogeneous activity modulations and their relationship to behavioral alterations is the key to understand the neural basis of anxiety.

#### 4.2.2.1 Examination of task-related neuronal activity reveals neural functioning susceptible to anxiety

Considering the abovementioned functional heterogeneity of VTA and mPFC neurons, it is critical to tease out which neuronal functions are specifically affected by anxiety in connection with a specific behavioral disruption. In a translational perspective, such specificity is of great importance in discovering therapeutic targets for specific behavioral symptoms related to stress and anxiety. Collectively, our findings demonstrate that the VTA and mPFC neuronal encoding of action is specifically more prone to disruptions in anxiety, while the sustained impact of anxiety also involves moderate alterations in baseline neuronal activity (Figure 4-1). This susceptibility of peri-action encoding to the effects of anxiety was observed throughout our

experiments, in which the action involved a complex decision making or distinct action-outcome contingencies. Specifically, we observed that mPFC neuronal encoding of the task rule required for the rule-based action selection was selectively impaired in anxiety (Section 3). In addition, we observed that the mPFC and VTA neuronal activity during a simple instrumental action was profoundly modulated as a function of punishment risk contingent on the action. By contrast, the impact of anxiety on neuronal activity at the time of the task outcome or at the time of the cue appeared to be less pronounced.

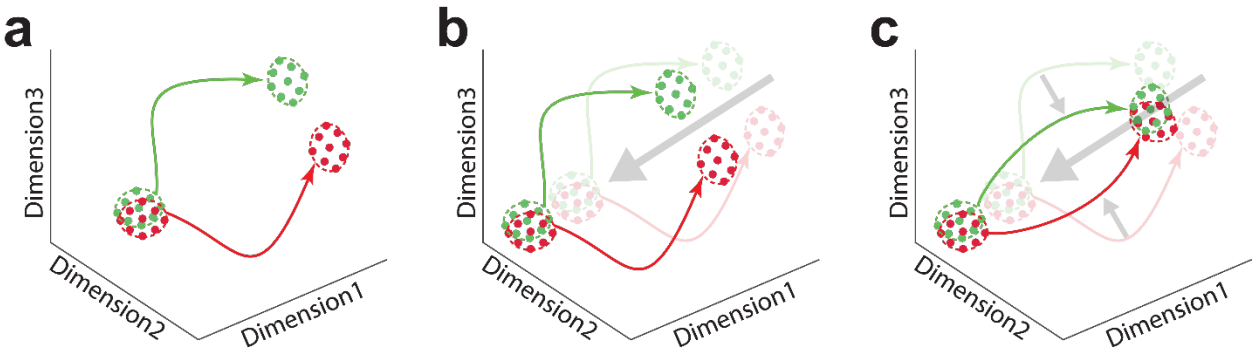


**Figure 4-1 Fictive illustrations of trial-by-trial neuronal population activity represented in the neural population state space (hypothetical data).**

(a) Trial-by-trial neural population states/trajectories during the peri-action epoch can be extracted by dimensionality reduction methods. Each dot represents the neural population state within the population state space defined based on the neuronal population activity co-modulation structure. The peri-action neural population trajectories may differ as a function of a task covariate relevant to the control of the action. For instance, a trajectory from one task rule (green) may be differentiated from that of another rule (red) in a cognitive decision-making task. Each line depicts a time-evolving neural population trajectory from the beginning and end of each trial. (b) Our data suggest that anxiety induces sustained changes in the ongoing activity of the individual neurons and neuronal populations (depicted with a gray arrow) that may be associated with sustained anxiety-related behavioral and affective changes

on a large time scale. (c) Furthermore, our neural data analyses reveal that anxiety specifically disrupts the peri-action activity of the individual neurons and neural populations (depicted with small gray arrows) on top of the sustained changes in the baseline activity (depicted with a large gray arrow). This specific alteration of the peri-action neuronal activity was associated with the disruption of goal-directed action involving motivational and cognitive processing in anxiety.

The selective susceptibility of the neuronal encoding of action to perturbation by anxiety reveals an important principle underlying the behavioral impact of anxiety: that is, the impact of anxiety may be more pronounced when the system is actively engaged in processing of task-relevant covariates to produce an adaptive behavior. To select and generate a goal-directed action, processing of diverse task-relevant covariates is required, which involves heterogeneous fine-tuned neuronal activity as a function of the task covariates. This dynamic state of the system may be more vulnerable to anxiogenic perturbations, resulting in cognitive errors or emotional responses as observed in our study and elsewhere (Arnsten, 2015). In support of this idea, we observed that the peri-action neuronal activity per se as well as the peri-action neuronal encoding of task covariates were more sensitive to anxiogenic manipulations. Furthermore, we noted that the peri-action neural oscillatory activity in the VTA-mPFC circuit displayed susceptibility to anxiety. We observed that mesoprefrontal theta oscillations arose specifically at the time of the action during the risky reward-seeking task in a non-anxious state, effectively phase-modulating the VTA and mPFC neuronal spike activity. Both neural oscillation and oscillation-mediated neural synchrony are known to arise as a net result of dynamic excitatory and inhibitory interactions amongst distinct types of principal neurons and local interneurons (Buzsaki et al.,

2012). The observed disruption of the peri-action neural oscillations supports the notion that a dynamic state of the neural system may enhance its vulnerability to anxiety.

#### 4.2.2.2 Functional heterogeneity may represent the mesocorticolimbic "appetitive" vs "aversive" network

We observed profound functional heterogeneity when we examined how mPFC and VTA neurons modulated their peri-action activity as a function of punishment risk contingent on the action. In both regions, we found that equivalent proportions of neurons exhibited excitatory vs inhibitory activity modulations – i.e., some increased their firing rates, while others decreased their firing rates as a function of punishment risk (Section 2, Figure 2-7b). While this functional heterogeneity could be interpreted as encoding of distinct motivational properties by different groups of neurons, as discussed in Section 2, critical questions remain: how do these distinct neuronal responses arise? Do neurons that show similar responses across different brain regions comprise functional networks that preferentially represent appetitive or aversive behavioral states? Specifically, do the VTA and mPFC neurons that increased or decreased their activity as a function of punishment risk comprise aversive vs appetitive neuronal networks?

Accumulating evidence suggests that neuron groups responding to appetitive vs aversive task events may be segregated by their distinct input-output connectivity – i.e., projection specificity (Beier et al., 2015; Lammel et al., 2011; Lammel et al., 2012; Menegas et al., 2015; Ye et al., 2016). Remarkably, recent findings indicate that distinct groups of neurons even within the same region possess distinct appetitive vs aversive tuning based on their input-output connectivity, in contrast to the classic way of thinking that tended to assign one brain region exclusively to either side. For example, a series of studies have demonstrated that distinct DA neuron groups were distinguished by their input-output connectivity and anatomical localization

within the VTA (Beier et al., 2015; Lammel et al., 2008; Lammel et al., 2011; Lammel et al., 2012). Optogenetic activation of these distinct circuits led to appetitive or aversive behavioral consequences, supporting the notion that distinct functional neural networks may exist in the mesocorticolimbic system (Gunaydin et al., 2014; Lammel et al., 2012). Likewise, Ye et al., (2016) found that distinct mPFC neuron groups emerged in response to appetitive or aversive behavioral experiences. Using brain-wide axonal projection mapping, the authors demonstrated that the mPFC neurons that selectively responded to appetitive vs aversive events preferentially projected to the NAc or LHb, respectively (Ye et al., 2016). Collectively, these results suggest that distinct functional neural networks, comprising neuron groups from overlapping and non-overlapping mesocorticolimbic regions, may represent distinct-valence experiences. In this framework, anxiety can be redefined as a neural state wherein the mesocorticolimbic neural networks of representing negative and positive valence are hyper- and hypo-active, respectively. Accordingly, the heterogeneous VTA and mPFC neuronal groups with distinct responses to punishment risk may represent the increased and decreased activation, respectively, of the aversive and appetitive networks in a risky situation. Admittedly, the lack of interrogation of projection specificity in our study prevents us from fully testing this hypothesis. Future studies using electrophysiology from neurons with their input-output connectivity revealed by viral tracing will be necessary for a rigorous test of this hypothesis.

#### 4.2.2.3 Oscillation-based neural synchrony may mediate the activation of an “aversive” cell assembly and deactivation of an “appetitive” cell assembly in anxiety

While the anatomical input-output connectivity may be the foundation for the appetitive and aversive neural networks, it alone may not be sufficient to resolve the “binding problem”: i.e., how are the neuron groups within the network recruited together selectively, in a temporally

specific manner, within the proper behavioral context? In this regard, the neural synchrony mediated by coherent oscillations may play a key role in activation or deactivation of a specific functional neural network depending on the behavioral context. We believe that the 8 Hz-oscillation-mediated neural synchrony in the VTA-mPFC circuit may play this role for the following reasons (Figure 4-2). First, if an oscillation-mediated synchrony is used for selective binding of appetitive or aversive neuron groups, the oscillation itself should be discriminative of the behavioral state. The mesoprefrontal 8 Hz oscillation satisfies this, as it exhibited sensitivity for punishment risk. Second, the 8 Hz oscillation appeared to be coherent across different brain regions; in addition, the VTA-driven 8 Hz oscillation could coordinate neuronal spike activity in both VTA and mPFC. This interregional coherence and synchrony are thought to be crucial criteria for an oscillation to support a brain-wide functional neural network. Third, a functional neural network is thought to emerge specifically at the moment when an appetitive (approach) or an aversive (avoidance) behavior is required – i.e., it should exhibit temporal specificity. The 8 Hz oscillation arose specifically during preparation and execution of the appetitive action in the absence of risk. Considering these properties, we propose that the 8 Hz-osillation-mediated neural synchrony promotes the formation of the appetitive neural network in an appetitive behavioral state by synchronizing the activity of the neurons emitting spikes during risk-free reward-seeking actions. Although we only recorded from the VTA and mPFC, it has been shown in many studies that neural oscillations, especially low-frequency oscillations, often represent a network-level phenomenon implicating multiple neural structures (Adhikari et al., 2010; Fujisawa and Buzsaki, 2011; Karalis et al., 2016b; Kopell et al., 2000). Therefore, a future study with simultaneous recording of more mesocorticolimbic structures will ultimately be needed to

test the hypothesis that the 8 Hz-mediated neural synchrony is a manifestation of the brain-wide formation of a network for appetitive behavior.

A critical remaining question is whether there is other oscillation-based neural synchrony between VTA and PFC that are selective for an aversive state. In our study, we have not observed the emergence of a distinct oscillation in the VTA-mPFC circuit that is clearly associated with an anxious state, while we observed the decline of the 8 Hz-mediated neural synchrony. However, we note that other groups recently have shown that a slower theta band oscillation (4 Hz) arose in mPFC in synchrony with the amygdala during a conditioned fearful state (Dejean et al., 2016; Karalis et al., 2016b; Likhtik et al., 2014). This suggests that the slower 4 Hz theta oscillation may contribute to the formation of an "aversive" cell assembly, in contrast to the faster 8 Hz theta oscillation that we believe contributes to an "appetitive" cell assembly. This scenario would predict that the appetitive cell assembly mediated by the faster theta rhythm may diminish in the presence of punishment risk, whereas we would expect the aversive cell assembly based on the slower theta to arise in the mesoprefrontal circuit. Consistent with this prediction, we showed that the mesoprefrontal 8 Hz-mediated synchrony significantly declined as a function of risk. However, we did not observe the emergence of a 4 Hz oscillation; we speculate that this is the case because animals in our task engaged in instrumental actions even in the presence of risk unlike the fear-conditioned animals that generated freezing, for the most part – i.e., primarily an avoidance response – in other studies.

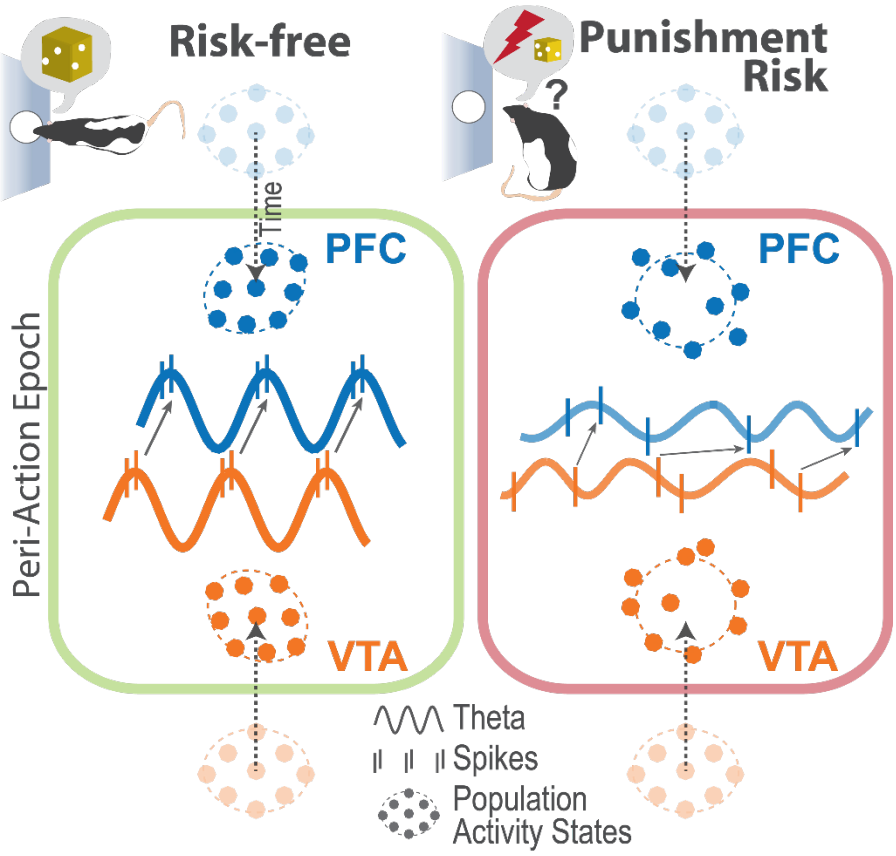


**Figure 4-2 Punishment risk disrupts individual neuron and neuronal population activity as well as 8 Hz-oscillation-mediated neural synchrony in the VTA-mPFC neural circuit.**

Punishment risk contingent on the action was represented by the majority of individual VTA and mPFC neurons with bidirectional modulation of their activity. This heterogeneous individual neuronal activity modulation gave rise to distinct neural population activity states, from which trial-by-trial risk-based behavior could be accurately inferred. At the neural circuit level, punishment risk reduced the 8 Hz-oscillation-mediated neural synchrony in the mesoprefrontal circuit that emerged during the purely appetitive action in the absence of punishment risk. Neural synchrony mediated by an 8 Hz oscillation may subserve binding of the mesoprefrontal neurons responding to the appetitive action into the “appetitive” neural network. Our observation of the decline in 8 Hz-mediated neural synchrony may reflect reduced activation of the appetitive neural network in the presence of punishment risk.

In sum, our findings and recent findings from others suggest that anxiety may be a state supported by the activation of a brain-wide aversive neural network and deactivation of the appetitive network, each of which involving distinct neural oscillations and oscillation-mediated neural synchrony. From a translational perspective, it will be important to address whether recovering the faster theta rhythmicity associated with appetitive behavior might promote recovery from pathological aversive behaviors observed in anxiety and other mood disorders.

## 4.3 CONCLUSION AND FUTURE DIRECTIONS

The current dissertation work focused on gaining a better understanding of the nature of VTA and PFC neural representations of anxiety and its impact on cognitive and motivated behavior. Some older models suggested that stress and resultant anxiety are associated with hyperactivity of the mesoprefrontal circuit, which leads to aberrant cognitive and motivational processing in the PFC. Our findings suggest that this simplistic model may partially fit the basal, non-task-related state of the mesoprefrontal circuit in anxiety. However, analyses of the neural and behavioral data during task events have revealed important aspects of the mesoprefrontal neural representation of anxiety and its behavioral impacts.

First, we found that mPFC and VTA neuronal activity and neuronal encoding of task covariates, before and during the action was specifically susceptible to anxiogenic perturbation. The peri-action period is a dynamic state, wherein complex functions amongst cue, action, and outcome are represented with fine-tuned patterns of neuronal activity that presumably facilitate the selection and generation of an adaptive action. We observed that the peri-action neuronal activity and the peri-action neuronal encoding of task covariates, such as the task rule, were

particularly prone to disruptions in anxiety. This suggests that a dynamic state of the nervous system may increase vulnerability to anxiogenic perturbations.

Second, we found that distinct mPFC and VTA neuron groups displayed excitatory or inhibitory activity modulations in anxiety. This functional heterogeneity suggests that distinct groups of neurons may be preferentially tuned for appetitive vs aversive behavioral states. Mounting evidence suggests that neuron groups with similar behavioral tuning tend to be anatomically connected to one another (Beier et al., 2015; Lammel et al., 2011; Lammel et al., 2012; Menegas et al., 2015; Ye et al., 2016); this supports the notion that distinct functional neural networks, comprising groups of neurons with similar behavioral valence tuning, may be activated or suppressed to promote an appetitive or aversive behavior. Extending this notion, we propose that coherent oscillation-mediated neural synchrony may bind distinct neuron groups across the mesocorticolimbic system into a cell assembly that gives rise to an aversive or appetitive behavior (Figure 4-2). Under this framework, anxiety may be best defined as a biased neural state supported by overactivation of the brain-wide aversive neural network and underactivation of the appetitive network, each of which involves distinct neural oscillations and oscillation-mediated neural synchrony. These neural states may promote representation of environmental stimuli of high salience and negative valence, and lead to execution of appropriate behavioral responses. Importantly, however, our data indicate that the behavioral coping may come at the expense of disruptions in flexible top-down control of behavior.

Our model must be further developed and verified in future studies. Within the PFC and mesoprefrontal neural circuit, further interrogations of neuronal activity, in combination with viral and/or optogenetic tagging of input-output connectivity and/or cell-type specificity, may allow us to draw connections among certain types of activity modulation of specific cell groups

with specific behavioral changes in anxiety. We suggest that distinct brain-wide functional neural networks, mediated by coherent oscillations across mesocorticolimbic structures, may bind neurons together into a cell assembly that respond preferentially to an appetitive or an aversive state. To test this notion experimentally, simultaneous multi-site electrophysiological recording will be necessary to capture the ebbs and flows of functional neural networks underlying anxiety-like behaviors.

Clinically, the current findings suggest that the VTA-mPFC circuit might be a promising target for a circuit-based intervention with currently available tools for deep brain stimulation or transcranial stimulation that have been effective in treating other psychiatric and neurological symptoms (Laxton et al., 2010; Mayberg et al., 2005; Stefani et al., 2007). To this end, our data suggest that recovering the VTA-driven theta oscillations in the mesoprefrontal and mesocorticolimbic networks could be a viable approach to drive goal-directed behavior, potentially overcoming the behavioral impact of anxiety.

# 5.0 BIBLIOGRAPHY

Abercrombie, E.D., Keefe, K.A., DiFrischia, D.S., and Zigmond, M.J. (1989). Differential effect of stress on in vivo dopamine release in striatum, nucleus accumbens, and medial frontal cortex. J Neurochem 52, 1655-1658.

Aberman, J.E., and Salamone, J.D. (1999). Nucleus accumbens dopamine depletions make rats more sensitive to high ratio requirements but do not impair primary food reinforcement. Neuroscience 92, 545-552.

Adhikari, A. (2014). Distributed circuits underlying anxiety. Front Behav Neurosci 8, 112.

Adhikari, A., Topiwala, M.A., and Gordon, J.A. (2010). Synchronized activity between the ventral hippocampus and the medial prefrontal cortex during anxiety. Neuron 65, 257-269.

Adhikari, A., Topiwala, M.A., and Gordon, J.A. (2011). Single units in the medial prefrontal cortex with anxiety-related firing patterns are preferentially influenced by ventral hippocampal activity. Neuron 71, 898-910.

Anderson, M.H., Hardcastle, C., Munafo, M.R., and Robinson, E.S. (2012). Evaluation of a novel translational task for assessing emotional biases in different species. Cogn Affect Behav Neurosci 12, 373-381.

Anderson, S.W., Bechara, A., Damasio, H., Tranel, D., and Damasio, A.R. (1999). Impairment of social and moral behavior related to early damage in human prefrontal cortex. Nature neuroscience 2, 1032-1037.

Arnsten, A.F. (2000). Stress impairs prefrontal cortical function in rats and monkeys: role of dopamine D1 and norepinephrine alpha-1 receptor mechanisms. Prog Brain Res 126, 183-192.

Arnsten, A.F. (2009). Stress signalling pathways that impair prefrontal cortex structure and function. Nature reviews Neuroscience 10, 410-422.

Arnsten, A.F. (2015). Stress weakens prefrontal networks: molecular insults to higher cognition. Nat Neurosci 18, 1376-1385.

Asaad, W.F., Rainer, G., and Miller, E.K. (2000). Task-specific neural activity in the primate prefrontal cortex. J Neurophysiol 84, 451-459.

Aso, Y., and Rubin, G.M. (2016). Dopaminergic neurons write and update memories with cell-type-specific rules. Elife 5.

Atack, J.R., Hutson, P.H., Collinson, N., Marshall, G., Bentley, G., Moyes, C., Cook, S.M., Collins, I., Wafford, K., McKernan, R.M., and Dawson, G.R. (2005). Anxiogenic properties of an inverse agonist selective for alpha3 subunit-containing GABA A receptors. Br J Pharmacol 144, 357-366.

Baeg, E.H., Kim, Y.B., Jang, J., Kim, H.T., Mook-Jung, I., and Jung, M.W. (2001). Fast spiking and regular spiking neural correlates of fear conditioning in the medial prefrontal cortex of the rat. Cerebral cortex 11, 441-451.

Balleine, B.W., and Dickinson, A. (1998). Goal-directed instrumental action: contingency and incentive learning and their cortical substrates. Neuropharmacology 37, 407-419.

Bar-Haim, Y., Lamy, D., Pergamin, L., Bakermans-Kranenburg, M.J., and van, I.M.H. (2007). Threat-related attentional bias in anxious and nonanxious individuals: a meta-analytic study. Psychological bulletin 133, 1-24.

Barik, J., Marti, F., Morel, C., Fernandez, S.P., Lanteri, C., Godeheu, G., Tassin, J.P., Mombereau, C., Faure, P., and Tronche, F. (2013). Chronic stress triggers social aversion via glucocorticoid receptor in dopaminoceptive neurons. Science 339, 332-335.

Barnett, L., and Seth, A.K. (2014). The MVGC multivariate Granger causality toolbox: a new approach to Granger-causal inference. J Neurosci Methods 223, 50-68.

Bechara, A., Tranel, D., and Damasio, H. (2000). Characterization of the decision-making deficit of patients with ventromedial prefrontal cortex lesions. Brain 123 ( Pt 11), 2189-2202.

Bechara, A., Tranel, D., Damasio, H., and Damasio, A.R. (1996). Failure to respond autonomically to anticipated future outcomes following damage to prefrontal cortex. Cerebral cortex 6, 215-225.

Beier, K.T., Steinberg, E.E., DeLoach, K.E., Xie, S., Miyamichi, K., Schwarz, L., Gao, X.J., Kremer, E.J., Malenka, R.C., and Luo, L. (2015). Circuit Architecture of VTA Dopamine Neurons Revealed by Systematic Input-Output Mapping. Cell 162, 622-634.

Berger, B., Thierry, A.M., Tassin, J.P., and Moyne, M.A. (1976). Dopaminergic innervation of the rat prefrontal cortex: a fluorescence histochemical study. Brain Res 106, 133-145.

Bertolino, A., Arciero, G., Rubino, V., Latorre, V., De Candia, M., Mazzola, V., Blasi, G., Caforio, G., Hariri, A., Kolachana, B., *et al.* (2005). Variation of human amygdala response during threatening stimuli as a function of 5'HTTLPR genotype and personality style. Biol Psychiatry 57, 1517-1525.

Birrell, J.M., and Brown, V.J. (2000). Medial frontal cortex mediates perceptual attentional set shifting in the rat. The Journal of neuroscience : the official journal of the Society for Neuroscience 20, 4320-4324.

Bishop, S., Duncan, J., Brett, M., and Lawrence, A.D. (2004). Prefrontal cortical function and anxiety: controlling attention to threat-related stimuli. Nature neuroscience 7, 184-188.

Bishop, S.J. (2007). Neurocognitive mechanisms of anxiety: an integrative account. Trends in cognitive sciences 11, 307-316.

Bishop, S.J. (2009). Trait anxiety and impoverished prefrontal control of attention. Nature neuroscience 12, 92-98.

Bissonette, G.B., Martins, G.J., Franz, T.M., Harper, E.S., Schoenbaum, G., and Powell, E.M. (2008). Double dissociation of the effects of medial and orbital prefrontal cortical lesions on attentional and affective shifts in mice. The Journal of neuroscience : the official journal of the Society for Neuroscience 28, 11124-11130.

Bissonette, G.B., Schoenbaum, G., Roesch, M.R., and Powell, E.M. (2015). Interneurons are necessary for coordinated activity during reversal learning in orbitofrontal cortex. Biol Psychiatry 77, 454-464.

Bokil, H., Andrews, P., Kulkarni, J.E., Mehta, S., and Mitra, P.P. (2010). Chronux: a platform for analyzing neural signals. J Neurosci Methods 192, 146-151.

Bradberry, C.W., Gruen, R.J., Berridge, C.W., and Roth, R.H. (1991a). Individual differences in behavioral measures: correlations with nucleus accumbens dopamine measured by microdialysis. Pharmacol Biochem Behav 39, 877-882.

Bradberry, C.W., Lory, J.D., and Roth, R.H. (1991b). The anxiogenic beta-carboline FG 7142 selectively increases dopamine release in rat prefrontal cortex as measured by microdialysis. J Neurochem 56, 748-752.

Brischoux, F., Chakraborty, S., Brierley, D.I., and Ungless, M.A. (2009). Phasic excitation of dopamine neurons in ventral VTA by noxious stimuli. Proc Natl Acad Sci U S A 106, 4894-4899.

Bromberg-Martin, E.S., Matsumoto, M., and Hikosaka, O. (2010). Dopamine in motivational control: rewarding, aversive, and alerting. Neuron 68, 815-834.

Brozoski, T.J., Brown, R.M., Rosvold, H.E., and Goldman, P.S. (1979). Cognitive deficit caused by regional depletion of dopamine in prefrontal cortex of rhesus monkey. Science 205, 929-932.

Bunge, S.A., Kahn, I., Wallis, J.D., Miller, E.K., and Wagner, A.D. (2003). Neural circuits subserving the retrieval and maintenance of abstract rules. Journal of neurophysiology 90, 3419-3428.

Burgos-Robles, A., Vidal-Gonzalez, I., and Quirk, G.J. (2009). Sustained conditioned responses in prelimbic prefrontal neurons are correlated with fear expression and extinction failure. The Journal of neuroscience : the official journal of the Society for Neuroscience 29, 8474-8482.

Burke, K.A., Takahashi, Y.K., Correll, J., Brown, P.L., and Schoenbaum, G. (2009). Orbitofrontal inactivation impairs reversal of Pavlovian learning by interfering with 'disinhibition' of responding for previously unrewarded cues. Eur J Neurosci 30, 1941-1946.

Buschman, T.J., Denovellis, E.L., Diogo, C., Bullock, D., and Miller, E.K. (2012). Synchronous oscillatory neural ensembles for rules in the prefrontal cortex. Neuron 76, 838-846.

Butts, K.A., Floresco, S.B., and Phillips, A.G. (2013). Acute stress impairs set-shifting but not reversal learning. Behavioural brain research 252, 222-229.

Butts, K.A., Weinberg, J., Young, A.H., and Phillips, A.G. (2011). Glucocorticoid receptors in the prefrontal cortex regulate stress-evoked dopamine efflux and aspects of executive function. Proc Natl Acad Sci U S A 108, 18459-18464.

Buzsaki, G., Anastassiou, C.A., and Koch, C. (2012). The origin of extracellular fields and currents--EEG, ECoG, LFP and spikes. Nat Rev Neurosci 13, 407-420.

Calhoon, G.G., and Tye, K.M. (2015). Resolving the neural circuits of anxiety. Nat Neurosci 18, 1394-1404.

Cardin, J.A., Carlen, M., Meletis, K., Knoblich, U., Zhang, F., Deisseroth, K., Tsai, L.H., and Moore, C.I. (2009). Driving fast-spiking cells induces gamma rhythm and controls sensory responses. Nature 459, 663-667.

Carr, D.B., and Sesack, S.R. (2000a). GABA-containing neurons in the rat ventral tegmental area project to the prefrontal cortex. Synapse 38, 114-123.

Carr, D.B., and Sesack, S.R. (2000b). Projections from the rat prefrontal cortex to the ventral tegmental area: target specificity in the synaptic associations with mesoaccumbens and mesocortical neurons. The Journal of neuroscience : the official journal of the Society for Neuroscience 20, 3864-3873.

Carter, C.S., Braver, T.S., Barch, D.M., Botvinick, M.M., Noll, D., and Cohen, J.D. (1998). Anterior cingulate cortex, error detection, and the online monitoring of performance. Science 280, 747-749.

Cha, J., Carlson, J.M., Dedora, D.J., Greenberg, T., Proudfit, G.H., and Mujica-Parodi, L.R. (2014). Hyper-reactive human ventral tegmental area and aberrant mesocorticolimbic connectivity in overgeneralization of fear in generalized anxiety disorder. J Neurosci 34, 5855-5860.

Cho, K.K., Hoch, R., Lee, A.T., Patel, T., Rubenstein, J.L., and Sohal, V.S. (2015). Gamma rhythms link prefrontal interneuron dysfunction with cognitive inflexibility in Dlx5/6(+/-) mice. Neuron 85, 1332-1343.

Christopoulos, G.I., Tobler, P.N., Bossaerts, P., Dolan, R.J., and Schultz, W. (2009). Neural correlates of value, risk, and risk aversion contributing to decision making under risk. The Journal of neuroscience : the official journal of the Society for Neuroscience 29, 12574-12583.

Cisler, J.M., and Koster, E.H. (2010). Mechanisms of attentional biases towards threat in anxiety disorders: An integrative review. Clin Psychol Rev 30, 203-216.

Clark, L., Bechara, A., Damasio, H., Aitken, M.R., Sahakian, B.J., and Robbins, T.W. (2008). Differential effects of insular and ventromedial prefrontal cortex lesions on risky decision-making. Brain 131, 1311-1322.

Clarke, H.F., Robbins, T.W., and Roberts, A.C. (2008). Lesions of the medial striatum in monkeys produce perseverative impairments during reversal learning similar to those produced by lesions of the orbitofrontal cortex. J Neurosci 28, 10972-10982.

Cohen, J.D., and Servan-Schreiber, D. (1992). Context, cortex, and dopamine: a connectionist approach to behavior and biology in schizophrenia. Psychol Rev 99, 45-77.

Cohen, J.Y., Amoroso, M.W., and Uchida, N. (2015). Serotonergic neurons signal reward and punishment on multiple timescales. Elife 4.

Cohen, J.Y., Haesler, S., Vong, L., Lowell, B.B., and Uchida, N. (2012). Neuron-type-specific signals for reward and punishment in the ventral tegmental area. Nature 482, 85-88.

Cohen, M.X., Krohn-Grimberghe, A., Elger, C.E., and Weber, B. (2007). Dopamine gene predicts the brain's response to dopaminergic drug. Eur J Neurosci 26, 3652-3660.

Cole, B.J., Hillmann, M., Seidelmann, D., Klewer, M., and Jones, G.H. (1995). Effects of benzodiazepine receptor partial inverse agonists in the elevated plus maze test of anxiety in the rat. Psychopharmacology 121, 118-126.

Courtin, J., Chaudun, F., Rozeske, R.R., Karalis, N., Gonzalez-Campo, C., Wurtz, H., Abdi, A., Baufreton, J., Bienvenu, T.C., and Herry, C. (2014). Prefrontal parvalbumin interneurons shape neuronal activity to drive fear expression. Nature 505, 92-96.

Darrah, J.M., Stefani, M.R., and Moghaddam, B. (2008). Interaction of N-methyl-D-aspartate and group 5 metabotropic glutamate receptors on behavioral flexibility using a novel operant set-shift paradigm. Behav Pharmacol 19, 225-234.

Davis, M. (2006). Neural systems involved in fear and anxiety measured with fear-potentiated startle. The American psychologist 61, 741-756.

Dejean, C., Courtin, J., Karalis, N., Chaudun, F., Wurtz, H., Bienvenu, T.C., and Herry, C. (2016). Prefrontal neuronal assemblies temporally control fear behaviour. Nature 535, 420-424.

Dias, R., Robbins, T.W., and Roberts, A.C. (1996). Dissociation in prefrontal cortex of affective and attentional shifts. Nature 380, 69-72.

Dias, R., Robbins, T.W., and Roberts, A.C. (1997). Dissociable forms of inhibitory control within prefrontal cortex with an analog of the Wisconsin Card Sort Test: restriction to novel situations and independence from "on-line" processing. J Neurosci 17, 9285-9297.

Dorow, R. (1987). FG 7142 and its anxiety-inducing effects in humans. Br J Clin Pharmacol 23, 781-782.

Durstewitz, D., Vittoz, N.M., Floresco, S.B., and Seamans, J.K. (2010). Abrupt transitions between prefrontal neural ensemble states accompany behavioral transitions during rule learning. Neuron 66, 438-448.

Duvarci, S., and Pare, D. (2014). Amygdala microcircuits controlling learned fear. Neuron 82, 966-980.

Euston, D.R., Gruber, A.J., and McNaughton, B.L. (2012). The role of medial prefrontal cortex in memory and decision making. Neuron 76, 1057-1070.

Evans, A.K., and Lowry, C.A. (2007). Pharmacology of the beta-carboline FG-7,142, a partial inverse agonist at the benzodiazepine allosteric site of the GABA A receptor: neurochemical, neurophysiological, and behavioral effects. CNS Drug Rev 13, 475-501.

Eysenck, M.W., Derakshan, N., Santos, R., and Calvo, M.G. (2007). Anxiety and cognitive performance: attentional control theory. Emotion 7, 336-353.

Fecteau, S., Knoch, D., Fregni, F., Sultani, N., Boggio, P., and Pascual-Leone, A. (2007). Diminishing risk-taking behavior by modulating activity in the prefrontal cortex: a direct current stimulation study. The Journal of neuroscience : the official journal of the Society for Neuroscience 27, 12500-12505.

Felix-Ortiz, A.C., Beyeler, A., Seo, C., Leppla, C.A., Wildes, C.P., and Tye, K.M. (2013). BLA to vHPC inputs modulate anxiety-related behaviors. Neuron 79, 658-664.

Fields, H.L., Hjelmstad, G.O., Margolis, E.B., and Nicola, S.M. (2007). Ventral tegmental area neurons in learned appetitive behavior and positive reinforcement. Annu Rev Neurosci 30, 289-316.

Floresco, S.B. (2013). Prefrontal dopamine and behavioral flexibility: shifting from an "inverted-U" toward a family of functions. Front Neurosci 7, 62.

Floresco, S.B., Block, A.E., and Tse, M.T. (2008). Inactivation of the medial prefrontal cortex of the rat impairs strategy set-shifting, but not reversal learning, using a novel, automated procedure. Behav Brain Res 190, 85-96.

Floresco, S.B., Magyar, O., Ghods-Sharifi, S., Vexelman, C., and Tse, M.T. (2006). Multiple dopamine receptor subtypes in the medial prefrontal cortex of the rat regulate set-shifting.

Neuropsychopharmacology : official publication of the American College of Neuropsychopharmacology 31, 297-309.

Forster, G.L., and Blaha, C.D. (2000). Laterodorsal tegmental stimulation elicits dopamine efflux in the rat nucleus accumbens by activation of acetylcholine and glutamate receptors in the ventral tegmental area. Eur J Neurosci 12, 3596-3604.

Fries, P. (2005). A mechanism for cognitive dynamics: neuronal communication through neuronal coherence. Trends in cognitive sciences 9, 474-480.

Fries, P. (2015). Rhythms for Cognition: Communication through Coherence. Neuron 88, 220-235.

Fujisawa, S., Amarasingham, A., Harrison, M.T., and Buzsaki, G. (2008). Behavior-dependent short-term assembly dynamics in the medial prefrontal cortex. Nat Neurosci 11, 823-833.

Fujisawa, S., and Buzsaki, G. (2011). A 4 Hz oscillation adaptively synchronizes prefrontal, VTA, and hippocampal activities. Neuron 72, 153-165.

Funahashi, S., Bruce, C.J., and Goldman-Rakic, P.S. (1989). Mnemonic coding of visual space in the monkey's dorsolateral prefrontal cortex. J Neurophysiol 61, 331-349.

Funahashi, S., Bruce, C.J., and Goldman-Rakic, P.S. (1990). Visuospatial coding in primate prefrontal neurons revealed by oculomotor paradigms. J Neurophysiol 63, 814-831.

Fuster, J.M. (1989). The Prefrontal Cortex: Anatomy Physiology and Neuropsychology of the Frontal Lobe. (New York: Raven).

Fuster, J.M., and Alexander, G.E. (1971). Neuron activity related to short-term memory. Science 173, 652-654.

Fuster, J.M., Bodner, M., and Kroger, J.K. (2000). Cross-modal and cross-temporal association in neurons of frontal cortex. Nature 405, 347-351.

Gamo, N.J., Lur, G., Higley, M.J., Wang, M., Paspalas, C.D., Vijayraghavan, S., Yang, Y., Ramos, B.P., Peng, K., Kata, A., *et al.* (2015). Stress Impairs Prefrontal Cortical Function via D1 Dopamine Receptor Interactions with Hyperpolarization-Activated Cyclic Nucleotide-Gated Channels. Biological psychiatry.

Gariano, R.F., and Groves, P.M. (1988). Burst firing induced in midbrain dopamine neurons by stimulation of the medial prefrontal and anterior cingulate cortices. Brain Res 462, 194-198.

Gillan, C.M., Kosinski, M., Whelan, R., Phelps, E.A., and Daw, N.D. (2016). Characterizing a psychiatric symptom dimension related to deficits in goal-directed control. Elife 5.

Giorgetta, C., Grecucci, A., Zuanon, S., Perini, L., Balestrieri, M., Bonini, N., Sanfey, A.G., and Brambilla, P. (2012). Reduced risk-taking behavior as a trait feature of anxiety. Emotion 12, 1373-1383.

Goldstein, L.E., Rasmusson, A.M., Bunney, B.S., and Roth, R.H. (1996). Role of the amygdala in the coordination of behavioral, neuroendocrine, and prefrontal cortical monoamine responses to psychological stress in the rat. The Journal of neuroscience : the official journal of the Society for Neuroscience 16, 4787-4798.

Gorelova, N., Seamans, J.K., and Yang, C.R. (2002). Mechanisms of dopamine activation of fast-spiking interneurons that exert inhibition in rat prefrontal cortex. Journal of neurophysiology 88, 3150-3166.

Gotham, A.M., Brown, R.G., and Marsden, C.D. (1988). 'Frontal' cognitive function in patients with Parkinson's disease 'on' and 'off' levodopa. Brain 111 ( Pt 2), 299-321.

Grace, A.A. (2016). Dysregulation of the dopamine system in the pathophysiology of schizophrenia and depression. Nature reviews Neuroscience 17, 524-532.

Granger, C.W.J. (1969). Investigating causal relations by econometric models and cross-spectral methods. Econometrica 37, 424-438.

Guarraci, F.A., and Kapp, B.S. (1999). An electrophysiological characterization of ventral tegmental area dopaminergic neurons during differential pavlovian fear conditioning in the awake rabbit. Behav Brain Res 99, 169-179.

Gunaydin, L.A., Grosenick, L., Finkelstein, J.C., Kauvar, I.V., Fenno, L.E., Adhikari, A., Lammel, S., Mirzabekov, J.J., Airan, R.D., Zalocusky, K.A., *et al.* (2014). Natural neural projection dynamics underlying social behavior. Cell 157, 1535-1551.

Hains, A.B., and Arnsten, A.F. (2008). Molecular mechanisms of stress-induced prefrontal cortical impairment: implications for mental illness. Learning & memory 15, 551-564.

Hamilton, J.P., Chen, M.C., Waugh, C.E., Joormann, J., and Gotlib, I.H. (2014). Distinctive and common neural underpinnings of major depression, social anxiety, and their comorbidity. Social cognitive and affective neuroscience.

Hariri, A.R., Drabant, E.M., Munoz, K.E., Kolachana, B.S., Mattay, V.S., Egan, M.F., and Weinberger, D.R. (2005). A susceptibility gene for affective disorders and the response of the human amygdala. Arch Gen Psychiatry 62, 146-152.

Hariri, A.R., Mattay, V.S., Tessitore, A., Fera, F., and Weinberger, D.R. (2003). Neocortical modulation of the amygdala response to fearful stimuli. Biol Psychiatry 53, 494-501.

Hariri, A.R., Mattay, V.S., Tessitore, A., Kolachana, B., Fera, F., Goldman, D., Egan, M.F., and Weinberger, D.R. (2002). Serotonin transporter genetic variation and the response of the human amygdala. Science 297, 400-403.

Harris, A.Z., and Gordon, J.A. (2015). Long-range neural synchrony in behavior. Annu Rev Neurosci 38, 171-194.

Hartley, C.A., and Phelps, E.A. (2012). Anxiety and decision-making. Biol Psychiatry 72, 113-118.

Herry, C., Ciocchi, S., Senn, V., Demmou, L., Muller, C., and Luthi, A. (2008). Switching on and off fear by distinct neuronal circuits. Nature 454, 600-606.

Hikosaka, O. (2010). The habenula: from stress evasion to value-based decision-making. Nat Rev Neurosci 11, 503-513.

Holly, E.N., and Miczek, K.A. (2016). Ventral tegmental area dopamine revisited: effects of acute and repeated stress. Psychopharmacology (Berl) 233, 163-186.

Homayoun, H., and Moghaddam, B. (2007). NMDA receptor hypofunction produces opposite effects on prefrontal cortex interneurons and pyramidal neurons. The Journal of neuroscience : the official journal of the Society for Neuroscience 27, 11496-11500.

Hong, S., Jhou, T.C., Smith, M., Saleem, K.S., and Hikosaka, O. (2011). Negative reward signals from the lateral habenula to dopamine neurons are mediated by rostromedial tegmental nucleus in primates. J Neurosci 31, 11457-11471.

Horvitz, J.C. (2000). Mesolimbocortical and nigrostriatal dopamine responses to salient non-reward events. Neuroscience 96, 651-656.

Hoshi, E., Shima, K., and Tanji, J. (1998). Task-dependent selectivity of movement-related neuronal activity in the primate prefrontal cortex. J Neurophysiol 80, 3392-3397.

Ikemoto, S. (2007). Dopamine reward circuitry: two projection systems from the ventral midbrain to the nucleus accumbens-olfactory tubercle complex. Brain Res Rev 56, 27-78.

Jedema, H.P., and Moghaddam, B. (1996). Characterization of excitatory amino acid modulation of dopamine release in the prefrontal cortex of conscious rats. J Neurochem 66, 1448-1453.

Jin, X., and Costa, R.M. (2010). Start/stop signals emerge in nigrostriatal circuits during sequence learning. Nature 466, 457-462.

Jocham, G., Klein, T.A., Neumann, J., von Cramon, D.Y., Reuter, M., and Ullsperger, M. (2009). Dopamine DRD2 polymorphism alters reversal learning and associated neural activity. J Neurosci 29, 3695-3704.

Joshua, M., Adler, A., Mitelman, R., Vaadia, E., and Bergman, H. (2008). Midbrain dopaminergic neurons and striatal cholinergic interneurons encode the difference between reward and aversive events at different epochs of probabilistic classical conditioning trials. J Neurosci 28, 11673-11684.

Karalis, N., Dejean, C., Chaudun, F., Khoder, S., Rozeske, R.R., Wurtz, H., Bagur, S., Benchenane, K., Sirota, A., Courtin, J., and Herry, C. (2016a). 4-Hz oscillations synchronize prefrontal-amygdala circuits during fear behavior. Nature neuroscience.

Karalis, N., Dejean, C., Chaudun, F., Khoder, S., Rozeske, R.R., Wurtz, H., Bagur, S., Benchenane, K., Sirota, A., Courtin, J., and Herry, C. (2016b). 4-Hz oscillations synchronize prefrontal-amygdala circuits during fear behavior. Nat Neurosci 19, 605-612.

Karlsson, M.P., Tervo, D.G., and Karpova, A.Y. (2012). Network resets in medial prefrontal cortex mark the onset of behavioral uncertainty. Science 338, 135-139.

Kehagia, A.A., Murray, G.K., and Robbins, T.W. (2010). Learning and cognitive flexibility: frontostriatal function and monoaminergic modulation. Curr Opin Neurobiol 20, 199-204.

Keren, G.L., C. (1979). Partial omega squared for ANOVA designs. Educational and Psychological Measurement 39.

Kerns, J.G., Cohen, J.D., MacDonald, A.W., 3rd, Cho, R.Y., Stenger, V.A., and Carter, C.S. (2004). Anterior cingulate conflict monitoring and adjustments in control. Science 303, 1023-1026.

Kim, S., and Lee, D. (2011). Prefrontal cortex and impulsive decision making. Biological psychiatry 69, 1140-1146.

Kim, S.Y., Adhikari, A., Lee, S.Y., Marshel, J.H., Kim, C.K., Mallory, C.S., Lo, M., Pak, S., Mattis, J., Lim, B.K., *et al.* (2013). Diverging neural pathways assemble a behavioural state from separable features in anxiety. Nature 496, 219-223.

Kim, Y., Wood, J., and Moghaddam, B. (2012). Coordinated activity of ventral tegmental neurons adapts to appetitive and aversive learning. PLoS One 7, e29766.

Kim, Y.B., Matthews, M., and Moghaddam, B. (2010). Putative gamma-aminobutyric acid neurons in the ventral tegmental area have a similar pattern of plasticity as dopamine neurons during appetitive and aversive learning. Eur J Neurosci 32, 1564-1572.

Knoch, D., Gianotti, L.R., Pascual-Leone, A., Treyer, V., Regard, M., Hohmann, M., and Brugger, P. (2006). Disruption of right prefrontal cortex by low-frequency repetitive transcranial magnetic stimulation induces risk-taking behavior. J Neurosci 26, 6469-6472.

Kobayashi, S., Nomoto, K., Watanabe, M., Hikosaka, O., Schultz, W., and Sakagami, M. (2006). Influences of rewarding and aversive outcomes on activity in macaque lateral prefrontal cortex. Neuron 51, 861-870.

Koizumi, A., Tanaka, A., Imai, H., Hiramatsu, S., Hiramoto, E., Sato, T., and de Gelder, B. (2011). The effects of anxiety on the interpretation of emotion in the face-voice pairs. Exp Brain Res 213, 275-282.

Konishi, S., Nakajima, K., Uchida, I., Kameyama, M., Nakahara, K., Sekihara, K., and Miyashita, Y. (1998). Transient activation of inferior prefrontal cortex during cognitive set shifting. Nature neuroscience 1, 80-84.

Kopell, N., Ermentrout, G.B., Whittington, M.A., and Traub, R.D. (2000). Gamma rhythms and beta rhythms have different synchronization properties. Proc Natl Acad Sci U S A 97, 1867-1872.

Kubota, K., and Niki, H. (1971). Prefrontal cortical unit activity and delayed alternation performance in monkeys. J Neurophysiol 34, 337-347.

Kumar, S., Hultman, R., Hughes, D., Michel, N., Katz, B.M., and Dzirasa, K. (2014). Prefrontal cortex reactivity underlies trait vulnerability to chronic social defeat stress. Nat Commun 5, 4537.

Lammel, S., Hetzel, A., Hackel, O., Jones, I., Liss, B., and Roeper, J. (2008). Unique properties of mesoprefrontal neurons within a dual mesocorticolimbic dopamine system. Neuron 57, 760-773.

Lammel, S., Ion, D.I., Roeper, J., and Malenka, R.C. (2011). Projection-specific modulation of dopamine neuron synapses by aversive and rewarding stimuli. Neuron 70, 855-862.

Lammel, S., Lim, B.K., Ran, C., Huang, K.W., Betley, M.J., Tye, K.M., Deisseroth, K., and Malenka, R.C. (2012). Input-specific control of reward and aversion in the ventral tegmental area. Nature 491, 212-217.

Laxton, A.W., Tang-Wai, D.F., McAndrews, M.P., Zumsteg, D., Wennberg, R., Keren, R., Wherrett, J., Naglie, G., Hamani, C., Smith, G.S., and Lozano, A.M. (2010). A phase I trial of deep brain stimulation of memory circuits in Alzheimer's disease. Ann Neurol 68, 521-534.

Lee, D. (2013). Decision making: from neuroscience to psychiatry. Neuron 78, 233-248.

Lesting, J., Narayanan, R.T., Kluge, C., Sangha, S., Seidenbecher, T., and Pape, H.C. (2011). Patterns of coupled theta activity in amygdala-hippocampal-prefrontal cortical circuits during fear extinction. PLoS One 6, e21714.

Levin, B.E., Llabre, M.M., and Weiner, W.J. (1989). Cognitive impairments associated with early Parkinson's disease. Neurology 39, 557-561.

Li, C.S., Chao, H.H., and Lee, T.W. (2009). Neural correlates of speeded as compared with delayed responses in a stop signal task: an indirect analog of risk taking and association with an anxiety trait. Cereb Cortex 19, 839-848.

Likhtik, E., Stujenske, J.M., Topiwala, M.A., Harris, A.Z., and Gordon, J.A. (2014). Prefrontal entrainment of amygdala activity signals safety in learned fear and innate anxiety. Nature neuroscience 17, 106-113.

Liu, R.J., Lee, F.S., Li, X.Y., Bambico, F., Duman, R.S., and Aghajanian, G.K. (2012). Brain-derived neurotrophic factor Val66Met allele impairs basal and ketamine-stimulated synaptogenesis in prefrontal cortex. Biol Psychiatry 71, 996-1005.

Livneh, U., and Paz, R. (2012). Amygdala-prefrontal synchronization underlies resistance to extinction of aversive memories. Neuron 75, 133-142.

Lodge, D.J., and Grace, A.A. (2006). The laterodorsal tegmentum is essential for burst firing of ventral tegmental area dopamine neurons. Proc Natl Acad Sci U S A 103, 5167-5172.

Luthi, A., and Luscher, C. (2014). Pathological circuit function underlying addiction and anxiety disorders. Nature neuroscience 17, 1635-1643.

Ma, L., Hyman, J.M., Lindsay, A.J., Phillips, A.G., and Seamans, J.K. (2014). Differences in the emergent coding properties of cortical and striatal ensembles. Nat Neurosci 17, 1100-1106.

Mackintosh, N.J. (1975). A theory of attention: variations in the associability of stimuli with reinforcement. Psychol Rev 82, 276-298.

Maner, J.K., Gailliot, M.T., Menzel, A.J., and Kunstman, J.W. (2012). Dispositional anxiety blocks the psychological effects of power. Pers Soc Psychol Bull 38, 1383-1395.

Mante, V., Sussillo, D., Shenoy, K.V., and Newsome, W.T. (2013). Context-dependent computation by recurrent dynamics in prefrontal cortex. Nature 503, 78-84.

Maren, S., and Holmes, A. (2016). Stress and Fear Extinction. Neuropsychopharmacology 41, 58-79.

Margolis, E.B., Mitchell, J.M., Ishikawa, J., Hjelmstad, G.O., and Fields, H.L. (2008). Midbrain dopamine neurons: projection target determines action potential duration and dopamine D(2) receptor inhibition. J Neurosci 28, 8908-8913.

Matsumoto, H., Tian, J., Uchida, N., and Watabe-Uchida, M. (2016). Midbrain dopamine neurons signal aversion in a reward-context-dependent manner. Elife 5.

Matsumoto, M., and Hikosaka, O. (2009). Two types of dopamine neuron distinctly convey positive and negative motivational signals. Nature 459, 837-841.

Matsumoto, M., Matsumoto, K., Abe, H., and Tanaka, K. (2007). Medial prefrontal cell activity signaling prediction errors of action values. Nat Neurosci 10, 647-656.

Mayberg, H.S., Lozano, A.M., Voon, V., McNeely, H.E., Seminowicz, D., Hamani, C., Schwalb, J.M., and Kennedy, S.H. (2005). Deep brain stimulation for treatment-resistant depression. Neuron 45, 651-660.

McAlonan, K., and Brown, V.J. (2003). Orbital prefrontal cortex mediates reversal learning and not attentional set shifting in the rat. Behav Brain Res 146, 97-103.

McClure, S.M., Laibson, D.I., Loewenstein, G., and Cohen, J.D. (2004). Separate neural systems value immediate and delayed monetary rewards. Science 306, 503-507.

Menegas, W., Bergan, J.F., Ogawa, S.K., Isogai, Y., Umadevi Venkataraju, K., Osten, P., Uchida, N., and Watabe-Uchida, M. (2015). Dopamine neurons projecting to the posterior striatum form an anatomically distinct subclass. Elife 4, e10032.

Meyer-Lindenberg, A., Buckholtz, J.W., Kolachana, B., A, R.H., Pezawas, L., Blasi, G., Wabnitz, A., Honea, R., Verchinski, B., Callicott, J.H., *et al.* (2006). Neural mechanisms of genetic risk for impulsivity and violence in humans. Proc Natl Acad Sci U S A 103, 6269-6274.

Meyers, E.M., Qi, X.L., and Constantinidis, C. (2012). Incorporation of new information into prefrontal cortical activity after learning working memory tasks. Proceedings of the National Academy of Sciences of the United States of America 109, 4651-4656.

Mikkelsen, J.D., Soderman, A., Kiss, A., and Mirza, N. (2005). Effects of benzodiazepines receptor agonists on the hypothalamic-pituitary-adrenocortical axis. European journal of pharmacology 519, 223-230.

Milad, M.R., and Quirk, G.J. (2002). Neurons in medial prefrontal cortex signal memory for fear extinction. Nature 420, 70-74.

Milad, M.R., and Quirk, G.J. (2012). Fear extinction as a model for translational neuroscience: ten years of progress. Annu Rev Psychol 63, 129-151.

Miller, E.K., and Cohen, J.D. (2001). An integrative theory of prefrontal cortex function. Annu Rev Neurosci 24, 167-202.

Milner, B. (1963). Effects of different brain lesions on card sorting: The role of the frontal lobes. Archives of Neurology 9, 100-110.

Mineka, S., Watson, D., and Clark, L.A. (1998). Comorbidity of anxiety and unipolar mood disorders. Annu Rev Psychol 49, 377-412.

Mingote, S., Weber, S.M., Ishiwari, K., Correa, M., and Salamone, J.D. (2005). Ratio and time requirements on operant schedules: effort-related effects of nucleus accumbens dopamine depletions. Eur J Neurosci 21, 1749-1757.

Mogg, K., and Bradley, B.P. (1998). A cognitive-motivational analysis of anxiety. Behav Res Ther 36, 809-848.

Moghaddam, B., Roth, R.H., and Bunney, B.S. (1990). Characterization of dopamine release in the rat medial prefrontal cortex as assessed by in vivo microdialysis: comparison to the striatum. Neuroscience 36, 669-676.

Morgan, M.A., and LeDoux, J.E. (1995). Differential contribution of dorsal and ventral medial prefrontal cortex to the acquisition and extinction of conditioned fear in rats. Behavioral neuroscience 109, 681-688.

Morrison, S.E., and Salzman, C.D. (2009). The convergence of information about rewarding and aversive stimuli in single neurons. J Neurosci 29, 11471-11483.

Mueller, D., Bravo-Rivera, C., and Quirk, G.J. (2010). Infralimbic D2 receptors are necessary for fear extinction and extinction-related tone responses. Biol Psychiatry 68, 1055-1060.

Murphy, B.L., Arnsten, A.F., Goldman-Rakic, P.S., and Roth, R.H. (1996a). Increased dopamine turnover in the prefrontal cortex impairs spatial working memory performance in rats and monkeys. Proc Natl Acad Sci U S A 93, 1325-1329.

Murphy, B.L., Arnsten, A.F., Jentsch, J.D., and Roth, R.H. (1996b). Dopamine and spatial working memory in rats and monkeys: pharmacological reversal of stress-induced impairment. J Neurosci 16, 7768-7775.

Nagano-Saito, A., Leyton, M., Monchi, O., Goldberg, Y.K., He, Y., and Dagher, A. (2008). Dopamine depletion impairs frontostriatal functional connectivity during a set-shifting task. The Journal of neuroscience : the official journal of the Society for Neuroscience 28, 3697-3706.

Nair-Roberts, R.G., Chatelain-Badie, S.D., Benson, E., White-Cooper, H., Bolam, J.P., and Ungless, M.A. (2008). Stereological estimates of dopaminergic, GABAergic and glutamatergic neurons in the ventral tegmental area, substantia nigra and retrorubral field in the rat. Neuroscience 152, 1024-1031.

Nakahara, K., Hayashi, T., Konishi, S., and Miyashita, Y. (2002). Functional MRI of macaque monkeys performing a cognitive set-shifting task. Science 295, 1532-1536.

Namburi, P., Beyeler, A., Yorozu, S., Calhoon, G.G., Halbert, S.A., Wichmann, R., Holden, S.S., Mertens, K.L., Anahtar, M., Felix-Ortiz, A.C., *et al.* (2015). A circuit mechanism for differentiating positive and negative associations. Nature 520, 675-678.

Naneix, F., Marchand, A.R., Di Scala, G., Pape, J.R., and Coutureau, E. (2009). A role for medial prefrontal dopaminergic innervation in instrumental conditioning. J Neurosci 29, 6599-6606.

Ninan, P.T., Insel, T.M., Cohen, R.M., Cook, J.M., Skolnick, P., and Paul, S.M. (1982). Benzodiazepine receptor-mediated experimental "anxiety" in primates. Science 218, 1332-1334.

Nyhus, E., and Barcelo, F. (2009). The Wisconsin Card Sorting Test and the cognitive assessment of prefrontal executive functions: a critical update. Brain and cognition 71, 437-451.

O'Doherty, J.P. (2004). Reward representations and reward-related learning in the human brain: insights from neuroimaging. Curr Opin Neurobiol 14, 769-776.

Omelchenko, N., and Sesack, S.R. (2009). Ultrastructural analysis of local collaterals of rat ventral tegmental area neurons: GABA phenotype and synapses onto dopamine and GABA cells. Synapse 63, 895-906.

Ouimet, A.J., Gawronski, B., and Dozois, D.J. (2009). Cognitive vulnerability to anxiety: A review and an integrative model. Clin Psychol Rev 29, 459-470.

Owens, D.G., Miller, P., Lawrie, S.M., and Johnstone, E.C. (2005). Pathogenesis of schizophrenia: a psychopathological perspective. The British journal of psychiatry : the journal of mental science 186, 386-393.

Pan, W.X., Brown, J., and Dudman, J.T. (2013). Neural signals of extinction in the inhibitory microcircuit of the ventral midbrain. Nat Neurosci 16, 71-78.

Park, J., Wood, J., Bondi, C., Del Arco, A., and Moghaddam, B. (2016). Anxiety Evokes Hypofrontality and Disrupts Rule-Relevant Encoding by Dorsomedial Prefrontal Cortex Neurons. J Neurosci 36, 3322-3335.

Paxinos, G., and Watson, C. (1998). The rat brain in stereotaxic coordinates. Academic Press.

Pearce, J.M., and Hall, G. (1980). A model for Pavlovian conditioning: variations in the effectiveness of conditioned but not unconditioned stimuli. Psychol Rev 87, 532-552.

Pehrson, A.L., Bondi, C.O., Totah, N.K., and Moghaddam, B. (2013). The influence of NMDA and GABA(A) receptors and glutamic acid decarboxylase (GAD) activity on attention. Psychopharmacology 225, 31-39.

Pellow, S., and File, S.E. (1986). Anxiolytic and anxiogenic drug effects on exploratory activity in an elevated plus-maze: a novel test of anxiety in the rat. Pharmacol Biochem Behav 24, 525-529.

Perugi, G., Del Carlo, A., Benvenuti, M., Fornaro, M., Toni, C., Akiskal, K., Dell'Osso, L., and Akiskal, H. (2011). Impulsivity in anxiety disorder patients: is it related to comorbid cyclothymia? J Affect Disord 133, 600-606.

Pezawas, L., Meyer-Lindenberg, A., Drabant, E.M., Verchinski, B.A., Munoz, K.E., Kolachana, B.S., Egan, M.F., Mattay, V.S., Hariri, A.R., and Weinberger, D.R. (2005). 5-HTTLPR polymorphism impacts human cingulate-amygdala interactions: a genetic susceptibility mechanism for depression. Nat Neurosci 8, 828-834.

Phelps, E.A., Delgado, M.R., Nearing, K.I., and LeDoux, J.E. (2004). Extinction learning in humans: role of the amygdala and vmPFC. Neuron 43, 897-905.

Pinto, L., and Dan, Y. (2015). Cell-Type-Specific Activity in Prefrontal Cortex during Goal-Directed Behavior. Neuron 87, 437-450.

Pitman, R.K., Rasmusson, A.M., Koenen, K.C., Shin, L.M., Orr, S.P., Gilbertson, M.W., Milad, M.R., and Liberzon, I. (2012). Biological studies of post-traumatic stress disorder. Nat Rev Neurosci 13, 769-787.

Popescu, A.T., Zhou, M.R., and Poo, M.M. (2016). Phasic dopamine release in the medial prefrontal cortex enhances stimulus discrimination. Proc Natl Acad Sci U S A.

Powell, N.J., and Redish, A.D. (2016). Representational changes of latent strategies in rat medial prefrontal cortex precede changes in behaviour. Nat Commun 7, 12830.

Purcell, R., Maruff, P., Kyrios, M., and Pantelis, C. (1998). Cognitive deficits in obsessive-compulsive disorder on tests of frontal-striatal function. Biological psychiatry 43, 348-357.

Quirk, G.J., and Beer, J.S. (2006). Prefrontal involvement in the regulation of emotion: convergence of rat and human studies. Current opinion in neurobiology 16, 723-727.

Raghunathan, R., and Pham, M.T. (1999). All Negative Moods Are Not Equal: Motivational Influences of Anxiety and Sadness on Decision Making. Organ Behav Hum Decis Process 79, 56-77.

Ragozzino, M.E. (2002). The effects of dopamine D(1) receptor blockade in the prelimbic-infralimbic areas on behavioral flexibility. Learning & memory 9, 18-28.

Ragozzino, M.E., Kim, J., Hassert, D., Minniti, N., and Kiang, C. (2003). The contribution of the rat prelimbic-infralimbic areas to different forms of task switching. Behav Neurosci 117, 1054-1065.

Raposo, D., Kaufman, M.T., and Churchland, A.K. (2014). A category-free neural population supports evolving demands during decision-making. Nature neuroscience 17, 1784-1792.

Rauch, S.L., Shin, L.M., and Phelps, E.A. (2006). Neurocircuitry models of posttraumatic stress disorder and extinction: human neuroimaging research--past, present, and future. Biological psychiatry 60, 376-382.

Redgrave, P., and Gurney, K. (2006). The short-latency dopamine signal: a role in discovering novel actions? Nat Rev Neurosci 7, 967-975.

Reinhard, J.F., Jr., Bannon, M.J., and Roth, R.H. (1982). Acceleration by stress of dopamine synthesis and metabolism in prefrontal cortex: antagonism by diazepam. Naunyn Schmiedebergs Arch Pharmacol 318, 374-377.

Rescorla, R.A., and Wagner, A.R. (1972). A theory of Pavlovian conditioning: variations in the effectiveness of reinforcement and nonreinforcement. In Classical conditioning II: Current Research and Theory, B.A. H., and P.W. F., eds. (New York: Appleton Century Crofts), pp. 64-99.

Rich, E.L., and Shapiro, M. (2009). Rat prefrontal cortical neurons selectively code strategy switches. The Journal of neuroscience : the official journal of the Society for Neuroscience 29, 7208-7219.

Richards, A., French, C.C., Calder, A.J., Webb, B., Fox, R., and Young, A.W. (2002). Anxiety-related bias in the classification of emotionally ambiguous facial expressions. Emotion 2, 273-287.

Rigotti, M., Barak, O., Warden, M.R., Wang, X.J., Daw, N.D., Miller, E.K., and Fusi, S. (2013). The importance of mixed selectivity in complex cognitive tasks. Nature 497, 585-590.

Rigotti, M., Ben Dayan Rubin, D., Morrison, S.E., Salzman, C.D., and Fusi, S. (2010). Attractor concretion as a mechanism for the formation of context representations. Neuroimage 52, 833-847.

Robinson, O.J., Vytal, K., Cornwell, B.R., and Grillon, C. (2013). The impact of anxiety upon cognition: perspectives from human threat of shock studies. Frontiers in human neuroscience 7, 203.

Roesch, M.R., Calu, D.J., and Schoenbaum, G. (2007). Dopamine neurons encode the better option in rats deciding between differently delayed or sized rewards. Nat Neurosci 10, 1615-1624.

Roesch, M.R., and Olson, C.R. (2004). Neuronal activity related to reward value and motivation in primate frontal cortex. Science 304, 307-310.

Rudebeck, P.H., Walton, M.E., Smyth, A.N., Bannerman, D.M., and Rushworth, M.F. (2006). Separate neural pathways process different decision costs. Nat Neurosci 9, 1161-1168.

Ruglass, L.M., Lopez-Castro, T., Cheref, S., Papini, S., and Hien, D.A. (2014). At the crossroads: the intersection of substance use disorders, anxiety disorders, and posttraumatic stress disorder. Current psychiatry reports 16, 505.

Russo, S.J., and Nestler, E.J. (2013). The brain reward circuitry in mood disorders. Nat Rev Neurosci 14, 609-625.

Schoenbaum, G., Roesch, M.R., Stalnaker, T.A., and Takahashi, Y.K. (2009). A new perspective on the role of the orbitofrontal cortex in adaptive behaviour. Nat Rev Neurosci 10, 885-892.

Schultz, W. (1997). Dopamine neurons and their role in reward mechanisms. Curr Opin Neurobiol 7, 191-197.

Schultz, W. (1998). Predictive reward signal of dopamine neurons. J Neurophysiol 80, 1-27.

Schultz, W. (2016). Dopamine reward prediction-error signalling: a two-component response. Nat Rev Neurosci 17, 183-195.

Schultz, W., Apicella, P., and Ljungberg, T. (1993). Responses of monkey dopamine neurons to reward and conditioned stimuli during successive steps of learning a delayed response task. J Neurosci 13, 900-913.

Seamans, J.K., Gorelova, N., Durstewitz, D., and Yang, C.R. (2001). Bidirectional dopamine modulation of GABAergic inhibition in prefrontal cortical pyramidal neurons. The Journal of neuroscience : the official journal of the Society for Neuroscience 21, 3628-3638.

Seo, H., and Lee, D. (2009). Behavioral and neural changes after gains and losses of conditioned reinforcers. J Neurosci 29, 3627-3641.

Sesack, S.R., and Bunney, B.S. (1989). Pharmacological characterization of the receptor mediating electrophysiological responses to dopamine in the rat medial prefrontal cortex: a microiontophoretic study. The Journal of pharmacology and experimental therapeutics 248, 1323-1333.

Shansky, R.M., Hamo, C., Hof, P.R., McEwen, B.S., and Morrison, J.H. (2009). Stress-induced dendritic remodeling in the prefrontal cortex is circuit specific. Cereb Cortex 19, 2479-2484.

Shin, L.M., Whalen, P.J., Pitman, R.K., Bush, G., Macklin, M.L., Lasko, N.B., Orr, S.P., McInerney, S.C., and Rauch, S.L. (2001). An fMRI study of anterior cingulate function in posttraumatic stress disorder. Biol Psychiatry 50, 932-942.

Simon, N.W., Wood, J., and Moghaddam, B. (2015). Action-outcome relationships are represented differently by medial prefrontal and orbitofrontal cortex neurons during action execution. J Neurophysiol 114, 3374-3385.

Sirota, A., Montgomery, S., Fujisawa, S., Isomura, Y., Zugaro, M., and Buzsaki, G. (2008). Entrainment of neocortical neurons and gamma oscillations by the hippocampal theta rhythm. Neuron 60, 683-697.

Sohal, V.S., Zhang, F., Yizhar, O., and Deisseroth, K. (2009). Parvalbumin neurons and gamma rhythms enhance cortical circuit performance. Nature 459, 698-702.

Solomon, M., Ozonoff, S., Carter, C., and Caplan, R. (2008). Formal thought disorder and the autism spectrum: relationship with symptoms, executive control, and anxiety. Journal of autism and developmental disorders 38, 1474-1484.

Somerville, L.H., Wagner, D.D., Wig, G.S., Moran, J.M., Whalen, P.J., and Kelley, W.M. (2013). Interactions between transient and sustained neural signals support the generation and regulation of anxious emotion. Cereb Cortex 23, 49-60.

Sotres-Bayon, F., Bush, D.E., and LeDoux, J.E. (2004). Emotional perseveration: an update on prefrontal-amygdala interactions in fear extinction. Learn Mem 11, 525-535.

Spellman, T., Rigotti, M., Ahmari, S.E., Fusi, S., Gogos, J.A., and Gordon, J.A. (2015). Hippocampal-prefrontal input supports spatial encoding in working memory. Nature 522, 309-314.

Stamatakis, A.M., and Stuber, G.D. (2012). Activation of lateral habenula inputs to the ventral midbrain promotes behavioral avoidance. Nat Neurosci 15, 1105-1107.

Stefani, A., Lozano, A.M., Peppe, A., Stanzione, P., Galati, S., Tropepi, D., Pierantozzi, M., Brusa, L., Scarnati, E., and Mazzone, P. (2007). Bilateral deep brain stimulation of the pedunculopontine and subthalamic nuclei in severe Parkinson's disease. Brain 130, 1596-1607.

Stefani, M.R., Groth, K., and Moghaddam, B. (2003). Glutamate receptors in the rat medial prefrontal cortex regulate set-shifting ability. Behav Neurosci 117, 728-737.

Stefani, M.R., and Moghaddam, B. (2005). Systemic and prefrontal cortical NMDA receptor blockade differentially affect discrimination learning and set-shift ability in rats. Behavioral neuroscience 119, 420-428.

Stefani, M.R., and Moghaddam, B. (2006). Rule learning and reward contingency are associated with dissociable patterns of dopamine activation in the rat prefrontal cortex, nucleus accumbens, and dorsal striatum. The Journal of neuroscience : the official journal of the Society for Neuroscience 26, 8810-8818.

Stefani, M.R., and Moghaddam, B. (2010). Activation of type 5 metabotropic glutamate receptors attenuates deficits in cognitive flexibility induced by NMDA receptor blockade. Eur J Pharmacol 639, 26-32.

Stokes, M.G., Kusunoki, M., Sigala, N., Nili, H., Gaffan, D., and Duncan, J. (2013). Dynamic coding for cognitive control in prefrontal cortex. Neuron 78, 364-375.

Strait, C.E., Blanchard, T.C., and Hayden, B.Y. (2014). Reward value comparison via mutual inhibition in ventromedial prefrontal cortex. Neuron 82, 1357-1366.

Sul, J.H., Kim, H., Huh, N., Lee, D., and Jung, M.W. (2010). Distinct roles of rodent orbitofrontal and medial prefrontal cortex in decision making. Neuron 66, 449-460.

Sutton, R.S., and Barto, A.G. (1998). Reinforcement Learning: An introduction (Cambridge, MA: MIT press).

Swanson, L.W. (1982). The projections of the ventral tegmental area and adjacent regions: a combined fluorescent retrograde tracer and immunofluorescence study in the rat. Brain Res Bull 9, 321-353.

Sylvers, P., Lilienfeld, S.O., and LaPrairie, J.L. (2011). Differences between trait fear and trait anxiety: implications for psychopathology. Clin Psychol Rev 31, 122-137.

Tan, K.R., Yvon, C., Turiault, M., Mirzabekov, J.J., Doehner, J., Labouebe, G., Deisseroth, K., Tye, K.M., and Luscher, C. (2012). GABA neurons of the VTA drive conditioned place aversion. Neuron 73, 1173-1183.

Thierry, A.M., Deniau, J.M., and Feger, J. (1979). Effects of stimulation of the frontal cortex on identified output VMT cells in the rat. Neurosci Lett 15, 102-107.

Thierry, A.M., Tassin, J.P., Blanc, G., and Glowinski, J. (1976). Selective activation of mesocortical DA system by stress. Nature 263, 242-244.

Tovote, P., Fadok, J.P., and Luthi, A. (2015). Neuronal circuits for fear and anxiety. Nat Rev Neurosci 16, 317-331.

Uhlhaas, P.J., and Singer, W. (2010). Abnormal neural oscillations and synchrony in schizophrenia. Nature reviews Neuroscience 11, 100-113.

Ungless, M.A., Argilli, E., and Bonci, A. (2010). Effects of stress and aversion on dopamine neurons: implications for addiction. Neurosci Biobehav Rev 35, 151-156.

Ungless, M.A., Magill, P.J., and Bolam, J.P. (2004). Uniform inhibition of dopamine neurons in the ventral tegmental area by aversive stimuli. Science 303, 2040-2042.

Valenti, O., Lodge, D.J., and Grace, A.A. (2011). Aversive stimuli alter ventral tegmental area dopamine neuron activity via a common action in the ventral hippocampus. J Neurosci 31, 4280-4289.

van der Meulen, J.A., Joosten, R.N., de Bruin, J.P., and Feenstra, M.G. (2007). Dopamine and noradrenaline efflux in the medial prefrontal cortex during serial reversals and extinction of instrumental goal-directed behavior. Cereb Cortex 17, 1444-1453.

van Zessen, R., Phillips, J.L., Budygin, E.A., and Stuber, G.D. (2012). Activation of VTA GABA neurons disrupts reward consumption. Neuron 73, 1184-1194.

Vijayraghavan, S., Wang, M., Birnbaum, S.G., Williams, G.V., and Arnsten, A.F. (2007). Inverted-U dopamine D1 receptor actions on prefrontal neurons engaged in working memory. Nat Neurosci 10, 376-384.

Wallis, J.D., Anderson, K.C., and Miller, E.K. (2001). Single neurons in prefrontal cortex encode abstract rules. Nature 411, 953-956.

Wassum, K.M., Ostlund, S.B., and Maidment, N.T. (2012). Phasic mesolimbic dopamine signaling precedes and predicts performance of a self-initiated action sequence task. Biol Psychiatry 71, 846-854.

White, I.M., and Wise, S.P. (1999). Rule-dependent neuronal activity in the prefrontal cortex. Exp Brain Res 126, 315-335.

White, J.A., Banks, M.I., Pearce, R.A., and Kopell, N.J. (2000). Networks of interneurons with fast and slow gamma-aminobutyric acid type A (GABAA) kinetics provide substrate for mixed gamma-theta rhythm. Proceedings of the National Academy of Sciences of the United States of America 97, 8128-8133.

Williams, G.V., and Goldman-Rakic, P.S. (1995). Modulation of memory fields by dopamine D1 receptors in prefrontal cortex. Nature 376, 572-575.

Wise, R.A. (2004). Dopamine, learning and motivation. Nat Rev Neurosci 5, 483-494.

Wise, S.P., Murray, E.A., and Gerfen, C.R. (1996). The frontal cortex-basal ganglia system in primates. Crit Rev Neurobiol 10, 317-356.

Ye, L., Allen, W.E., Thompson, K.R., Tian, Q., Hsueh, B., Ramakrishnan, C., Wang, A.C., Jennings, J.H., Adhikari, A., Halpern, C.H., *et al.* (2016). Wiring and Molecular Features of Prefrontal Ensembles Representing Distinct Experiences. Cell 165, 1776-1788.

Young, A.M. (2004). Increased extracellular dopamine in nucleus accumbens in response to unconditioned and conditioned aversive stimuli: studies using 1 min microdialysis in rats. J Neurosci Methods 138, 57-63.

Yu, B.M., Cunningham, J.P., Santhanam, G., Ryu, S.I., Shenoy, K.V., and Sahani, M. (2009). Gaussian-process factor analysis for low-dimensional single-trial analysis of neural population activity. Journal of neurophysiology 102, 614-635.

Zweifel, L.S., Argilli, E., Bonci, A., and Palmiter, R.D. (2008). Role of NMDA receptors in dopamine neurons for plasticity and addictive behaviors. Neuron 59, 486-496.